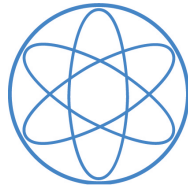


PHYSIK-DEPARTMENT

LEHRSTUHL FÜR EXPERIMENTALPHYSIK E12



**Development of an ultra-sensitive detection
method for transuranium elements with
respect to ocean water samples from
Fukushima**

Dissertation

von

Karin M. Hain





Fakultät für Physik der Technischen Universität München
Lehrstuhl für Experimentalphysik E12

Development of an ultra-sensitive detection method for transuranium elements with respect to ocean water samples from Fukushima

Karin Margarete Hain

Vollständiger Abdruck der von der Fakultät für Physik der Technischen Universität München zur Erlangung des akademischen Grades eines

Doktors der Naturwissenschaften (Dr. rer. nat.)

genehmigten Dissertation.

Vorsitzender: apl. Prof. Dr. Norbert Kaiser

Prüfer der Dissertation: 1. Univ.-Prof. Dr. Walter Henning
2. Univ.-Prof. Dr. Stefan Schönert

Die Dissertation wurde am 09.03.2016 bei der Technischen Universität München eingereicht und durch die Fakultät für Physik am 30.03.2016 angenommen.

Abstract

The development of a detection method for the identification of a possible emission of actinides into the Pacific Ocean by the Fukushima Daiichi Nuclear Power Plant (FDNPP) accident, was the major aim of this PhD thesis. It is shown in this work that in addition to the isotopic plutonium ratio $^{240}\text{Pu}/^{239}\text{Pu}$, which is an important signature for different contamination sources, the $^{241}\text{Pu}/^{239}\text{Pu}$ ratio has to be determined, to distinguish between a Fukushima entry of actinides and nuclear weapon fallout in the Pacific Ocean. Furthermore, this study was aiming for the improvement of the data on the neptunium (^{237}Np) distribution in the ocean. For the detection of the trace concentrations of actinides in the order of mBq/m^3 in a small sample volume of 20 L ocean water, the ultra-sensitive method accelerator mass spectrometry (AMS) was chosen. A chemical separation procedure for Pu and Np based on extraction chromatography was developed using mass spectrometry and radiometric analysis to determine the chemical recovery. ^{241}Am , which causes isobaric background to ^{241}Pu in mass spectrometric measurements, was separated with a suppression of at least 10^{-4} from Pu by this method. The detection method adjusted to Pu and Np was successfully verified by analyzing the concentration of Pu in certified reference material with AMS at the Maier-Leibnitz-Laboratory (MLL) in Munich. Due to a temporary closure of the MLL, 12 sea water samples, collected in autumn 2012, were prepared at the Radiochemie München and measured at the Vienna Environmental Research Laboratory (VERA). The sampling station closest to the FDNPP was located at a distance of 39.6 km. Three of the samples showed a slightly elevated $^{240}\text{Pu}/^{239}\text{Pu}$ ratio of up to $0.23_{-0.03}^{+0.04}$ compared to global fallout ($^{240}\text{Pu}/^{239}\text{Pu} = 0.180 \pm 0.007$), whereas all measured $^{241}\text{Pu}/^{239}\text{Pu}$ ratios were clearly consistent with nuclear weapon fallout ($^{241}\text{Pu}/^{239}\text{Pu} < 2.4 \cdot 10^{-3}$). An upper limit for the dissolved amount of ^{239}Pu released by the Fukushima accident of 10 MBq was estimated from the average $^{241}\text{Pu}/^{239}\text{Pu}$ ratio of $6_{-2}^{+6} \cdot 10^{-4}$ at the sampling station located closest to FDNPP. Pu with the signature of weapon grade Pu was found off the US West Coast. A preceding emission from Hanford Site seems most likely. The data for ^{237}Np indicate a distribution in the water column different from Pu.

Zusammenfassung

Die primäre Zielsetzung dieser Arbeit war, einen möglichen Eintrag an Transuranium Elementen in den Pazifischen Ozean durch den Reaktorunfall von Fukushima zu identifizieren. Das Plutonium (Pu) Isotopenverhältnis $^{240}\text{Pu}/^{239}\text{Pu}$ wurde bereits in der Vergangenheit erfolgreich als Fingerabdruck verschiedener Kontaminationsquellen verwendet. Wie in der vorliegenden Arbeit gezeigt wird, muss im Pazifischen Ozean zur Unterscheidung einer Emission von Aktiniden durch Fukushima und Fallout aus Kernwaffentests, zusätzlich das $^{241}\text{Pu}/^{239}\text{Pu}$ Verhältnis bestimmt werden. Ein weiteres Ziel dieser Studie war die Verbesserung der Datenlage bezüglich der Neptunium (^{237}Np) Verteilung im Ozean. Um Spurenkonzentration von Aktiniden in der Größenordnung mBq/m^3 in relativ kleinen Probenvolumina von 20 L Meerwasser nachweisen zu können, wurde die ultra-sensitive Beschleuniger Massenspektrometrie eingesetzt (AMS). Im Rahmen dieser Arbeit wurde eine chemische Prozedur zur Pu und Np Trennung basierend auf Extraktionschromatographie entwickelt, und deren Ausbeute mittels Massenspektrometrie und radiometrischer Analyse bestimmt. Mit dieser chemischen Separationsmethode konnte ^{241}Am , welches bei allen massenspektrometrischen Messungen isobaren Untergrund von ^{241}Pu verursacht, um vier Größenordnungen unterdrückt werden. Die auf Pu und Np optimierte Nachweismethode wurde erfolgreich am Maier-Leibnitz-Laboratorium (MLL) in München validiert, indem die Pu und Np Konzentrationen in einem zertifizierten Referenzmaterial mittels AMS analysiert wurden. Aufgrund einer temporären Schließung des MLL, wurden 12 Wasserproben, welche im Herbst 2012 im Pazifik genommen wurden, an der Radiochemie München aufbereitet und am Vienna Environmental Research Laboratory (VERA) gemessen. Die dem Kernkraftwerk Fukushima am nächsten gelegene Probenposition befand sich in einem Abstand von 39.6 km. Drei Proben zeigten im Vergleich zu globalen Fallout ($^{240}\text{Pu}/^{239}\text{Pu} = 0.180 \pm 0.007$) ein leicht erhöhtes $^{240}\text{Pu}/^{239}\text{Pu}$ Verhältnis von bis zu $0.23_{-0.03}^{+0.04}$, wohingegen alle $^{241}\text{Pu}/^{239}\text{Pu}$ Verhältniss eindeutig kompatibel mit denen von Kernwaffen-Fallout ($^{241}\text{Pu}/^{239}\text{Pu} < 2.4 \cdot 10^{-3}$) waren. Anhand des durchschnittlichen $^{241}\text{Pu}/^{239}\text{Pu}$ Verhältnisses der dem Kernkraftwerk am nächsten gelegenen Probenposition von $6_{-2}^{+6} \cdot 10^{-4}$, konnte eine Obergrenze von 10 MBq für das durch den Reaktorunfall freigesetzte und im Meerwasser gelöste ^{239}Pu abgeschätzt werden. Pu, welches vor der Westküste der USA gefunden wurde, zeigte die Signatur von waffenfähigem Pu, was durch eine zurückliegende Freisetzung durch Hanford Site erklärt werden könnte.

Die ^{237}Np Daten deuten auf eine andere Verteilung in der Wassersäule als für Pu hin.

Contents

| | |
|---|-----------|
| 1. Introduction | 13 |
| 2. Chemical and physical characteristics of the relevant transuranium elements | 17 |
| 2.1. Discovery and nuclear properties of Pu and Np | 17 |
| 2.2. Chemistry | 19 |
| 2.2.1. Oxidation states | 19 |
| 2.2.2. Behaviour in sea water | 22 |
| 2.3. Radiotoxicity | 23 |
| 2.4. Production of transuranium elements | 24 |
| 2.5. Anthropogenic sources of transuranium elements in the environment | 25 |
| 2.6. Concentrations and detection of Pu and Np in the Pacific Ocean | 28 |
| 3. The Fukushima accident | 31 |
| 3.1. The nuclear power plant Fukushima Daiichi I | 32 |
| 3.2. Chronology of the accident | 35 |
| 3.2.1. Unit 1 | 36 |
| 3.2.2. Unit 2 and 3 | 38 |
| 3.2.3. Unit 4 | 40 |
| 3.3. Radiological consequences | 41 |
| 3.4. Inventory of FDNPP I at the moment of SCRAM | 45 |
| 3.5. Identification of a possible entry of actinides into the Pacific Ocean | 49 |
| 4. Ocean water samples and AMS sample preparation | 53 |
| 4.1. Sampling of sea water | 53 |
| 4.1.1. IAEA-443: Irish Sea Water | 53 |
| 4.1.2. Pacific Ocean water | 54 |
| 4.2. Chemical Pu and Np extraction | 56 |
| 4.2.1. Concentration using a rotary evaporator | 58 |
| 4.2.2. Spike material IRMM-085 | 59 |
| 4.2.3. Fe(OH) ₃ co-precipitation | 60 |
| 4.2.4. Extraction chromatography using TEVA resin | 62 |
| 4.2.5. Combination with UTEVA resin for further U suppression | 66 |

Contents

| | |
|---|------------|
| 4.2.6. Final AMS sample | 68 |
| 4.2.7. Blank samples | 69 |
| 4.3. Preparation of a $^{237}\text{Np}/^{242}\text{Pu}$ standard sample | 70 |
| 5. Chemical recovery of the separation procedure | 71 |
| 5.1. Experimental settings | 71 |
| 5.2. Applied detection methods | 72 |
| 5.2.1. α - and γ -spectrometry | 72 |
| 5.2.2. ICP-MS | 74 |
| 5.3. Results for Pu and Np recovery | 76 |
| 6. AMS setup and measurements | 79 |
| 6.1. Introduction to AMS | 79 |
| 6.2. AMS setup for the detection of heavy nuclides ($m > 140$) at the MLL . . . | 80 |
| 6.2.1. AMS injector | 81 |
| 6.2.2. Tandem accelerator | 82 |
| 6.2.3. Beam transport | 83 |
| 6.2.4. Detection system | 83 |
| 6.3. AMS setup at VERA laboratory | 85 |
| 6.4. Measurement procedure for Pu and Np | 87 |
| 6.4.1. Challenges of measuring $^{239-241}\text{Pu}$ and ^{237}Np | 87 |
| 6.4.2. Injector and beam tuning | 89 |
| 6.4.3. Detector calibration | 89 |
| 6.4.4. Measurement principle | 93 |
| 6.4.5. Detection efficiency | 96 |
| 6.5. Analysis of uncertainties | 97 |
| 7. Results and Discussion of the Ocean Water Samples | 99 |
| 7.1. IAEA-443 | 99 |
| 7.2. Pu in Pacific Ocean Water | 101 |
| 7.2.1. Concentration | 101 |
| 7.2.2. Isotopic ratios | 105 |
| 7.3. Np in Pacific Ocean Water | 107 |
| 7.3.1. Concentration | 107 |
| 7.3.2. Isotopic ratios | 108 |
| 7.4. Upper limit of dissolved ^{239}Pu activity released by the FDNPP accident . . | 110 |
| 7.5. Discussion of BD17-0m | 113 |
| 8. Conclusion and Outlook | 117 |

| | |
|--|------------|
| A. α- and γ-decay energies | 119 |
| B. Individual sample results | 121 |
| C. Results for Pu and Np recovery | 125 |
| D. Further chemical separation techniques | 127 |
| D.1. Solvent extraction | 127 |
| D.2. Ion exchange chromatography | 127 |
| E. Purification and characterization of the ^{237}Np solution | 131 |
| E.0.1. Purification of the ^{237}Np solution provided by the RCM | 131 |
| E.0.2. Characterization of the final ^{237}Np solution and standard sample preparation | 133 |
| F. Prepared $^{237}\text{Np}/^{242}\text{Pu}$ standard samples | 135 |
| G. Certificates | 137 |
| H. List of Pacific ocean water samples | 141 |

1. Introduction

Since the detonation of the first nuclear weapon in 1945, anthropogenic transuranium elements (TRU) continuously entered the environment due to reprocessing plants, nuclear accidents and in particular nuclear weapon testing. In comparison, the natural abundance of TRU mainly produced in uranium ores, is negligible. As events like the Fukushima accident in 2011 and the most recent nuclear weapon test by North Korea in 2016 have shown, there is a significant risk for TRU release also in the future. Consequently, it is important to study the physio-chemical behaviour of TRU in the environment to predict locally increased concentrations and possibilities to enter the human food-chain. Especially plutonium (Pu) shows a variety of processes in natural waters and a considerable radiotoxicity mainly due to its long-lived isotopes ^{239}Pu and ^{240}Pu , which are the reasons for a large number of publications on these isotopes, whereas the research in particular on Np is considered to lag 20-30 years behind [1]. The isotopic ratio $^{240}\text{Pu}/^{239}\text{Pu}$ has proven very useful as signature for different contamination sources. In this way, a different transport of Pu according to the type of nuclear weapon fallout in the Pacific Ocean was observed [2].

Since March 2011, when the Fukushima Daiichi Nuclear Power Plant (FDNPP) accident happened, there is another possible source for TRU in the Pacific Ocean apart from nuclear weapon fallout. Pu released into the atmosphere by the FDNPP has already been identified in soil and litter samples collected close to the NPP (Nuclear Power Plant), but the detected concentrations are not of radiological concern [3, 4]. Even though several studies could demonstrate that also the amount of Pu which might have been emitted into the Pacific Ocean is not radiologically relevant, a general release of TRU could not be definitively excluded so far. It is known that during the accident considerable amounts of partially highly contaminated effluents originating from the inner structure of the reactor, have entered the Pacific Ocean [5]. A release of TRU from the molten fuel would represent a physio-chemical form different from the weapon fallout. This allows to study its distribution and behaviour in the ocean.

The most sensitive detection method for long-lived isotopes, Accelerator Mass Spectrometry (AMS), was applied in this study to answer the question of a possible release of TRU, in particular Pu and Np into the Pacific Ocean by the FDNPP. It is shown in this work,

1. Introduction

that the $^{240}\text{Pu}/^{239}\text{Pu}$ ratio is not sufficient to clearly identify a FDNPP entry, but the $^{241}\text{Pu}/^{239}\text{Pu}$ has to be determined in addition. However, as ^{241}Pu concentrations in ocean water due to fallout are very low, an ultra-sensitive technique like AMS had to be used to detect this isotope in comparable small sample volumes of 20 L per sampling station. Samples were collected in autumn 2012 by the GEOTRACES program [6]. It was decided to use these valuable samples also to improve the overall data on the ^{237}Np distribution in the Pacific Ocean.

The AMS set-up at the Maier-Leibnitz-Laboratory (MLL) has already proven to reach the required sensitivities for the respective Pu isotopes in environmental samples like manganese nodules [7], but the beam line, now used for the detection of actinides, has been upgraded in the meantime [8, 9]. Consequently, not only the measurement procedure but also the sample preparation method had to be adjusted to the present application. The primary aim of the sample preparation was the chemical separation of ^{241}Pu , an almost pure β^- emitter, from its daughter nuclide ^{241}Am , which cannot be distinguished by mass-spectrometric means. In order to increase the overall detection efficiency for Pu and Np, both elements also have to be separated chemically, so that AMS samples for each element can be produced from one water sample. For this purpose, a procedure based on extraction chromatography using TEVATM resin already proposed in earlier publications [10, 11] was developed further. Several reagents applied in these procedures [12] had to be eliminated from the separation method, as their use is off-limits in the laboratory of the MLL. For the estimation of the chemical yields, the procedure also had to meet the requirements of α and γ spectrometry and ICP-MS (Inductively Coupled Plasma Mass Spectrometry), apart from the demands of AMS. After the successful validation of the separation method with certified reference material provided by the IAEA (International Atomic Energy Agency), it was applied to the Pacific Ocean water samples. However, due to a temporary closure of the MLL, samples were prepared at the Radiochemie München (RCM) and measured at the Vienna Environmental Research Accelerator (VERA), where actinide detection is already well established [13, 14].

This work starts with an introduction to the nuclear and chemical properties of TRU with focus on Pu and Np, which determine their concentrations and behaviour in sea water. Different sources and the respective isotopic ratios are discussed, in particular for the Pacific Ocean. Chapter 3 gives an overview of the events during the FDNPP accident. Apart from the radioactive release, also results of previous Pu studies after the accident are presented in this chapter and the applied method to identify an entry of actinides into the Ocean is explained. In chapter 4, the ocean samples and the applied chemical separation procedure is described. The results for the chemical Pu and Np recovery and the applied detection techniques can be found in chapter 5. The AMS set-up at the MLL and the measurement procedure is presented in chapter 6 and differences to the set-up at

VERA are discussed. The results of the Pu and Np concentrations and isotopic ratios in Pacific Ocean water are shown in chapter 7 along with the results for the IAEA reference material. Implications for the release from the FDNPP accident or other sources are discussed. At the end, a conclusion and an outlook to the remaining Pacific Ocean water samples are given.

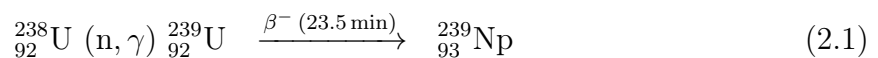
In this work, atomic ratios play an important role. Unless otherwise mentioned, any ratio written as e.g. $^{240}\text{Pu}/^{239}\text{Pu}$ refers to the atomic ratio, not the mass or activity ratio which are explicitly denoted as e.g. $m(^{240}\text{Pu})/m(^{239}\text{Pu})$ or $A(^{240}\text{Pu})/A(^{239}\text{Pu})$, respectively.

2. Chemical and physical characteristics of the relevant transuranium elements

Nuclear activities of mankind lead to an enrichment of actinides in the environment and are generally based on neutron induced fission of uranium (U). Neutron capture on U which does not fission causes the build-up of the transuranium elements (TRU). This chapter describes the production paths of this group of elements along with the nuclear and in particular the chemical properties of the isotopes studied in this project, which define their behaviour in sea water but also during sample preparation. These elements are plutonium (Pu) and neptunium (Np) in the first place, but also americium (Am) whose chemical properties are essential for sample preparation.

2.1. Discovery and nuclear properties of Pu and Np

The first transuranium element was discovered by McMillan and Abelson in 1940, who produced element 93, which was later given the name neptunium, via the reaction



which then further decays with a half-life 2.355 d to ${}^{239}\text{Pu}$, also by β^- emission. In 1940 and 1941, Pu was synthesized for the first time by G. T. Seaborg and his co-workers [15] at Berkeley National Laboratory. For this purpose, uranium oxid was bombarded by deuterons which had been accelerated by an cyclotron to an energy of 16 MeV. In this (d, 2n) reaction, ${}^{238}\text{Np}$ was produced in the first place which decayed via β^- emission with a half-life of 2.1 days to ${}^{238}\text{Pu}$. Np and Pu could be distinguished by the in-growth of α -activity due to the decay of ${}^{238}\text{Pu}$.

In addition, Seaborg also found naturally occurring Pu in pitchblende concentrate from Canada in 1948 [16], and could show later in cooperation with C. A. Levine that it was isotopically pure ${}^{239}\text{Pu}$ [17]. He identified a ${}^{239}\text{Pu}$ concentration of $m({}^{239}\text{Pu})/m(\text{ore}) = 10^{-12}$

2. Chemical and physical characteristics of the relevant transuranium elements

in the Canadian pitchblende. These trace amounts of ^{239}Pu could be explained by neutron capture on ^{238}U and subsequent β -decay as presented by eq. (2.1). The presence of neutrons in the ore were thought to originate from spontaneous fission of uranium, (α, n) reactions or spallation reactions of cosmic rays [15, 16]. Also trace amounts of the long-lived neptunium isotope, ^{237}Np , can be found in nature. Relative atomic concentrations of $^{237}\text{Np}/^{238}\text{U} = 2 \cdot 10^{-12}$ were detected in Katanga Pitchblende [18].

| Isotope | $T_{1/2}$ | Decay | $\sigma(\text{n}_{th}, \text{f})$ [b] | $\sigma(\text{n}_{th}, \gamma)$ [b] |
|-------------------|----------------------|-----------------------------------|---------------------------------------|-------------------------------------|
| ^{236}Pu | 2.858 a | α , sf | 160 | - |
| ^{239}Pu | $2.41 \cdot 10^4$ a | α , sf | 752 | 270 |
| ^{240}Pu | $6.56 \cdot 10^3$ a | α , sf | 0.059 | 290 |
| ^{241}Pu | 14.35 a | β^- , sf, α | 1010 | 370 |
| ^{242}Pu | $3.75 \cdot 10^5$ a | α , sf | < 0.2 | 19 |
| ^{244}Pu | $8.00 \cdot 10^7$ a | α , sf | - | 1.7 |
| ^{236}Np | 22.5 h | ϵ , β^- | 2700 | |
| | $1.54 \cdot 10^5$ a | α , ϵ , β^- | 3000 | |
| ^{237}Np | $2.144 \cdot 10^6$ a | α , sf | 0.020 | 170 |
| ^{239}Np | 2.355 d | β^- | < 1 | 19 |

Table 2.1.: Nuclear characteristics of most relevant Pu and Np isotopes, with $T_{1/2}$: half life, $\sigma(\text{n}_{th}, \text{f})$: cross-section for thermal neutron induced fission, sf: spontaneous fission, $\sigma(\text{n}_{th}, \gamma)$: neutron capture cross-section. [19].

Table Tab. 2.1 lists the nuclear characteristics of Pu and Np isotopes which are either relevant for nuclear power production, nuclear weapons or radioanalytical application. Considering the cross-sections for thermal fission, ^{239}Pu , ^{241}Pu and ^{236}Np are candidates to be used as nuclear fuel. However, ^{241}Pu and ^{236}Np are produced only in minor quantities in a nuclear reactor (compare Ch. 2.4) and in addition, the half-life of ^{241}Pu is rather short. ^{236}Pu and ^{242}Pu are frequently used as tracer in radioanalytics, especially for the detection with α -spectrometry (see Ch. 5). Due to their long half-lives, ^{239}Pu , ^{240}Pu , and ^{237}Np receive special attention regarding final storage of nuclear waste and long-term environmental contamination. Because of its daughter product ^{241}Am ($T_{1/2} = 432.2$ a) which decays to ^{237}Np , also ^{241}Pu has to be considered in this context. The short-lived isotope ^{239}Np can be easily detected by γ -spectrometry and can be easily obtained from its mother nuclide ^{243}Am via α -decay, which favors this nuclide as tracer in radioanalytics.

2.2. Chemistry

It is well-known that the chemical behaviour of the actinides is rather complex due to their $[\text{Rn}]5f6d7s$ electron configuration with the 5f, 6d and 7s orbitals being at almost equal energy level. Therefore, for the actinides with lower atomic number until Am, the 5f orbitals are not efficiently shielded by the outer 6d orbitals, so that they can also participate in chemical bonds. With increasing nuclear charge, the attraction of the 5f orbitals by the nuclear core is enhanced so that those orbitals are hardly available for chemical bonds [12]. Consequently, a rather different chemical behaviour of U, Np, and Pu can be expected compared to the heavier Am and Cm. The actinides below Am show a diversity of chemical processes which makes it hard to predict their ways of migration in the environment. These processes are for example redox reactions, complexation, sorption, precipitation, and also biosorption by microbes [20]. These actinides can exist in at least two oxidation states simultaneously in the same solution, which determine the chemical behaviour.

2.2.1. Oxidation states

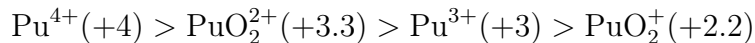
The oxidation states of actinides can be influenced by a number of parameters as for example pH, redox potential, complexing ligands which makes the understanding of their chemical behaviour in aqueous systems quite challenging. However, actinides in a certain oxidation state show a similar behaviour [20]. Therefore, chemical effects related to the oxidation state will be explained for plutonium in the following and can be transferred to other actinides.

Plutonium

The most complex chemical properties of all actinides can be attributed to Pu, as it exists in the oxidation states +III, +IV, +V, and +VI in solutions. Oxidation state +VII has been also found, but as its existence is rather rare [21, 12], it will be neglected in this work. Pu can occur in at least four common oxidation states simultaneously in solutions depending on the pH and the Eh (redox potential with respect to a standard hydrogen electrode) value of the solution as all oxidation states are instable [22, 12]. The chemical properties of the different oxidation states are strongly affected by hydrolysis which therefore has to be considered first. In an aqueous solution, Pu(III) and Pu(IV) are present as hydrated cations Pu^{3+} and Pu^{4+} whereas Pu(V) and Pu(VI) quickly hydrolyze forming ionic bonds which results in the so-called plutonyl ions, PuO_2^+ and PuO_2^{2+} , respectively. Consequently, the effective charge of the different ion species decreases in the following

2. Chemical and physical characteristics of the relevant transuranium elements

order:



where the respective charge is given in brackets. Since the complexation strength significantly depends on the effective charge, it decreases in a similar order. Therefore, the complex formation is most pronounced for Pu^{4+} leading to very stable complexes with strong ligands such as fluoride (F^-), carbonate (CO_3^{2-}) or phosphate (PO_4^{3-}) but also hydroxide (OH^-) (more detailed information can be found in [21]). Especially complexes with OH^- , i.e. hydrolysis, have a big influence on the solubility and sorption of Pu in aqueous systems. One of the most important implications of the strong hydrolysis of Pu^{4+} is a very efficient sorption of Pu(IV) to surfaces [22]. At environmental concentrations, this is the dominating process to remove Pu from the water column (see Ch. 2.2.2). A very convenient way to represent the dependence of the oxidation states and hydrolysis on Eh and pH is a Eh-pH diagram, as it is shown for the Pu-O-H system in Fig. 2.1 (a) [23]. It shows the dominating aqueous species and stable solid phases calculated from thermodynamic databases, which was the LLNL (Lawrence Livermore National Laboratory) database in this case. Using different thermodynamic models can lead to significantly different plots. However, the most important trend that all databases have in common, is that III and IV predominate at reducing conditions and low pH, whereas V and VI stabilize at oxidizing conditions and high pH. Oxidation states III and IV are commonly referred to as reduced and V and VI as oxidized species. A similar behaviour can be observed for Np and therefore, the same denotation will be applied. However, this situation can be highly effected by the presence of complexing agents, so that the Eh-pH-diagram can be considerably modified. For examples, it can be expected that pentavalent Pu carbonates dominate even at low pH [21]. Concerning redox reactions, Pu shows a very specific behaviour as the redox couples Pu(III)/Pu(IV) and Pu(V)/Pu(VI) are reversible. That means the reactions $\text{III} \rightleftharpoons \text{IV}$ and $\text{V} \rightleftharpoons \text{VI}$ happen very fast whereas redox reactions between a hydrated species and a plutonyl ion are very slow since bonds between Pu and O have to be modified in this case. Consequently, Pu can be usually found as a mixture of the two oxidation states which form a reversible redox couple [22]. This has some major implications on selective chemical procedures such as ion exchange, extraction chromatography or precipitation, which are usually based on one specific oxidation state.

By interaction with itself, Pu can react by disproportionation in acidic solutions, for example in the following way:



However, the expected concentrations of Pu in environmental samples are on trace level, so that disproportionation reactions can be neglected. This also holds for Np and therefore

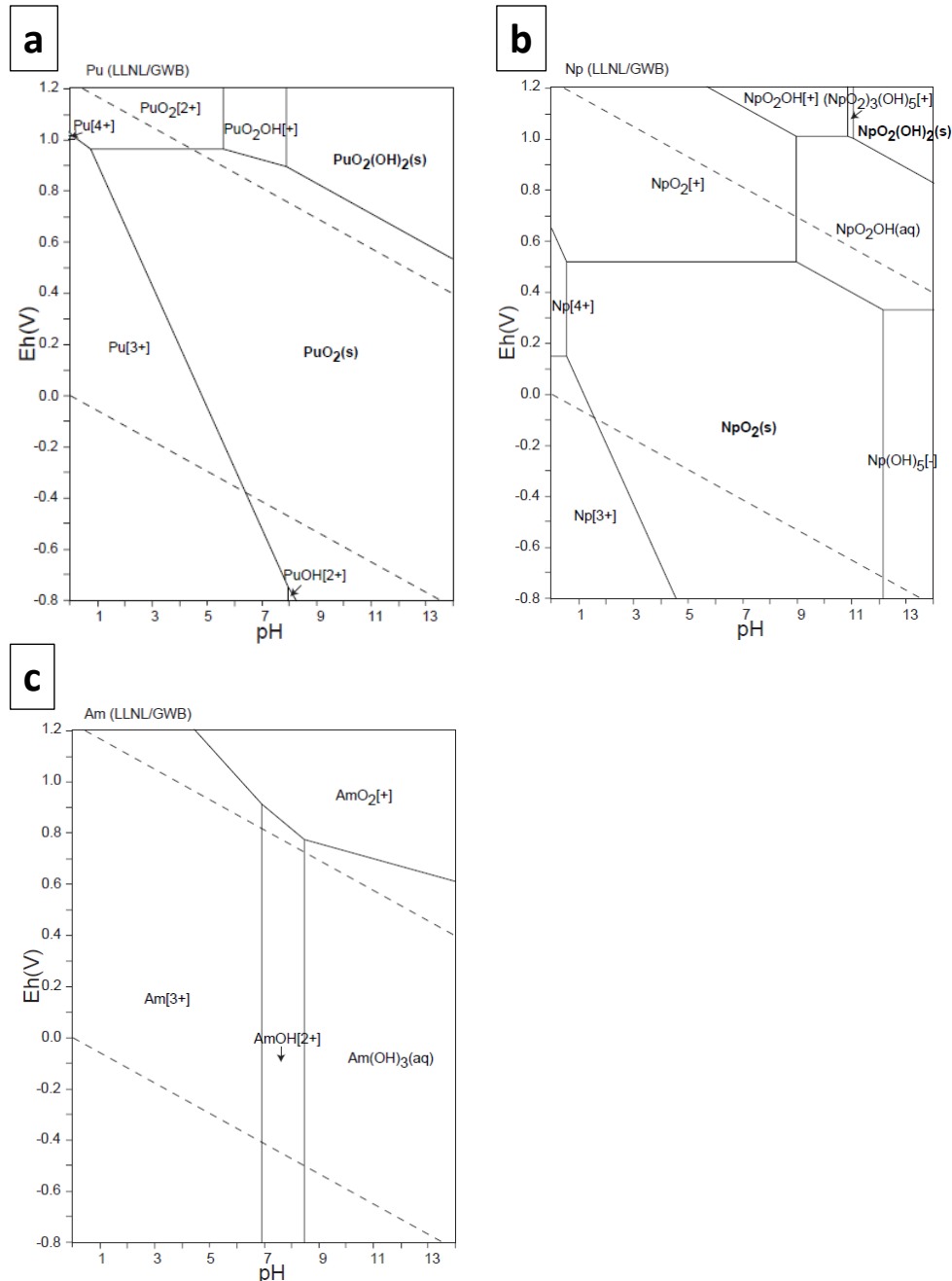


Figure 2.1.: Eh-pH diagram for the Pu-O-H system (a), the Np-O-H system (b) and the Am-O-H system (c) at a concentration of 10^{-10} M, 298.15 K, 10^5 Pa. The two dashed diagonal lines represent the stability field of water. Taken from [23].

is not discussed further in this work. Furthermore, the hydrolyzed Pu⁴⁺ which is readily formed even at pH = 0 can form colloids and various polymers. The mechanisms of colloid formation are still not fully understood and are an issue of current research [24, 25]. However, polymerization starts at concentrations larger than 10^{-6} M (mol/L) which corresponds to approximately $5 \cdot 10^{17}$ atoms/L [20] which is several orders of magnitude

2. Chemical and physical characteristics of the relevant transuranium elements

larger than the expected environmental concentrations and hence is not an issue to be taken into account in this work.

Neptunium

Similar to Pu, in principle Np can exist in all oxidation states between +III and +VII. However, the Eh-pH-diagram for Np in Fig. 2.1 (b) shows that in contrast to Pu, oxidation states +IV and +V dominate over a large range of pH and Eh values and thus, are considered as the most important ones. The oxidized Np readily forms the neptunyl ion NpO_2^+ in an aquatic environment, which only weakly hydrolyzes to NpO_2OH at $\text{pH} > 7$. By contrast, Np^{4+} is hydrolyzed already at highly acidic conditions ($\text{pH} = 1$). The higher effective charge of Np^{4+} in general leads to a significantly higher complexation strength compared to weakly complexing pentavalent Np [12, 22]. Disproportionation reactions and colloid formation can also be observed for tetravalent Np if the concentrations are sufficiently high.

Americium

The most important feature of Am chemistry is, that Am exists in the oxidation state +III at usual redox potentials over the full pH range in aqueous systems. Oxidation state +IV can only be obtained if a strong oxidizing agent is added to Am in an alkaline solution [25]. In contrast to Pu and Np also hydrolysis is not that pronounced which means that Am(III) starts to hydrolyze to $\text{Am}(\text{OH})_2$ at around $\text{pH} = 6$ (compare Fig. 2.1 (c)).

2.2.2. Behaviour in sea water

In natural waters, a large number of parameters determine the oceanic behaviour of TRU. This is not only the redox potential, the pH and the concentration and type of complexing agents, which can be changing with respect to the location in the ocean, but also the physical and chemical form how the TRU entered the water column in addition to biological processes. In general, the pH of the Pacific Ocean water ranges from 7.2 at around 55°N to 8.1 at 25°N [26]. The redox potential strongly depends on the ion species in the water, but for a usual composition of sea water an Eh value between 0.4 and 0.75, i.e. oxidizing conditions, can be expected [27]. Looking on the Eh-pH-diagrams for the simple actinide-O-H systems in Fig. 2.1, this gives oxidation state +IV for Pu and for Np +IV and predominantly +V. However, at low concentrations the stability of Pu(V) is increased when it is complexed by carbonate ions, so that this oxidation state can also be present, especially in oxidizing water layers. Typical concentrations of the most

important inorganic constituents of sea water are listed in Tab. 2.2. The dominance of oxidation state IV for Pu and V for Np leads to substantial differences in the behaviour in sea water. Pu(IV) either quickly hydrolyzes to form the hardly soluble $\text{Pu}(\text{OH})_4$ or is absorbed by suspended or colloidal particles, which results in a fast sedimentation. It has been shown, that in the dissolved phase Pu(V) is the prevailing chemical form, whereas for particulate Pu, Pu(IV) prevails [28]. Consequently, in coastal areas with shallow waters and high particle concentrations, Pu is removed from the water column much faster than in the open ocean [29]. Similar to Pu(V), also Np(V) primarily stays in the dissolved phase and can be transported over long distances. In studies of the Np oxidation state in the Irish Sea, less than 1% of Np was found to be present in +IV in the sea water whereas the original proportion was 45 % when emitted from the reprocessing plant Sellafield [30]. This percentage of the more soluble Np(V) increases even further with increasing distance to Sellafield [29]. Furthermore, there is the possibility of remobilization of TRU from sediments, e.g. by changing chemical conditions in the sediment or bioturbation, which means that the TRU bearing particles may be decomposed, so that the TRU are released back to the water [31].

| Ion | Concentration [g/L] |
|--------------------|---------------------|
| HCO_3^- | 0.140 |
| SO_4^{2-} | 2.65 - 2.71 |
| Cl^- | 1.90 - 1.94 |
| Ca^{2+} | 0.380 - 0.399 |
| Mg^{2+} | 1.27 - 1.29 |
| Na^+ | 10.6 - 10.8 |
| K^+ | 0.380 - 0.399 |

Table 2.2.: Typical concentration of most important inorganic constituents in sea water. The anionic species can form complexes with the actinides. Source [21].

A short overview of the physio-chemical behaviour of TRU and its dependence on the source is given in Ch. 2.6. For a more detailed discussion of the characteristics of TRU in ocean water, please refer to [20, 29, 31, 32].

2.3. Radiotoxicity

The radiotoxicity of incorporated TRU is considered as rather high, which is mainly due to the α -decay of most isotopes and the long retention times in the human body. Consequently, the long-lived isotopes $^{239,240}\text{Pu}$, ^{241}Am and ^{237}Np are of major concern for

2. Chemical and physical characteristics of the relevant transuranium elements

long-term effects, when incorporated via ingestion or especially inhalation. All elements mentioned are preferentially deposited in the liver and bones, even though they are present as Pu(+IV), Am(+III) and Np(+IV) in the human blood [33]. However, studies in mice and rats indicate a 2-3 times higher ability of ^{239}Pu to induce bone cancer than ^{241}Am , whereas ^{237}Np seems to be even a factor 3 more effective than ^{239}Pu , if normalized to the dose. This is probably caused by the different spatial and time distribution. Based on data obtained from mammalian studies, it was estimated that the average half-life for the residence time of Pu in the skeleton of man is around 100 years and in the liver around 40 years. This retention time can be probably also transferred to ^{241}Am [34]. If Pu is inhaled, e.g. as PuO_2 bearing aerosols, it is accumulated in the lymph nodes of the bronchial system and can lead to lymphopenia [35]. In general, it should be pointed out, that animal studies on carcinogenesis are performed with high doses of ^{239}Pu , that is several Gy [33]. In comparison, the mortality rate of workers involved in the research with Pu for the Manhattan Project who were exposed to an average effective dose of 1.25 Sv, has not been found to be elevated [36]. With a half-life of 432.2 a, ^{241}Am has the highest specific activity and thus has to be given special attention.

In addition to the radiotoxicity, it should be also considered, that the actinides belong to the group of heavy metals and thus also involve a high chemical toxicity. Due to the low specific activity of ^{237}Np , it has been reported that rats showed symptoms of chemical poisoning after ^{237}Np injection, before radiation induced effects have been observed [37].

2.4. Production of transuranium elements

The most important production paths of TRU in a nuclear reactor starting from uranium fuel is presented in Fig. 2.2. As ^{235}U used in a thermal reactor is enriched to only 3 %, the dominating reaction taking place is the n capture on ^{238}U which starts the major path for TRU built-up (bold arrows). As ^{239}U , with a half-life of only several minutes, is very short-lived (indicated by gray symbols), it rapidly decays to ^{239}Pu via the also short-lived ^{239}Np . Due to the long half-lives of the row of α decaying Pu isotopes, subsequent n-captures towards higher masses are possible. The β^- unstable nuclide ^{241}Pu represents an important branching point for the build-up of ^{241}Am , in particular after the chain reaction is stopped. The main TRU production path leads to ^{244}Am via the β^- decay of the short-lived ^{243}Pu . Successive n-capture on previously produced nuclides followed by β^- decay may built up even heavier elements, like curium, berkelium or even californium. Certainly, the yield of those heavier nuclides decreases, the larger the number of n-captures which are required. A second, minor production path is started by n-capture on ^{235}U if it does not induce fission but forms ^{236}U . Because of its long half-life of around 10^7 a

2.5. Anthropogenic sources of transuranium elements in the environment

with respect to α -decay, there is a large probability that another n is captured, so that the short-lived ^{237}U is formed which quickly decays towards ^{237}Np . A considerable part of ^{237}Np production via ^{237}U starts with a (n,2n) reaction on ^{238}U , which is especially important for nuclear devices, where there are high densities of fast neutrons. There are a lot more processes possible, which feed or re-feed into the described paths, as for example α -decay. However, because of the long half-lives its share in the general built-up is negligible if a usual fuel cycle length of around one year for FDNPP I [5] is considered.

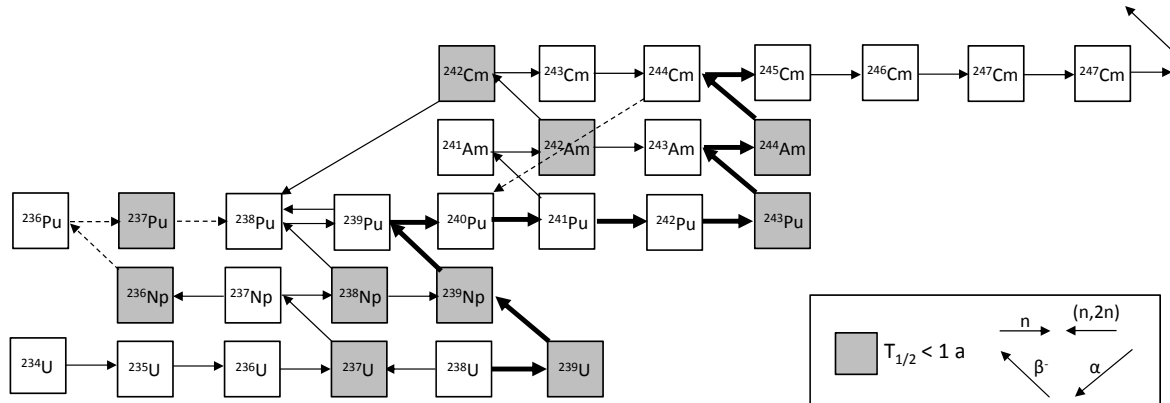


Figure 2.2.: Production paths of the transuranium elements, with bold arrows representing the major path in a thermal nuclear power plant. Dashed arrows represent built-up of low importance. Further explanations are given in the text.

The production of TRU in a nuclear device, like an atomic bomb, is somewhat different and also more complex because of the utilization of either highly enriched ($> 90\%$) ^{235}U or ^{239}Pu in fission weapons [38], or natural/depleted U ($\geq 99.3\%$ ^{238}U) as blankets in fusion (thermonuclear) weapons. Especially, in thermonuclear explosions, during a very short time period ($10^{-8}\text{ s} - 10^{-6}\text{ s}$), extremely high fluences of fast neutrons ($10^{23} - 10^{25}$ neutrons/cm 2) can produce very neutron rich nuclides, which then decay via β^- emission to more stable nuclides [29]. Consequently, the production paths and isotopic ratios depend on the yield and hence, the design of the specific device.

2.5. Anthropogenic sources of transuranium elements in the environment

Apart from the naturally occurring Pu and Np mentioned before, the concentrations in the environment today are clearly dominated by anthropogenic Pu and Np mainly released in nuclear weapon tests, nuclear accidents and by reprocessing plants. It is well known that large amounts of actinides have been emitted into the Atlantic Ocean by the reprocessing

2. Chemical and physical characteristics of the relevant transuranium elements

plants La Hague (France) and in particular Sellafield (UK). A maximum annual discharge of 55 TBq $^{239+240}\text{Pu}$ in 1974 by Sellafield has been reported [39], showing a large variation in $^{240}\text{Pu}/^{239}\text{Pu}$ ratios from 0.06 in the 1960's up to 0.25 in the 1980's and 90's [40]. The variation in isotopic ratios can be attributed to a general change in the operation mode of Sellafield. In the beginning, the main purpose was the production of weapon grade Pu, whereas nowadays Sellafield reprocesses spent nuclear fuel from nuclear power plants with a high burn-up of ^{239}Pu . If ^{239}Pu is produced for nuclear weapons, irradiation times have to be kept short to prevent build-up of ^{240}Pu , which has a high spontaneous fission rate and could lead to pre-initiation of the nuclear device. Consequently, the $^{240}\text{Pu}/^{239}\text{Pu}$ ratio of weapon grade Pu has to be below 0.07 [41]. In general, there is only little known about ^{237}Np discharges from reprocessing plants, but a total release of 6 – 8 TBq until 1989 was estimated from the detection of ^{237}Np in sediment cores [42]. Strong variations from 0.19 to 0.41 % in the activity ratio $^{237}\text{Np}/^{239+240}\text{Pu}$ were observed in sediments of the Irish Sea [1]. In Japan, the Tokai reprocessing plant, located south of Fukushima prefecture has been operated from 1977 - 2006, but no major release of $^{239+240}\text{Pu}$ was detected [43].

The most serious accident of a nuclear power plant, which caused a considerable contamination with TRU in Europe, was the Chernobyl accident in 1986. It was estimated, that in total 0.015 PBq ^{238}Pu , 0.013 PBq ^{239}Pu , 0.018 PBq ^{240}Pu and 2.6 PBq ^{241}Pu were released into the atmosphere [44]. From these data an isotopic ratio for $^{240}\text{Pu}/^{239}\text{Pu}$ of 0.37 and $^{241}\text{Pu}/^{239}\text{Pu}$ of 0.12 at the time of the accident can be derived. Information of the ^{237}Np emission is less abundant than for Pu, but an estimate that 3 – 6 % of the core inventory of refractory elements in general were released, is available. Using a ^{237}Np core inventory of Unit 4 of 0.26 PBq [45], an emission of around 0.01 TBq and an isotopic ratio $^{237}\text{Np}/^{239}\text{Pu}$ of 0.07 is obtained. Further information on additional accidental release of actinides into the environment can be found in [29, 40].

The largest contribution to the global inventory of actinides originates from the fallout of atmospheric nuclear weapon tests. From 1945 until 1980, in total 502 tests were conducted with the most active period between end of the 50's and beginning of the 60's. Until the Partial Test Ban Treaty in 1963, USA, USSR and UK were mainly responsible for the atmospheric nuclear explosions [46, 47]. A global inventory due to nuclear weapon fallout of 325 kCi (12 PBq) $^{239+240}\text{Pu}$ and a release of 1.5 t (39 TBq) ^{237}Np was estimated [48, 49]. Concerning nuclear fallout from weapon testing two different types have to be distinguished [50]:

- global fallout: produced by high yield (megaton TNT equivalent) detonations, generated by thermonuclear devices, which are able to push through the Tropopause and stabilize their fireball in the stratosphere. The residence time of the debris in the stratosphere is in the order of years, so that this type of fallout was transported

2.5. Anthropogenic sources of transuranium elements in the environment

over larger distance and was distributed almost all over the globe, but especially on the northern hemisphere.

- tropospheric or close-in fallout: produced also by low yield (kiloton TNT equivalent) detonations of fission devices which stabilize their fireball in the troposphere. The residence time of the debris in the troposphere is only several weeks, as weather phenomena occur in this layer of the atmosphere, so that the debris is precipitated with water droplets. Tropospheric fallout is restricted to the surroundings of the test site.

The average isotopic Pu ratios of global fallout on the northern hemisphere (71-30°N) were found to be $^{240}\text{Pu}/^{239}\text{Pu} = 0.180 \pm 0.014$ (2σ error) and $^{241}\text{Pu}/^{239}\text{Pu} = 0.00089 \pm 0.00013$ (decay corrected to Nov 2015, 2σ error) [51]. Whereas the USSR mainly conducted their atmospheric tests at high altitudes and hence, contributed significantly to global fallout, the tests of the USA at the Pacific Proving Grounds (PPG, Marshall Islands) happened near the surface, so that a considerable part of the debris was injected into the troposphere [2]. Therefore, the Pacific Proving Grounds are a major source for close-in fallout, which accounts for almost 60% of the Pu inventory of the North Pacific Ocean [52]. Close-in fallout shows elevated Pu ratios of $^{240}\text{Pu}/^{239}\text{Pu} = 0.24 - 0.34$ [2] and $^{241}\text{Pu}/^{239}\text{Pu} = 0.0017 - 0.0024$ [53, 4] (decay corrected to 11/2015), with only little information on the atomic $^{241}\text{Pu}/^{239}\text{Pu}$ ratio available. The average $^{237}\text{Np}/^{239}\text{Pu}$ ratio on the northern hemisphere was determined to 0.48 ± 0.07 (2σ error) [51]. Apart from a detected $^{237}\text{Np}/^{239}\text{Pu}$ ratio of 0.42 ± 0.04 in fallout from the Castle-Bravo test (15 megaton) [54], no information on the average $^{237}\text{Np}/^{239}\text{Pu}$ ratio due to close-in fallout was found. However, it was argued that ^{237}Np ratios are much more device dependent than Pu ratios which can lead to larger variation of detected ratios in environmental samples [51].

| | $^{240}\text{Pu}/^{239}\text{Pu}$ | $^{241}\text{Pu}/^{239}\text{Pu}$ | $^{237}\text{Np}/^{239}\text{Pu}$ |
|---|-----------------------------------|-----------------------------------|-----------------------------------|
| | | (decay corrected to Nov 15) | |
| Spent fuel reprocessing | 0.25 | - | - |
| Weapon grade plutonium | < 0.07 | - | - |
| Chernobyl accident | 0.37 | 0.05 | 0.07 |
| Global fallout (Northern Hemisphere) | 0.18 | 0.00089 | 0.48 |
| Tropospheric close-in fallout (PPG) | 0.24-0.34 | 0.0017-0.0024 | 0.42 |

Table 2.3.: Summary of isotopic ratios originating from different sources.

Tab.2.3 gives an overview over the known characteristic isotopic ratios from different

2. Chemical and physical characteristics of the relevant transuranium elements

sources. Especially the $^{240}\text{Pu}/^{239}\text{Pu}$ ratio can serve as a signature to determine the origin of a Pu contamination.

2.6. Concentrations and detection of Pu and Np in the Pacific Ocean

The two major sources for TRU in the Pacific Ocean before the Fukushima accident are global fallout and tropospheric close-in fallout from nuclear weapon tests. It has become evident, that the physio-chemical behaviour of Pu from global fallout is different from close-in fallout Pu in ocean water, which was explained by the type of particles Pu is attached to when it enters the water [2]. Global fallout particles are mainly composed of iron oxides which are sub- μm in size and which result from the vaporization followed by the condensation of nuclear weapon material. These particles have been found to dissolve in the ocean water rather quickly, i.e. in the order of several hours to days. By contrast, fallout from the PPG is based on calcium hydroxide from coral matrices which are vaporized during the blast of the surface-based tests. By the interaction with Mg in the sea water, a structure containing $\text{Mg}(\text{OH})_2$ which is insoluble in water, is formed. Consequently, the sedimentation rate for close-in fallout is supposed to be enhanced and close-in fallout is removed more quickly from the water column than global fallout. This picture was supported by the detection of increased $^{240}\text{Pu}/^{239}\text{Pu}$ ratios of up to 0.365 in deep water and ocean sediments [2]. Nevertheless, the detection of $^{240}\text{Pu}/^{239}\text{Pu}$ ratios up to 0.30 in sediments off the east coast of Japan and also in the South China Sea (summarized in [55]) proves that close-in fallout can be transported over considerable distances by ocean currents, in particular by the North Equatorial Current. During the transport, water masses showing a Pu signature from close-in fallout mix with water having a global fallout signature, so that in general with larger distances to the PPG, the $^{240}\text{Pu}/^{239}\text{Pu}$ ratio drops towards global fallout values.

Fig. 2.3 presents depth profiles of the Pu concentration detected in the North-West Pacific Ocean by different studies. The most characteristic feature of this profile, which has been reported several times before for different locations in the Pacific Ocean, is the subsurface maximum at around 500 m depth [52, 40]. It was suggested that the maximum is formed by the decomposition of sinking, Pu carrying, particles by biochemical processes [52, 31, 32]. Considering the year of the studies, it is evident that the maximum in the most recent results is much less pronounced and shifted to greater depth. Settling particles as explanation for the shift have been already excluded, whereas other possible explanations are still intensively debated [32]. Several involved processes were included in a 5-layer model by K. Hirose [56], which is able to reproduce vertical Pu profiles in the water

2.6. Concentrations and detection of Pu and Np in the Pacific Ocean

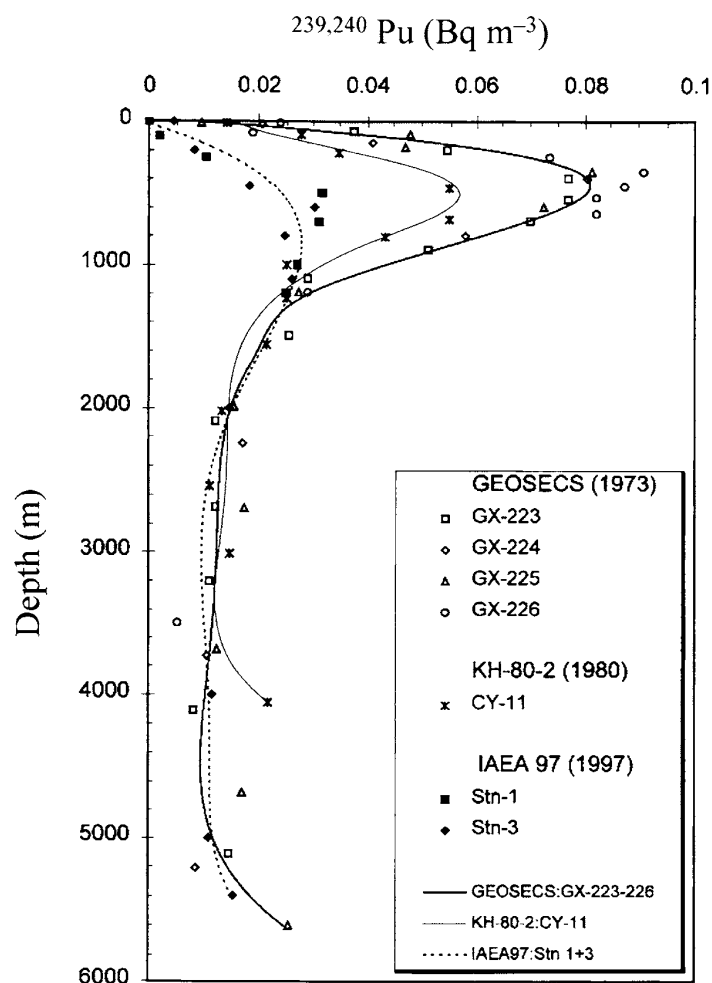


Figure 2.3.: Measured depth profiles of $^{239,240}\text{Pu}$ at GEOSECS (Geochemical Sections), Hakuho Maru and IAEA stations in the central NW Pacific Ocean. Taken from [29].

column. More soluble species like ^{137}Cs or ^{90}Sr also show a decrease in the subsurface maximum over the years so that it was attributed to the physical ocean circulation [32]. But the maximum of ^{137}Cs and ^{90}Sr is located closer to the surface and the center of the peak has not moved to greater depth or significantly broadened with time. Another typical feature of the Pu depth profile is the increase of concentration near the bottom. The most widely accepted explanation is the contribution of close-in fallout in these deep water layers [57]. To my present knowledge, there has been no comprehensive study on the behaviour of neptunium in the Pacific Ocean. Most of the limited knowledge about its transport in sea water was obtained from samples of Irish Sea water, where enhanced concentrations due to the reprocessing plant Sellafield have been found. Considering the behaviour of Pu, however, it can be expected that also the behaviour of Np depends on the physical and chemical form, how it enters the ocean which is different for the

2. Chemical and physical characteristics of the relevant transuranium elements

Pacific Ocean compared to the Irish Sea. Probably to a lesser extent than Pu, due to its enhanced mobility. It was estimated, that research on Np in sea water is lagging behind other actinides by 20-30 years [1].

As most actinides are α -emitters, α -spectrometry is the most frequently used detection method, because no expensive instrumentation is required and it is easily accessible. However, Fig. 2.3 demonstrates, that Pu concentration in the NW Pacific Ocean are below 30 mBq/m^3 and are further decreasing, which means that large sample volumes of around 200 L each have to be processed, to obtain an α source with reasonable counting statistics. This is even more problematic for ^{237}Np , because of its 100 times lower specific activity. Furthermore, sample preparation for α -spectrometry often is quite work-intensive, as many actinides emit α particles with a similar energy, so that the corresponding elements have to be chemically separated (compare Appendix C and Ch. 5.2.1). An individual detection of ^{239}Pu and ^{240}Pu is therefore not possible by means of α -spectrometry. In order to determine the $^{240}\text{Pu}/^{239}\text{Pu}$ ratio, mass spectrometric methods have to be applied. In particular ICP-MS (Inductively Coupled Plasma Mass Spectrometry) has recently become very popular for the routine analysis of actinides, as sample loading and operation is rather straightforward. Very low detection limits of 0.11 fg/mL ($10 \mu\text{Bq/m}^3$ in the initial water sample) ^{239}Pu [58] and 2.5 fg/mL [59] after chemical U separation, have been reported. A major drawback for ICP-MS in this project was its susceptibility to the salt content in the sample solution (see Ch. 5). In comparison, a detection limit of around $0.7 \mu\text{Bq/m}^3$ for ^{239}Pu and 0.1 nBq/m^3 for ^{237}Np in the initial sample was obtained by AMS in the present study. Due to its low availability, the advanced instrumentation and hence, its elevated costs, AMS cannot be applied for routine actinide studies. The detection of the almost pure β^- emitter ^{241}Pu is challenging for radiometric methods, as the emitted β^- -particles and γ -rays have rather low energies of 20 keV and 149 keV, respectively [19]. But the direct detection with mass spectrometry is also not possible due to the in-growth of its daughter nuclide ^{241}Am . Therefore, a chemical Am separation is required for mass spectrometric measurements (see Ch. 4.2). Alternatively, ^{241}Pu is detected indirectly via α -spectrometry of ^{241}Am or, at elevated concentrations, by liquid scintillation counting [60]. The detection of ^{237}Np by mass-spectrometric techniques, in general, is hampered by the lack of a suitable spike material, which is generally available. An additional method, applied for ^{237}Np detection of is NAA (Neutron Activation Analysis), which of course requires access to a neutron source, e.g. a reactor.

3. The Fukushima accident

On March 11, 2011 the Great East Japan Earthquake with a magnitude of 9.0 on the Richter scale occurred and led to the emergency shutdown (SCRAM: Safety Control Rod Activator Mechanism) of all operating reactors of the Fukushima Daiichi nuclear power plant (FDNPP). This means the control rods were fully inserted automatically into the reactor core to stop the chain reaction. However, the earthquake caused a tsunami which arrived at the FDNPP around 40 minutes later. With a maximum height of the waves of around 14 m, the water could easily overcome the 5.7 m high tsunami protection walls [61]. Consequently, most of the diesel generators were flooded, which were required as the site had been disconnected from power grid by the earthquake. This led to the complete loss of power in Unit 1-4 (Fukushima Daiichi I) while a shared use between Unit 5 and 6 (Fukushima Daiichi II) of the remaining functional diesel generator could be achieved. Without electricity, the cooling of the core, i.e. the removal of the decay heat, could not be maintained. Even though fresh and sea water was injected into the core of Unit 1-3 by water cannons later on, the water level had decreased such that the fuel elements were at least partially exposed to air. This has caused a (partial) melt-down of the reactor cores in Unit 1-3. Hydrogen explosions destroyed the reactor buildings of Unit 1, 3 and also 4 which was not in operation when the earthquake occurred. A large amount of radioactivity was released into the environment by this explosions mainly in the form of cesium (Cs) and iodine (I), since these chemical elements are volatile. In addition, a considerable amount of contaminated water was released into the ocean due to leakage from Unit 2 and 3 and because low-level radioactive water was intentionally discharged into the sea.

Similar to the Chernobyl accident, also the Fukushima accident was rated as a level 7 (major accident) event on the INES (International Nuclear and Radiological Event Scale) which is the highest level [62]. However, the total amount of radioactivity released into the environment during the Fukushima accident was estimated to be around a factor of 10 lower than in the case of the Chernobyl accident [63, 64, 5]. This chapter gives an overview over the sequence of events which might have led to the emission of TRU into the Pacific Ocean. A method to distinguish between a possible entry of FDNPP and nuclear weapon fallout in the Pacific Ocean, based on the isotopic Pu ratios of FDNPP at SCRAM, is

3. The Fukushima accident

presented. The following description of the site layout of FDNPP I and the course of events during the accident are mainly based on the reports by the IAEA [5, 65], TEPCO (The Tokyo Electric Power Company) [66], GRS (Gesellschaft für Reaktorsicherheit) [67], the Japanese Government [68], INPO (The Institute of Nuclear Power Operations) [61], the National Diet of Japan [69] and Hirose et al. [70].

3.1. The nuclear power plant Fukushima Daiichi I

The FDNPP is located on the east coast of Japan (37.422° N, 141.034° E) [71] in Fukushima prefecture (compare Fig. 4.2 in Ch. 4.1) and consisted of six reactor units as shown on the photography on Fig. 3.1. FDNPP has been operated by TEPCO since 1971. FDNPP II, consisting of Unit 5 and 6, where the reactor cores were shut down due to regular inspection, will not be considered further. The cooling of the spent fuel pools of both units could be ensured, because one out of three Diesel generators for Unit 6 was not flooded and hence, could provide emergency power to Unit 6 and later also to Unit 5. Therefore, it can be assumed that no considerable amounts of actinides were emitted from FDNPP II.



Figure 3.1.: Picture of the 6 units of FDNPP before the accident. The protection walls against tsunamis in front of the NPP are clearly visible. Taken from [65].

The most important technical specifications of FDNPP I (Unit 1-4) are given in the table presented in Fig. 3.2. All four reactors were Boiling Water Reactors (BWR) based on the BWR3 (Unit 1) or BWR4 (Unit 2-4) design by General Electric (GE) from the mid 60's [72]. Unit 1, which was the first one of the four units which was constructed on this site, contained a smaller reactor core, i.e. a smaller number of fuel elements and hence,

3.1. The nuclear power plant Fukushima Daiichi I

produced a smaller power output of 460 MW thermal compared to 784 MW thermal. Except for Unit 3, all reactors were using UO_2 enriched to around 2.2% in ^{235}U as fuel at the time when the accident occurred. The reactor core of Unit 3 was loaded with 32 fuel elements of MOX (Mixed Oxide Fuel) which is a mixture of uranium and plutonium oxide. Since this number of MOX fuel rods represents only a small fraction of the whole core with 548 fuel elements, the MOX has only a minor influence on the average isotopic composition of the core concerning plutonium (compare Ch. 3.4).

| | Unit 1 | Unit 2 | Unit 3 | Unit 4 |
|--------------------------------------|----------------------------------|----------------------------------|------------------------------------|----------------------------------|
| General | | | | |
| Company | GE | GE, Toshiba | Toshiba | Hitachi |
| Reactor type | BWR 3 | BWR 4 | BWR 4 | BWR 4 |
| Commercial operation | 1971 | 1974 | 1976 | 1978 |
| Electric/Thermal power output (MW) | 460 / 1380 | 784 / 2381 | 784/2381 | 784 / 2381 |
| Reactor core and fuel | | | | |
| Mass (tHM) | 68 | 94 | 94 | 94 |
| Number of fuel elements | 400 | 548 | 548 | 548 |
| Fuel | UO_2 | UO_2 | $\text{UO}_2 + 5.48\% \text{ MOX}$ | UO_2 |
| Enrichment primary core | 2,1 | 2,2 | 2,2 | 2,2 |
| Number of fuel rods per fuel element | 60 | 60 | 60 | 60 |
| Cladding material | Zircalloy-2 | Zircalloy-2 | Zircalloy-2 | Zircalloy-2 |
| Containment | | | | |
| Type | Mark I | Mark I | Mark I | Mark I |
| Control rods | | | | |
| Number of control rods | 97 | 137 | 137 | 137 |
| Material | $\text{B}_4\text{C} / \text{Hf}$ | $\text{B}_4\text{C} / \text{Hf}$ | $\text{B}_4\text{C} / \text{Hf}$ | $\text{B}_4\text{C} / \text{Hf}$ |

Figure 3.2.: Technical Data of Unit 1-4 of FDNPP during normal operation. Adapted from [73].

The BWR3 and BWR4 are equipped with a Mark I containment [72, 74], which comprises a bulb-shaped drywell and the torus-shaped wetwell and which is often referred to as primary containment vessel (PCV). The drywell surrounds the reactor pressure vessel (RPV) and the wetwell contains the suppression chamber which is directly connected to the drywell, so that in case of an overpressure steam from the RPV can be released into the suppression chamber. The suppression chamber serves as an additional heat sink and the steam condensates. The same holds, if there is a leakage from the RPV into the drywell in order to protect the containment from overpressure which might damage the containment. The containment is filled with nitrogen gas in order to prevent the explosive reaction of oxygen with hydrogen which can be built up in case of an accident (see Ch. 3.2). If the cladding of the fuel rods which is made out of Zircaloy is exposed to high

3. The Fukushima accident

temperatures, the following chemical reaction forming hydrogen takes place:



One of the characteristics of a BWR is that the steam produced in the reactor core is dried at the top of the RPV and directly guided onto the turbine. This means that also radioactive isotopes present in the coolant are transported to the turbine leading to a controlled area in the turbine building. As a consequence only two cooling loops are required (compare Fig. 3.3), with the second loop being supplied with seawater. Another typical feature of the BWR is that the spent fuel pool is located outside of the containment. For the FDNPP this means that the spent fuel pools were only covered by the roof of the reactor building made out of sheet metal panels. The turbine buildings are located on the sea side of the respective units and also host the generators and the diesel generators for the emergency power, the later ones being installed on the first basement. One exhaust chimney is shared between Unit 1 and 2, and Unit 3 and 4, respectively.

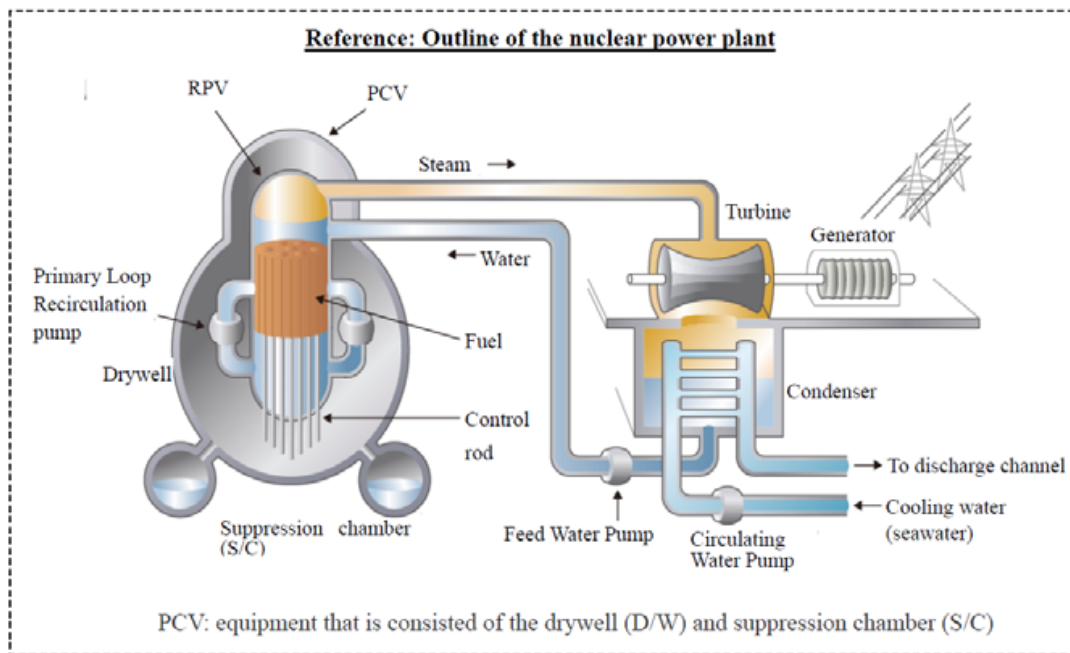


Figure 3.3.: Principle plant layout of FDNPP I. As usual for a Boiling Water Reactor, the steam produced in the reactor is directly guided onto the turbine which drives the generator. The steam then condensates in a heat exchanger (condenser) which uses sea water as heat sink in the secondary loop. The water in the primary loop is then pumped back into the reactor pressure vessel. The primary containment vessel encloses the reactor pressure vessel and the suppression chamber (S/C). Picture taken from [66].

Due to the slightly different reactor design of Unit 1 compared to Unit 2-4, also the decay

heat removal and emergency cooling systems are partly different. When the chain reaction is stopped, the reactor still produces around 1.6% of its initial power 1 h after shutdown because of the decay of the fission products. Therefore, the BWR 3 and the BWR 4 design have to be actively cooled to avoid core damage or even meltdown. For this purpose, the BWR 3 uses a so-called reactor shutdown cooling system (SHC) where the coolant from the RPV is guided to a heat exchanger. Here the heat is transferred to sea water and the cooled-down water from the primary loop is pumped back into the RPV. Furthermore, Unit 1 is equipped with an isolation condenser (IC), which is a passive system, guiding the steam from the RPV to a heat exchanger located above the RPV, where the steam condensates and then flows back into the RPV. As no pumps are required, DC battery power is sufficient just to open and close the respective valves. In Unit 2-4 the residual heat removal (RHR) system is installed to remove decay heat in normal operation mode by bypassing the turbine and guiding the steam directly to the condenser. In case of an accident coolant is taken from the suppression chamber, guided to a heat exchanger and then injected into the RPV. However, this can only be done at low pressures in the RPV, so that this mode of the RHR represents a part of the emergency low pressure coolant injection (LPCI) system. Furthermore, Unit 2-4 were equipped with a reactor core isolation system (RCIC) which removes water from the suppression chamber or the condensate storage tank and pumps it into the RPV to keep the water level constant. The electricity for the pumps is produced by turbines driven by the steam from the RPV. The exhaust from the turbine is guided back to the suppression chamber. Similar to the RCIC also the high pressure injection (HPCI) system which is part of the emergency core cooling system, is able to inject water into the RPV against the full pressure of the reactor core. The HPCI was installed in all units of FDNPP I and is based on the same working principle as the RCIC but provides higher flow rates of the coolant. Both systems only need DC battery power for the control of the valves. The second part of the emergency core coolant system is the core spray system (CS) with which also all units were equipped. Water from the suppression chamber is injected into the RPV above the core by electrical pumps which works only at low pressures inside the RPV. For a more detailed description of the respective core cooling system, refer to [66, 67, 72].

3.2. Chronology of the accident

The following report describes the events in Unit 1-4 after the earthquake, as it is understood at present time. It has to be noticed that there are still large uncertainties especially regarding the extent of core damage in Unit 1-3. This is because an inspection of the RPV and the reactor cores is still not possible (Feb. 2016) due to the high radiation levels inside the reactor building and the immense destruction of the reactor buildings caused by the

3. *The Fukushima accident*

hydrogen explosions. Therefore, present knowledge about the status of the reactor cores are based on model calculations. Those results vary depending on the assumptions made for the periods of time the reactor cores were not supplied with coolant which are not well known at any times.

Due to the earthquake on March 11th, 2011 at 2:46 pm, the FDNPP was disconnected from the external power grid and the reactors of Unit 1-3, which were in normal operation, were automatically shut down (SCRAM). AC power was provided by the emergency diesel generators which also started automatically. The subsequent chain of events in the different units are described separately in the following sections and is mainly based on the report by the IAEA [5] and GRS [67], as they are the most recent summarizing publications.

3.2.1. Unit 1

After the shutdown, the reactor was separated from the turbine to prevent the emission of steam from the containment. The IC started to remove the decay heat and hence, to reduce the increasing pressure in the RPV. When the regular pressure was reached, the IC was manually switched off. At the arrival of the tsunami around 40 min later, the diesel generator and also the batteries were flooded, so that no electricity was available. Consequently, monitoring of the whole unit, e.g. the water temperature or level in the reactor but also the status of the valves, was not possible. The IC could not be restarted, as the respective valves could not be opened, so that the reactor was left without any cooling system. Furthermore, the tsunami damaged the seawater pumps which means that the heat exchanger of the cooling systems lost the necessary heat sink.

As the pressure in the RPV rose, non-electrical valves were opened to release steam into the condensation chamber automatically which decreased the pressure in the RPV but increased the overall pressure in the containment. A first attempt to take the IC back into operation at 6.18 pm was thought to be successful when steam coming from the reactor building was observed. Since it was not clear, why the release of steam stopped shortly after, it was assumed that the IC was not working correctly. Because fracturing of the piping could occur, the IC was switched off manually again. Assuming that there was no cooling system active shortly before the tsunami arrived, TEPCO concluded that the water level dropped to the top edge of the fuel elements at 6 pm and first damage of the fuel happened at around 6:40 pm. It was already noticed at the day of the accident at 9:51 pm that the reactor core must have been already severely damaged when high radiation levels were measured on the first floor.

Shortly before midnight of March, 11th, the readout of the containment pressure could be

3.2. Chronology of the accident

restored. A pressure of 0.6 MPa compared to the design value of 0.528 MPa was measured. The pressure further increased to 0.84 MPa at 2:30 am of March 12th, so that preparations for the venting of the system were started. In the following, the pressure stabilized at a slightly lower pressure, which indicates a leakage from the containment. At 4:00 am the pressure inside the RPV was sufficiently low that freshwater could be injected by a mobile pump on a fire truck which has been connected to a fire protection water injection port at the turbine building. However, this cooling could not be sustained continuously and it is assumed that only 20-50% of the water arrived at the reactor core. A continuous freshwater supply using a fire truck pump was put into operation at 9:15 am.

From 9 am on, efforts to open the respective valves either manually or by a mobile pneumatic compressor in order to vent the PCV were made. At 2:30 pm a decrease of the pressure from 7.5 bar to 5.8 bar inside the containment was observed, so that it was assumed that venting had been successful. At 2:53 pm freshwater injection was stopped because the fire protection tanks almost had run empty. Consequently, measures to inject seawater were taken and a connection from a sea water pool at Unit 3 was quickly established. In the meanwhile, a mobile power supply was also successfully connected to Unit 1 and efforts were done to provide AC power via a low voltage grid. Both activities, i.e. the injection of seawater and the AC power supply, were interrupted by a hydrogen explosion on the service floor at 3:36 pm. This explosion led to the severe damage of the upper structure of the reactor building and the secondary containment. As a consequence, the dose rate at the boundary of the NPP increased to around 1 mSv/h and the site around Unit 1-4 was evacuated.

Because some of the infrastructure for the seawater injection just installed before the hydrogen explosion was also damaged by the ejected debris, the cooling by seawater through the core spray line could not be taken into operation before 07:04 pm the same day. In the time since freshwater injection was stopped, the core was without cooling. In the night of March, 14th, at 01:10 am seawater cooling was lost again, as the reservoir at Unit 3 was nearly depleted. It took until 08:00 pm till the seawater injection line, now directly from the Pacific Ocean, could be restored. Consequently, there was no cooling of the reactor core for more than 18 h.

On March, 25th, the injection of coolant was switched back to borated freshwater. Before, from March 19th to 23rd, Unit 1 had been successfully connected to the external power grid via temporary power cables, so that external power finally was available and the situation stabilized.

It can be assumed that the reactor core melted almost completely and also the RPV was partially destroyed when the hot melted fuel accumulated on the bottom of the RPV. Consequently, the core melt leaked through the RPV and was stopped by the bottom of

3. *The Fukushima accident*

the drywell. The melt penetrated around 65 cm into the wall of the drywell [75].

3.2.2. **Unit 2 and 3**

Due to the earthquake the reactor cores of Unit 2 and 3 were separated from the turbine by automatic closure of the valves in the primary steam pipe. The RCIC in both units was switched on manually in order to stabilize the water level in the RPV. With the arrival of the tsunami all DC power was lost from Unit 2 whereas in Unit 3 DC power was available for some time after the tsunami.

In Unit 2 the monitoring of the status of the system, i.e. the status of the valves and the water level in the core, was no longer possible. Also the RHR failed, so that the pressure in the RPV started to rise. Shortly before the complete blackout, the RCIC was started again. However, without DC power no control was possible and thus the status of the RCIC was uncertain. On the evening of March, 11th, a mobile generator was installed, so that the reactor water level indication was restored and it was found to be stable above the reactor core [61]. It was concluded that the RCIC was working since the tsunami had arrived, but could not be controlled. The next day the reactor building was damaged by the hydrogen explosion in Unit 1, creating an opening which probably prevented a hydrogen explosion in Unit 2 in the aftermath.

On March, 13th, as a precautionary measure, preparations were made to vent Unit 2. However, the containment pressure was too low to allow venting. Consequently, venting was not successful and no decrease of the pressure in the containment was observed. In the following, fire engines were connected to the fire protection lines of Unit 2 to inject seawater from the pool at Unit 3 in case the RCIC should fail. Due to the explosion in the upper part of Unit 3 on March 14th at 11:01 am, much of the infrastructure for the alternative seawater injection was destroyed by the ejected building debris. Furthermore, a major valve in the vent line of Unit 2 had closed, because the temporary power supply had been also affected by the explosion. At 12:00 pm the water level started to decrease and pressure in the RPV increased as the RCIC obviously had stopped working which means that the reactor core was left without any coolant injection.

At 02:43 pm the alternative water injection was restored but could not inject into the RPV as the pressure was above the pressure supplied by the fire engine pump. A depressurization of the RPV was not achieved before 07:03 pm after several unsuccessful attempts to open the required valves. At 07:20 pm, it was discovered that the fire engine pump which had been started already in the afternoon, had run out of fuel. Hence, it is uncertain how long and what amount of water the pump had injected into the RPV. After re-fueling of the engine, the sea water injection started at 07:54 pm. To present knowl-

3.2. Chronology of the accident

edge, at that time, the reactor core had not been supplied with water for 11 h and the fuel elements were exposed at around 6 pm leading to the damage of the fuel approximately one hour later. During the evening the RPV pressure started to increase again making it necessary to open more safety relief valves to release steam into the containment. But further attempts to vent the containment failed, so that the design value of the drywell was exceeded at 10:50 pm.

On March 15th, a sudden drop of the pressure in the suppression chamber which could not be explained and rising radiation levels on the site indicated the failure of the PCV. Furthermore, white smoke or steam coming from an upper floor of Unit 2 was observed.

In Unit 3, the monitoring of the water level in the RPV and also the control of the RCIC first was possible as DC power from batteries was partially available. The RCIC was adjusted to keep the water level constantly above the reactor core. In this way, heat was transferred from the RPV to the S/C leading to an overall increase of containment pressure. Even though the batteries were not yet empty, the RCIC stopped working at 11:36 am on March 12th and could not be restarted. Left without coolant injection, the water level in the RPV started to drop, so that the HPCI started automatically at 12:35 and stabilized the water level. As the steam turbine of the HPCI consumes steam from the RPV, consequently, also the pressure in the RPV decreased. During the night, the pressure dropped below the operational range of the HPCI causing concerns about the reliability and integrity of the HPCI. To present knowledge, the fuel elements were exposed to air at 02:30 am. The HPCI was switched off manually at 02:00 am when the inlet pressure decreased below the automatic shut-off pressure of the turbine but did not cause the HPCI to stop. An alternative water injection with a fire pump was not possible as the RPV pressure had already increased quickly after the HPCI was switched off. Several attempts to depressurize the RPV failed, so that a re-start of the HPCI and RCIC was tried, which was not achieved. Measures were taken to inject water via fire protection lines with fire engines and to vent the containment on the morning of March 13th. After several hours without cooling and heating up of the reactor core, depressurization of the RPV was finally successful and first fresh water, and after emptying the reservoir, sea water from the backwash pit was injected at 09:25 am. The venting of the containment which also had heated up considerably, was achieved at 09:20 am.

Similar to Unit 1, sea water injection was interrupted on March 14th when the pit was discovered to be almost empty at 01:10 am. A restart of the alternative coolant injection was possible two hours later. At 11:01 am a hydrogen explosion occurred, which almost completely destroyed the upper part of the reactor building above the service floor (see Fig. 3.4). Fire pumps and hoses were severely damaged and workers were injured by the explosion. Therefore, alternative sea water injection into Unit 3 could not be maintained.

3. The Fukushima accident

The sea water injection, now directly from the Pacific Ocean, was resumed 03:30 pm but was stopped again when the engine ran out of fuel at 07:20 pm and was restarted at 07:54 pm (compare Unit 1).



Figure 3.4.: Photograph of the four units of FDNPP I after the accident. Whereas the reactor building of Unit 3 and 4 and the upper part of Unit 1 were destroyed by hydrogen explosions, the reactor building of Unit 2 looks intact, apart from the opening of the so-called blowout-panel. [69].

On March 20th, Unit 2, and on March 22th Unit 3 also, were successfully connected to the external grid and off-site power was restored. The alternative water injection in both units was switched from seawater to borated fresh water around March 25th and the fire pump was replaced by a motor driven pump.

3.2.3. Unit 4

Unit 4 was undergoing regular inspection since Nov, 2010, so that all fuel elements had been removed from the reactor and had been stored in the spent fuel pool. At the time of the earthquake the spent fuel pool was isolated from the reactor by a closed gate and the temperature of the coolant was around 27°C [61]. Due to the tsunami, also Unit 4 lost all AC power from the emergency diesel generator and also the batteries were destroyed, so that also DC power was not available. However, due to the low power output of the stored fuel elements, attention did not focus on Unit 4 before March 15th, at 6:14 am, when a hydrogen explosion occurred which completely destroyed the upper part of the reactor building. Still, the origin of the hydrogen is not fully clarified, but the most widely accepted theory is that hydrogen from the venting of Unit 3 had accumulated in the piping going to the exhaust chimney which is also connected to Unit 4. Because of the

blackout, the valves of the exhaust air system in Unit 4 had been opened, which explains how the hydrogen from Unit 3 might have arrived at Unit 4 causing the explosion there. It was determined in the aftermath of the accident, that the fuel elements had not been significantly damaged, which means the water level had not dropped below the top of the fuel. Consequently, it is rather improbable that hydrogen was produced in the spent fuel pool of Unit 4. But at the time of the accident, the hydrogen explosion led to concerns that the fuel might have been exposed. Therefore, different measures to increase the water level were initiated, e.g. spraying (sea-)water by water cannons or helicopters into the pool. As most of the water missed the spent fuel pool, water was injected by a concrete pump vehicle from March, 22nd, on. In June, an alternative water supply using a mobile pump could be realized and the situation was stabilized.

3.3. Radiological consequences

During the FDNPP accident a large amount of radioactivity was released into the environment. It was estimated, that in total (100 – 500) PBq of ^{131}I [5, 66, 68, 76], (6 – 40) PBq of ^{137}Cs [5, 66, 68, 76, 77], around 10 PBq of ^{134}Cs [66, 76] and (500 – 15, 000) PBq [5, 66, 77] of noble gases, especially ^{133}Xe , were emitted into the atmosphere. Cs, I and the noble gases dominate the contamination of the environment, as these elements are highly volatile and can easily leak from the damaged RPV and containment or were released during venting. This is a major difference to the Chernobyl accident, where also considerable amounts of less volatile nuclides, such as ^{90}Sr or actinides were emitted to the atmosphere, as a part of the reactor core was ejected during the accident. However, the radioactive release in case of the Fukushima accident led to local hot-spots with more than 150 mSv/year dose rate (compare Fig. 3.5). As a consequence, people living within a 20 km zone around the NPP site were evacuated on March 12th. Winds blowing from south-east on March 15th and 16th caused a corridor north-west of the NPP with high radiation levels, which is evident in Fig. 3.5, so that the evacuation zone had to be extended in April 2011, including also Iitate Village. Due to the short half-lives of ^{131}I ($T_{1/2} = 8.02\text{ d}$) and ^{133}Xe ($T_{1/2} = 5.25\text{ d}$) [19] those two isotopes quickly decayed, so that the dose to the population was dominated by ^{137}Cs ($T_{1/2} = 30.17\text{ a}$) after 2011.

Dose assessment studies of UNSCEAR [78] and WHO [62], come to the conclusion that the effective dose received by an adult during the first year after the accident in a non-evacuated area of Fukushima prefecture is below 10 mSv/a. That is lower than the reference level for planned residual dose in emergency exposure situations recommended by the ICRP (International Commission on Radiological Protection) which is between (20 – 100) mSv per year. The detection of Pu in soil and litter samples attributed to

3. The Fukushima accident

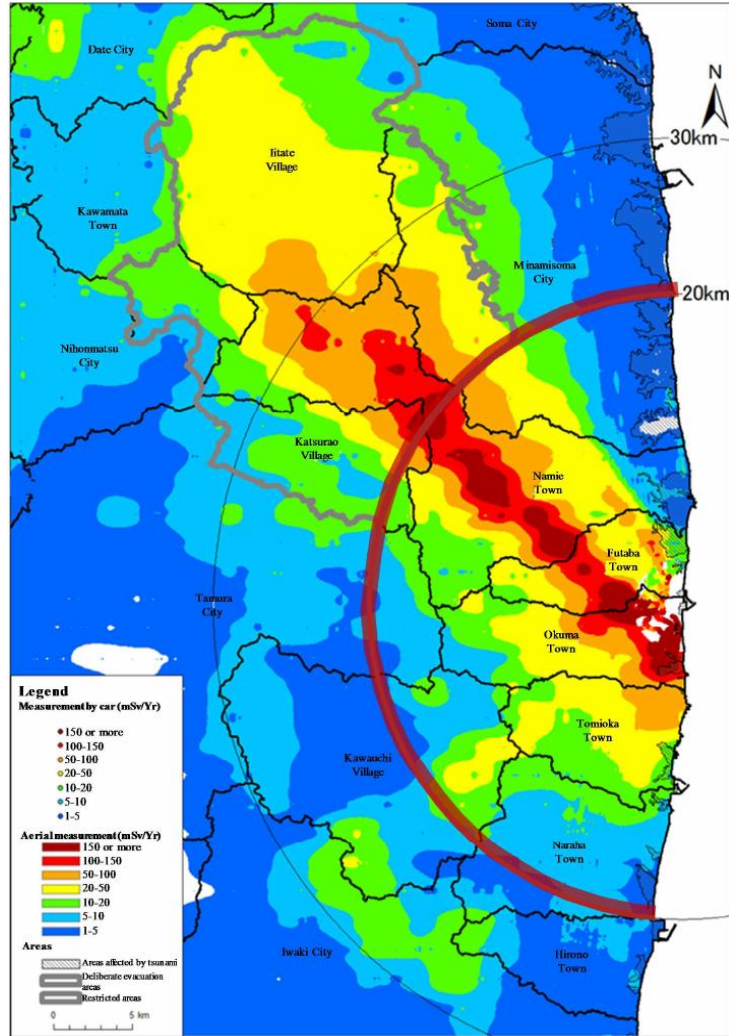


Figure 3.5.: Map of measured aerial dose rates, which clearly indicates a highly contaminated corridor to the northwest (NW) of the FDNPP (November 2011). This led to the extension of the 20 km evacuation zone (red circle) to the districts in the NW, the so-called Deliberate Evacuation Area. Taken from [76].

the FDNPP (see Ch. 3.5) by Zheng et al. [3] of maximum 1.400 mBq/g $^{239+240}\text{Pu}$ and 34.8 mBq/g ^{241}Pu demonstrate that the amount of Pu ejected into the atmosphere is not of radiological concern for the population. Considering the progress of the accident with the melted fuel staying inside of the containment, it was expected from model calculations that little volatile elements like Sr or the actinides are hardly released into the air [79, 80]. These theoretical predictions match the measured concentrations in environmental samples very well. It was estimated that around $(0.002 \pm 0.003)\%$ of the total Pu core inventory of Unit 1 and Unit 3 were released into the environment by venting [79]. This corresponds to an activity of $10^9 - 10^{10} \text{ Bq}$ $^{239+240}\text{Pu}$ and $10^{11} - 10^{12} \text{ Bq}$ ^{241}Pu , depending on the model used for the calculation (compare Ch. 3.5 and [4]).

Even though PuO_2 and NpO_2 are hardly soluble and therefore preferentially stay in the fuel matrix, there is the possibility that during the specific conditions of the meltdown, a small fraction were leached from the melt by the coolant or escaped from the fuel as bound to particles. To estimate, which amounts of contaminated effluents in general were released into the ocean during the accident, the so-called source term, i.e. the type and amount of radioactivity emitted into the Pacific Ocean, is discussed in more detail in the following. However, this does not imply that a possible emission of Pu or Np shows the same distribution in the ocean as the radioactive contamination, which is mainly due to ^{137}Cs .

Emission to the Pacific Ocean

In general, two main source terms for the release to the Pacific Ocean can be distinguished: first wet and dry deposition on the surface of the ocean from the atmosphere and secondly, the direct discharge of contaminated liquids into the ocean. In the first days of the accident until March 15th, wind was blowing from western directions transporting the radioactive plume to the ocean. The estimates for the indirect deposition from the atmosphere show large variability as no direct measurements of the dose rate above the ocean surface were performed in March when the major releases occurred [78, 5]. For this reason, the amount of ^{137}Cs , for example, deposited on the ocean surface, ranges from 0.18 to 10 PBq ([5] and references therein). In accordance with the findings by Zheng et al. [3] concerning the atmospheric release of Pu, also the concentration of Pu related to the accident found in aerosol samples at a distance of 120 km from the NPP is negligible [14]. Consequently, the indirect deposition on the ocean surface only plays a minor role for the entry of actinides into the Pacific Ocean.

Direct release of contaminated effluents happened at several occasions. For example, highly contaminated water with a dose rate of more than 1000 mSv/h was found in the turbine building of Unit 2, accumulated in a trench for electric cables on April 2nd. From this trench, the contaminated water leaked into the Pacific Ocean through a 20 cm crack on the surface [68]. Because of the high concentrations of $^{134+137}\text{Cs} = 1.8 \cdot 10^9 \text{ Bq/kg}$ and $^{131}\text{I} = 5.2 \cdot 10^9 \text{ Bq/kg}$ it was concluded that the water had originated from inside the PCV [5]. On April 6th, the outflow of water from the cable trench was stopped by pouring concrete and macromolecule polymers [66]. It was estimated that in total 520 m³ water with a total activity of 4.7 PBq was released into the Pacific Ocean between April 1st and 6th [66, 68].

As there were concerns that further leakage of highly contaminated water from the turbine building of Unit 2 might occur, it was decided to discharge approximately 10,400 tons of low activity water from the Radioactive Waste Treatment Facilities in order to increase

3. The Fukushima accident

storage capacities for the water from Unit 2. The discharge of $1.5 \cdot 10^{11}$ Bq into the ocean happened between April 4th to 10th [68]. Furthermore, on May 11th, it was found that contaminated water from the turbine building of Unit 3 had flown out into the ocean. In total 250 m^3 water corresponding to a total activity of Cs and I of $2 \cdot 10^{13}$ Bq [66] had been released.

It should be mentioned that also in the following years after 2011, radioactive effluents leaked into the Pacific Ocean as for example from storage tanks in April 2013 [67]. However, the major entry of radionuclides into the ocean happened shortly after the accident in 2011 and the activity in the sea water is decreasing since then. This is demonstrated by Fig. 3.6, which shows the results from monitoring the specific activity inside the port of FDNPP at a exemplary measurement point at the intake of Unit 3 from May 2011 to July 2013. Starting from an extremely high concentration of around 1 GBq/L, the specific activity quickly drops below the density limits specified by reactor regulation at the beginning of 2012. The activity concentration of ^{131}I decreases much faster because of its short half-life of only 8.02 d [19]. The decrease in the concentration of ^{134}Cs and ^{137}Cs apart from some temporary increases is mainly due to the dilution with the water masses, especially by the mixing of the Kuroshio and Oyashio Current [81]. It was shown in ocean model calculations and measurements, that the Cs contamination was transported eastwards [82, 83] and arrived at the Canadian coast in 2013, with a maximum concentration detected of 2 Bq/m^3 in 2014 [84].

Apart from the highly volatile elements I and Cs, in seawater also radiostrontium (^{89}Sr , $T_{1/2} = 50.5 \text{ d}$ and ^{90}Sr , $T_{1/2} = 28.64 \text{ a}$) has been found in surface waters offshore the FDNPP. The results of these measurements have been summarized and analyzed by Povinec et al. [86]. Even though the concentrations are not of radiological concern ($10 \text{ Bq/m}^3 - 9 \text{ kBq/m}^3$ of ^{90}Sr at a distance of 15 km from the coast), it was estimated by Povinec et al. that the total amount of 1 PBq ^{90}Sr was directly released to the ocean. The isotopic ratio $^{90}\text{Sr}/^{137}\text{Cs}$ of around 0.1 in seawater is rather high compared to the corresponding ratios of 0.1 – 0.0001 which were found in soil samples from atmospheric deposit [80]. This indicates that the direct release of low-volatile elements as Sr to the seawater is of greater significance than by atmospheric deposition in case of the FDNPP accident, which could be also the case for Pu and Np. However, so far, the concentrations of Pu found in seawater were consistent with those detected before the Fukushima accident [87, 58] (for more detailed information, see Ch. 3.5).

There are several different estimates on the source term already published, with some of them being summarized in Tab. 3.1 in order to demonstrate the order of magnitude and variation between the different studies.

3.4. Inventory of FDNPP I at the moment of SCRAM

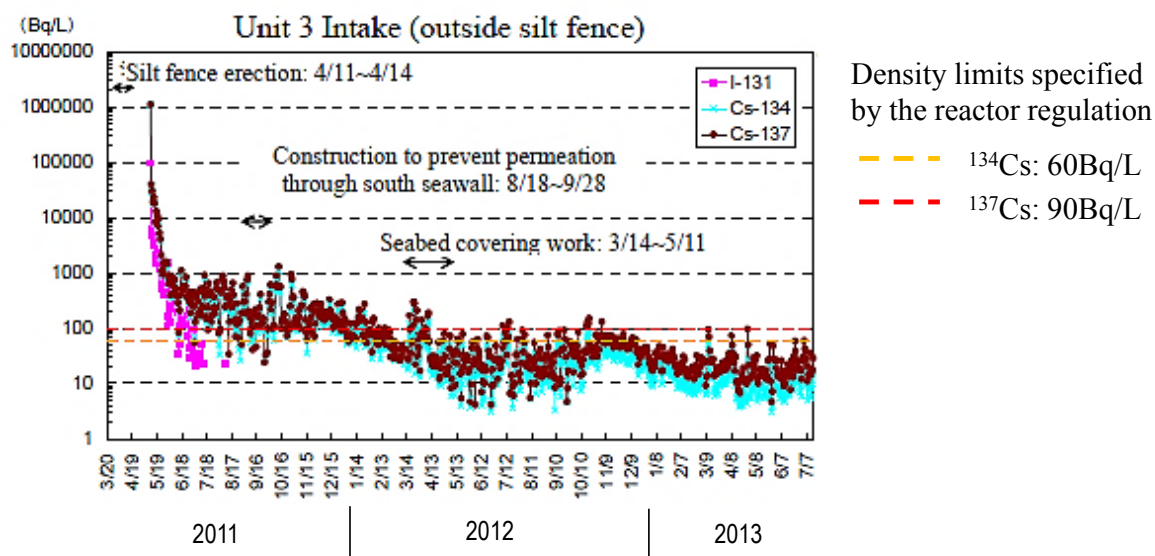


Figure 3.6.: Detected concentrations of ^{131}I (pink), ^{134}Cs (cyan) and ^{137}Cs (dark red) close to the intake of Unit 3 in the time between March 2011 and July 2013. From a initially very high specific activity of 1 GBq/L, the concentration quickly decreases in the first three months. The curve of ^{131}I ends in August 2011, as the activity has dropped below the detection limit. Modified from [85].

3.4. Inventory of FDNPP I at the moment of SCRAM

In order to distinguish a possible entry of actinides into the Pacific Ocean due to the FDNPP accident from other sources (compare Ch. 2.5), the characteristics of the reactor cores with respect to the actinides have to be well-known. This means the inventory and composition of the fuel at the moment of the accident. In the following, all results on the reactor inventory refer to the moment of emergency shut-down, when the chain reaction was stopped. Consequently, neutrons for the build-up of actinides starting from ^{238}U and ^{235}U were no longer available. After the SCRAM, the dominating process is the radioactive decay of the fission and activation products. The decay of the short-lived nuclides like ^{241}Pu and thus the built-up of its daughter nuclide ^{241}Am , has to be considered when comparing measurement results with the theoretical calculations presented in this chapter. For an overview over the most important actinide nuclides, which were built up during operation of the reactor and possible decay channels after shutdown, the corresponding section of the chart of nuclides is shown in Fig. 3.7.

The most widespread method to calculate the composition of nuclear fuel is the application of the ORIGEN code, which was developed in the early 70s' at Oak Ridge National Laboratory [93]. Since then, different revised versions of the program (e.g. ORIGEN2 [94],

3. The Fukushima accident

| Reference | Direct release | | Atmospheric deposition | |
|-----------------------------------|--|--|------------------------|-------------------------|
| | ^{131}I [PBq] | Cs [PBq] | ^{131}I [PBq] | Cs [PBq] |
| TEPCO (2012) [66] | 2.81 (Apr.-May) | 1.9 (Apr.-May) | - | - |
| Bailly du Bois et al. (2012) [88] | - | 12 - 41 ^{137}Cs (Mar-Jul) | - | 0.076 (80 km radius) |
| Buesseler et al. (2011) [89] | 2 ^{137}Cs in area of 150.000 km ² (March-June) | | | |
| Honda et al. (2012) | | | 0.18 ^{137}Cs | |
| Kobayashi et al. (2013) [90] | 11 (March 26 - June 30) | 3.5 ^{137}Cs | 99 | 7.6 ^{137}Cs |
| Kawamura et al. (2011) [91] | 57 | 5 ^{137}Cs (March 12th - April 30th) | 67 | 6 |

Table 3.1.: Comparison of the results for the source term of the radioactive contamination of the Pacific Ocean due to the FDNPP accident obtained by different studies.

ORIGEN-ARP [95]) have become available in order to improve the predictions for nuclide inventories and to increase the speed of the calculations. Basically, reactor codes solve coupled, linear differential equations of the simple form

$$\frac{dX_i}{dt} = \text{Production rate} - \text{Removal rate} \quad (3.2)$$

with X_i being the atomic density of nuclide i . If considered in more detail, however, there are many different production and removal channels in the fuel matrix which were discussed for the relevant actinides in Ch. 2.4. Especially when the fuel element was already irradiated for some time in the reactor, there is a large number of parameters which have to be taken into account. For example, the time evolution of the concentration of a nuclide crucially depends on the position and energy dependent neutron flux. However, the neutron flux itself is affected by the fuel composition at that time, so that the concentration of a certain nuclide strongly depends on the irradiation history and thus, the burn-up of the fuel elements. In order to keep the burn-up homogeneous in the core, only a certain number of fuel elements is replaced by fresh fuel during a refueling cycle. Furthermore, the fuel geometry, the moderator density and the void coefficient (in case of a BWR) [96], among others, play an important role.

Detailed information on the refueling cycles and power, i.e. irradiation history of the reactor cores of FDNPP I had not been available to the public before 2012 [97]. Therefore, early studies on the core inventories had to make assumptions on some of these parameters, which lead to some variations in the results even though the same reactor code was used.

3.4. Inventory of FDNPP I at the moment of SCRAM

| | | | | | | | |
|--|---|--|---|--|---|---|--|
| Am 237 73.6 m sf ε γ 280, 438, 474 909..., g α 6.042... | Am 238 98 m sf ε γ 963, 919, 561 605..., g α 5.94 | Am 239 11.9 h sf ε γ 278, 228..., e ⁻ g α 5.774, 5734... | Am 240 50.8 h sf ε γ 988, 889... e ⁻ α 5.378... α→g | Am 241 432.6 a sf α 5.486, 5.443... γ 60, 26..., e ⁻ , g σ 60 + 640 σ 3.15 | Am 242 141 a 16.02 h sf IT (49), e ⁻ α 5.206... γ (42...), e ⁻ g σ 1700 σ 380 σ 5900 σ 2100 | Am 243 7364 a sf α 5.275, 5.233... γ 75, 44..., e ⁻ σ 75 + 5 σ 0.079 | Am 244 26 m 10.1 h sf ε β ⁻ 0.4 γ 744, 898 154... e ⁻ , g σ 1600 σ 2200 |
| Pu 236 2.858 a sf α 5.768, 5.721... γ (48, 109...), e ⁻ sf Mg28 σ 160 | Pu 237 45.2 d sf α 5.334... γ 60..., e ⁻ σ 2300 | Pu 238 87.7 a sf α 5.499, 5.456... γ (43, 100...), e ⁻ sf Si, Mg σ 510, σ 17 | Pu 239 24110 a sf α 5.157, 5.144... γ (13, 52...), e ⁻ m, sf σ 270, σ 752 | Pu 240 6561 a sf α 5.168, 5.124... γ (45...), e ⁻ , g sf σ 290, σ 0.059 | Pu 241 14.325 a sf β ⁻ 0.02, g α 4.896... γ (149...), e ⁻ σ 370, σ 1010 | Pu 242 3.750·10 ⁵ a sf α 4.901, 4.856... γ (45...), e ⁻ , g sf σ 18, σ < 0.2 | Pu 243 4.956 h sf β ⁻ 0.6... γ 84... g σ < 100 σ 200 |
| Np 235 396.1 d ε, g α 5.025, 5.008... γ (26, 84...), e ⁻ σ 160 + ? | Np 236 22.5 h 1.54·10 ⁵ a ε, β ⁻ 0.5... γ (642...), e ⁻ σ 2700 | Np 237 2.144·10 ⁶ a sf α 4.790, 4.774... γ 29, 87..., e ⁻ σ 170, σ 0.020 | Np 238 2.117 d β ⁻ 1.2..., γ 984 1029, 1026, 924..., e ⁻ , g σ 2600 | Np 239 2.356 d β ⁻ 0.4, 0.7... γ 106, 278 228..., e ⁻ , g σ 32 + 19, σ 1 | Np 240 7.22 m 61.9 m β ⁻ 2.2... γ 555 597..., e ⁻ IT σ 566, 974 601, 448... g | Np 241 13.9 m β ⁻ 1.3... γ 175, (133...) g | Np 242 2.2 m 5.5 m β ⁻ 2.7... γ 736, 780 1473... 159... g |
| U 234 0.0054 a 2.455·10 ⁹ a α 4.775, 4.722... γ (53, 121...), e ⁻ sf, Mg28, Ne24, Ne26 α 96, σ 0.07 | U 235 0.7204 a 26 m 7.038·10 ⁸ a α 4.395, 4.364... IT γ 186, 144... (0.08) sf, Ne, Mg e ⁻ , σ 95, σ 586 | U 236 120 ns 2.342·10 ⁷ a α 4.494 4.445... 1783... γ (49 113...) γ 642... e ⁻ , sf, Mg30 α 5.1 | U 237 6.75 d β ⁻ 0.2... γ 60, 208..., e ⁻ σ ~100 σ < 0.35 | U 238 99.2742 a 280 ns IT 2513... γ 1879... sf, β ⁻ , σ 2.7 σ 3E-6 | U 239 23.45 m β ⁻ 1.2, 1.3... γ 75, 44..., e ⁻ σ 22, σ 15 | U 240 14.1 h β ⁻ 0.4... γ 44, (190...) e ⁻ m | |
| Pa 233 27.0 d β ⁻ 0.3, 0.6... γ 312, 300, 341... e ⁻ σ 20 + 19 σ < 0.1 | Pa 234 1.159 m 6.70 h β ⁻ 2.3... γ (1001...) 767... IT (74...), e ⁻ σ < 500 | Pa 235 24.4 m β ⁻ 1.4... γ (128 - 659) m | Pa 236 9.1 m β ⁻ 2.0, 3.1... γ 642, 687 1763..., g βsf? | Pa 237 8.7 m β ⁻ 1.4, 2.3... γ 854, 865, 529 541... | Pa 238 2.3 m β ⁻ 1.7, 2.9... γ 1015, 635 448, 680... g | Pa 239 1.8 h β ⁻ γ 522, 562, 638 681 | |

Figure 3.7.: Section of the chart of nuclides showing the actinide region with the most relevant nuclides for a thermal nuclear power plant. Image produced with Nucleonica [92].

For example, Kirchner et al. used the activity ratios of a number of radionuclides detected in air samples from Europe which had been attributed to the accident in order to estimate a mean burn-up of Unit 1-3 of 26.7 GWd/t (Gigawatt days per ton of fuel) [98]. Still, there is no information on the composition of the MOX fuel published which was confirmed by TEPCO [5]. However, with 5.48 % of the fuel elements of Unit 3, the MOX fraction is very small, so that it can be either neglected or the composition of spent fuel can be used as an approximation [99]. A detailed summary of the core parameters of the FDNPP required for the inventory calculations and on the assumptions made in different studies can be found in [5].

Tab. 3.2 gives the results of different studies on the average inventory of the relevant nuclides $^{239-241}\text{Pu}$, ^{237}Np and ^{241}Am in addition to the corresponding isotopic atom ratios. In order to make the results from the different studies comparable, the nuclide inventories were normalized to 1 tHM (ton Heavy Metal) where an initial mass of 69 tHM for Unit 1 and 94 tHM for Unit 2 and 3 [99], respectively, was used. The composition of the spent fuel pools were not considered in this table, as there is no indication up to now, that there was a direct release of radioactive effluents into the ocean from there. Consequently, an emission of actinides from the spent fuel pools is also not expected. In general, the different results for the inventories for one nuclide agree within 10 % to 30 % and thus show the reliability of those reactor core calculations. The results can also be reproduced when starting

3. The Fukushima accident

| | JAEA | Schwantes et al. | Kirchner et al. | Hannstein (GRS) |
|--------------------------------------|-----------------------|-------------------------|------------------------|------------------------|
| | [97] | [79] | [98] | [101] |
| | Unit (1-3) | Unit (1+3) | Unit (1-3) | Unit (2) |
| Code | ORIGEN2 | ORIGEN-ARP | ORIGEN-ARP | Serpent 2.1.21 |
| Nuclide | | | | |
| ²³⁹ Pu | 1.02·10 ¹³ | 8.93·10 ¹² | 9.7·10 ¹² | 9.39·10 ¹² |
| ²⁴⁰ Pu | 1.28·10 ¹³ | 1.46·10 ¹³ | 1.4·10 ¹³ | 1.10·10 ¹³ |
| ²⁴¹ Pu | 3.17·10 ¹⁵ | 2.91·10 ¹⁵ | 2.8·10 ¹⁵ | 3.00·10 ¹⁵ |
| ²³⁷ Np | 7.09·10 ⁰⁹ | N.D. | N.D. | 6.65·10 ⁰⁹ |
| ²⁴¹ Am | 6.05·10 ¹² | 3.59·10 ¹² | 3.6·10 ¹² | 4.63·10 ¹² |
| Atomic ratio | | | | |
| ²⁴⁰ Pu/ ²³⁹ Pu | 0.34 | 0.44 | 0.39 | 0.32 |
| ²⁴¹ Pu/ ²³⁹ Pu | 0.18 | 0.19 | 0.17 | 0.19 |
| ²³⁷ Np/ ²³⁹ Pu | 0.06 | - | - | 0.06 |
| ²⁴¹ Pu/ ²⁴¹ Am | 17 | 27 | 26 | 22 |

Table 3.2.: Results for average inventory of FDNPP I in Bq/tHM and the corresponding atomic ratios calculated in different analyses.

from the core parameters of Unit 2 and using a different code than ORIGEN, such as Serpent [100, 101]. In general, the isotopic ratios for Pu, ²⁴⁰Pu/²³⁹Pu and ²⁴¹Pu/²³⁹Pu, of the FDNPP are significantly higher than for the most prominent source of contamination in the environment, the nuclear bomb fallout. Thus, the isotopic ratios of Pu can be used as fingerprint to identify Pu emitted into the ocean by the accident, which will be discussed in more detail in the next section. At SCRAM the number of ²⁴¹Pu atoms is more than one order of magnitude higher than its isobar ²⁴¹Am. 5 a after the accident, the isotopic ratio ²⁴¹Pu/²⁴¹Am has already decreased by a factor of around 4.4. Data for the ²³⁷Np inventory are hardly available as it is not of immediate radiological concern because of its long half-life ($T_{1/2} = 2.144 \cdot 10^6$ a). Consequently, the isotopic ratio ²³⁷Np/²³⁹Pu of 0.06 obtained by Nishihara et al. [97] and confirmed by V. Hannstein [101] is subject to increased uncertainties. However, compared to the ²³⁷Np/²³⁹Pu ratio of 0.45 attributed to global fallout [49], the characteristic ratio of the FDNPP is a factor 7.5 lower.

3.5. Identification of a possible entry of actinides into the Pacific Ocean

From the theoretical predictions discussed in the previous section, Pu which entered the environment by the FDNPP accident should show increased $^{240}\text{Pu}/^{239}\text{Pu}$ and $^{241}\text{Pu}/^{239}\text{Pu}$ ratios compared to the fallout from nuclear weapon testing. These predictions were supported by the findings of Zheng et al. [3], who reported on increased $^{240}\text{Pu}/^{239}\text{Pu}$ and $^{241}\text{Pu}/^{239}\text{Pu}$ ratios in soil and litter samples at a maximum distance of 32 km from the FDNPP. The results of these measurements are plotted in Fig. 3.8 along with the respective ratios of global and atmospheric fallout in Japan and also for the fallout from the Chernobyl accident. The detected ratios of 0.303–0.330 for $^{240}\text{Pu}/^{239}\text{Pu}$ and 0.103–0.135 for $^{241}\text{Pu}/^{239}\text{Pu}$ were in good agreement with the theoretical predictions from the reactor core calculations (compare Ch. 3.4), they were attributed to the FDNPP accident. The specific $^{239+240}\text{Pu}$ activity, i.e. the $^{239+240}\text{Pu}$ concentration, in those samples with increased isotopic ratios, however, was comparable to other soil samples with global fallout signature. This already demonstrates, that a simple comparison of Pu concentrations before and after the accident is not sufficient to answer the question concerning a possible release into the environment in general, but especially into the ocean. It can be expected that due to the low solubility of PuO_2 , only small amounts of Pu were transferred from the fuel to the coolant, which was then diluted in a large volume of sea water. An estimation of the increase in the overall concentrations in the Pacific Ocean is not possible, as the transfer rate of Pu to the coolant, especially under the extreme conditions of a core meltdown, is hardly known. However, it can be assumed that the increase in concentration is not detectable when just distributions are compared, as Pu concentrations can vary significantly, e.g. one order of magnitude with depth [57]. Consequently, no significant increase from the pre-accident Pu levels was observed by Bu et al. using ICP-MS [58, 102], who studied a distribution of concentrations at a number of sampling locations off the Fukushima coast.

For this reason, most studies on the emission of Pu into the environment by the FDNPP determine the isotopic ratios of Pu, especially $^{240}\text{Pu}/^{239}\text{Pu}$, in addition. Fig. 3.8 clearly shows that for the identification of a Pu contamination on the Japanese mainland, it is sufficient to determine just the mentioned ratio. It is quite different for the other two most prominent sources for Pu, the global and atmospheric fallout ($^{240}\text{Pu}/^{239}\text{Pu}=0.18-0.19$). When seawater or sediment samples from the Pacific Ocean are considered, also the tropospheric close-in fallout from the PPG [50] has to be taken into account. This type of fallout which entered the ocean close to the PPG (compare Ch. 2.5), can have $^{240}\text{Pu}/^{239}\text{Pu}$ ratios of up to 0.34 [2]. By mixing with water masses dominated by global fallout, tropospheric close-in fallout lead to increased $^{240}\text{Pu}/^{239}\text{Pu}$ ratios of around

3. The Fukushima accident

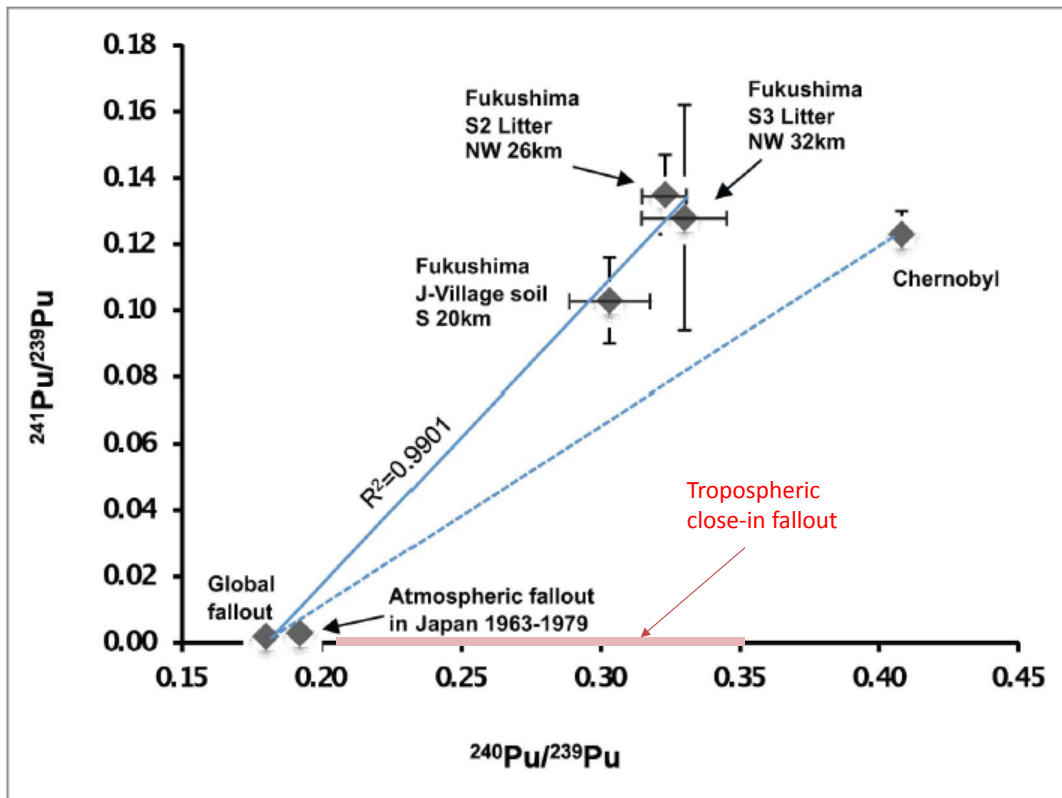


Figure 3.8.: $^{240}\text{Pu}/^{239}\text{Pu}$ and $^{241}\text{Pu}/^{239}\text{Pu}$ ratios measured in soil and litter samples close to FDNPP in comparison to respective ratios of global fallout, atmospheric fallout in Japan and fallout from the Chernobyl accident. Both ratios together serve as a clear signature of Pu from the FDNPP accident, also in sea water, as it can be also distinguished from tropospheric close-in fallout whose characteristic ratios are marked in red. Modified from [3].

0.27 off the east coast of Japan in water and sediments even before the accident [55]. The range of detected values for the isotopic ratio of tropospheric close-in fallout is marked in red in Fig. 3.8. First studies, which measured similarly elevated $^{240}\text{Pu}/^{239}\text{Pu}$ ratios in seawater after the accident, were therefore not able to make a clear statement on a release of Pu into the Pacific Ocean [4, 87, 58, 102].

A considerable part of ^{241}Pu ($T_{1/2} = 14.35$ a) produced during the weapon testings in the 1950's and 60's has already decayed. Consequently, the isotopic ratio $^{241}\text{Pu}/^{239}\text{Pu}$ of 0.00194 for global fallout on the northern hemisphere [51] and for local tropospheric close-in fallout of up to 0.0044 [53] (decay corrected to January 1st, 2000) is clearly different from the FDNPP signature of 0.18. The determination of both isotopic Pu ratios will provide reliable information about an additional entry of Pu due to the FDNPP accident and its distribution in the Pacific Ocean. As discussed in Ch. 2.6, a mass-spectrometric technique

3.5. Identification of a possible entry of actinides into the Pacific Ocean

had to be applied, for a separate detection of ^{239}Pu and ^{240}Pu . Because of the small sample volume of only 20 L and the expected low concentrations of especially ^{241}Pu in the ocean water, Accelerator Mass Spectrometry (AMS) was chosen as detection method. However, the detection of ^{241}Pu , an almost pure β^- emitter, poses a problem for mass spectrometric techniques due to the isobaric interference of its daughter nuclide ^{241}Am . Therefore, a highly efficient and reliable chemical suppression of Am is required. In addition, in order to increase the overall detection efficiency for Pu and Np, also those two elements have to be separated chemically, so that AMS samples for each element can be produced from one water sample. As demonstrated in Ch. 2.5 and 2.6, there is only little data on ^{237}Np concentrations and isotopic ratios in the Pacific Ocean before the accident available. So far, no measurements on ^{237}Np in the environment after the accident has been published and also little information on the ^{237}Np inventories from theoretical predictions can be found (compare Ch. 3.4). For this reason, the determination of the ^{237}Np concentrations in the present seawater samples will contribute considerably to improve the data on ^{237}Np in the environment in general. The description of the seawater samples and the chemical sample preparation procedure developed in the frame of this PhD thesis are discussed in the next chapter.

4. Ocean water samples and AMS sample preparation

4.1. Sampling of sea water

Two different types of ocean water were studied regarding the ^{239}Pu , ^{240}Pu , ^{241}Pu and ^{237}Np concentration in this work. First, Atlantic Ocean (Irish Sea) water with a well-known and rather high concentration of the mentioned actinides to test the developed detection method, i.e. the chemical separation and the AMS measurement procedure. And secondly, selected Pacific Ocean water samples which potentially might show a FD-NPP signature in addition to background samples which were collected at a large distance to the Japanese coast.

4.1.1. IAEA-443: Irish Sea Water

5L of the certified reference material IAEA-443 were purchased from the International Atomic Energy Agency (IAEA). This material is water collected in the Irish Sea in 1993 at two sampling locations ($54^{\circ}24.89'\text{N}$ - $3^{\circ}33.62'\text{W}$ and $54^{\circ}23.2'\text{N}$ - $3^{\circ}33.45'\text{W}$) close to the reprocessing plant Sellafield in UK [103]. In total, 3600 liters were sampled in which increased concentrations of especially anthropogenic radionuclides can be expected due to the release from the reprocessing plant into the ocean. The water was acidified to $\text{pH} < 1$ already on the ship to destroy organic compounds and microorganisms. Furthermore, it has been shown that acidification reduces the adsorption of actinides on exposed surfaces like the container walls [104]. The water was distributed to altogether 28 laboratories to detect the concentrations of different natural and anthropogenic radionuclides by gamma- and alpha-spectrometry, beta-counting and mass-spectrometry.

Depending on the number of laboratories which determined a specific isotope concentration and the relative uncertainty of the stated concentration, the certificate distinguishes between certified and information values [105]. Whereas the combined massic activity (activity relative to mass) of $^{239+240}\text{Pu}$ does fulfill the requirements for a certified value,

4. Ocean water samples and AMS sample preparation

| Radionuclide | Information value | Combined expanded uncertainty |
|----------------------|--------------------------|--------------------------------------|
| | [mBq/kg] | [mBq/kg] |
| $N(^{239}\text{Pu})$ | 8.2 | 0.8 |
| $N(^{240}\text{Pu})$ | 7.0 | 0.6 |
| $N(^{241}\text{Pu})$ | 161 | 19 |

Table 4.1.: Information values on the massic activities of ^{239}Pu , ^{240}Pu and ^{241}Pu in the reference material IAEA-443. Decay corrected to 01/01/07. [105]

the massic activities of ^{239}Pu and ^{240}Pu detected by ICP-MS and high resolution alpha-spectrometry are specified only as information value [103]. In addition to the information value for ^{241}Pu , which was determined by alpha-spectrometry (calculated from the ^{241}Am in-growth), liquid scintillation, and mass spectrometry, the massic activities of ^{239}Pu and ^{240}Pu from the reference sheet are listed in Tab. 4.1.

The massic activity of ^{237}Np of (7 ± 3) mBq/kg was determined by one laboratory only, using gamma-spectrometry and therefore is neither a certified nor an information value. Consequently, this value can only be used as an estimate for the order of magnitude of the ^{237}Np concentration. For further information on the reference material and also the corresponding uncertainties, refer to [103, 105].

4.1.2. Pacific Ocean water

Samples were collected on the cruise KH-12-4 (GP02) of the ship R/V Hakuho Maru which left Tokyo (Japan) on August 23, 2012 and arrived in Vancouver (Canada) on October 2, 2012. The route of the ship in the North Pacific Ocean and the different sampling stations are shown in Fig. 4.1. The cruise was part of the GEOTRACES program which aims at the investigation of the biochemical cycles and distribution of trace elements and the corresponding isotopes in the marine environment [6]. For the collection of the sea water, Teflon-coated Niskin bottles (12 L) mounted on a CTD-CMS (Carousel Multi Sampling System) and a large-volume water sampler (250 L x 4) were used. The water was filtered and acidified to $\text{pH} < 1$ with HNO_3 directly on board of the ship.

42 samples with around 20 L each were provided by Prof. M. Yamada from the Hirosaki University. A complete list of all samples received by the TUM with the exact coordinates of the sampling locations can be found in Appendix H. However, considering the behaviour of actinides in sea water (compare Ch. 2.2.3), with especially Pu showing a fast sedimentation, and the date of the cruise, it can be expected that only the two sampling stations located closest to FDNPP possibly show a detectable signature from the

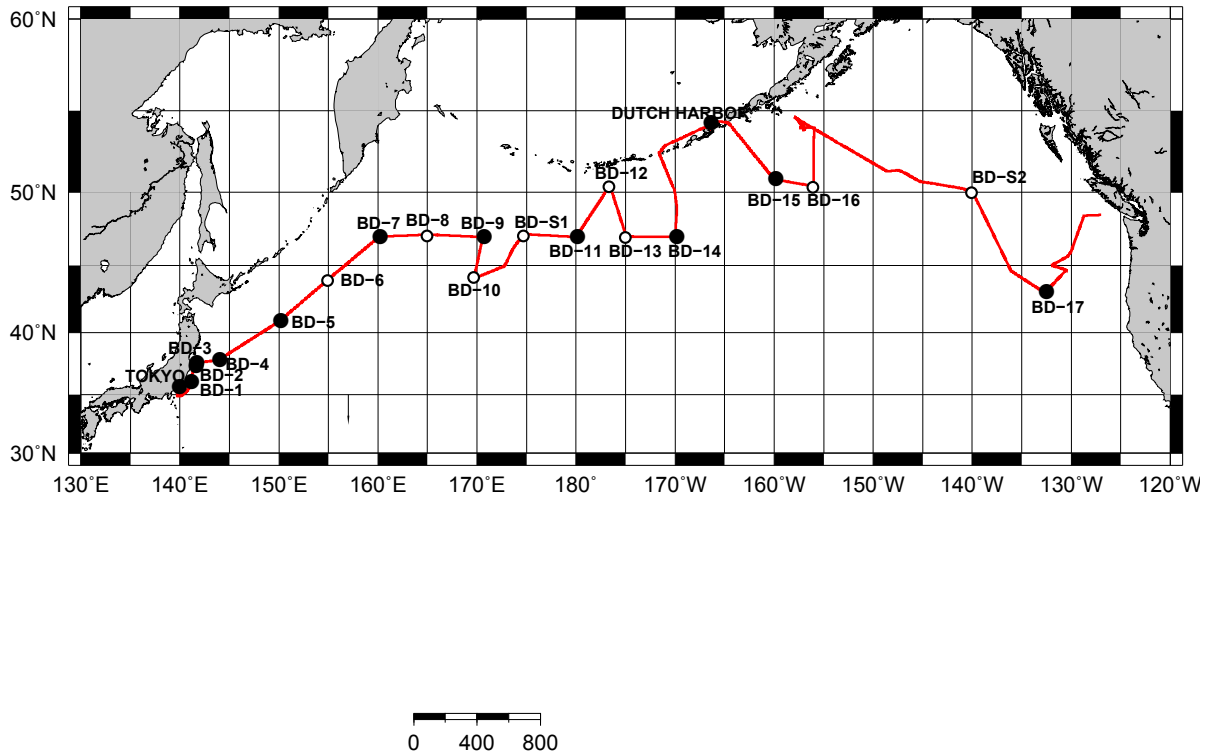


Figure 4.1.: Track of cruise KH-12-4 from Tokyo to Vancouver (Aug. 23th, 2012 - Oct. 2nd, 2012) presented as red line. Sampling stations BD1 - BD17 are marked with black or white circles.

NPP. Consequently, all samples from station BD02 and three samples from BD04 listed in Tab. 4.2 were prepared for the AMS measurements in addition to 4 background samples collected at stations which were located at larger distances to the Japanese coast. The distances to the FDNPP in the table were calculated from the geographic coordinates of the FDNPP (37.422° N, 141.034° E) [71] and of the samples using the spherical law of cosines assuming the earth as a perfect sphere.

The sampling stations closest to the FDNPP, BD02 and BD04, are also marked on the map in Fig. 4.2 showing the central part of Japan to illustrate their location with respect to the FDNPP. The green arrow in this figure is pointing on the location of FDNPP and the dashed white circles indicate the approximate distance to the NPP given in the white boxes. The southward directed Oyashio Current off the coast of Fukushima prefecture [81] favors the transport of radionuclides in southern directions [106], so that the location of BD02 southeast of FDNPP might be advantageous for the detection of Pu emitted from the FDNPP.

4. Ocean water samples and AMS sample preparation

| Sample type | Station | Depth [m] | Distance to FDNPP [km] |
|-----------------------|---------|-----------|------------------------|
| Fukushima relevant | BD02 | 0 | 39.06 |
| | BD02 | 20 | 39.06 |
| | BD02 | 50 | 39.06 |
| | BD02 | 100 | 39.06 |
| | BD02 | (B-10) | 39.06 |
| | BD04 | 50 | 254.1 |
| | BD04 | 300 | 254.1 |
| | BD04 | 500 | 254.1 |
| Background samples | BD07 | 100 | 1890 |
| | BD11 | 4000 | 3346 |
| | BD15 | 1000 | 4811 |
| | BD17 | 0 | 7037 |

Table 4.2.: Pacific Ocean water samples which were prepared for the analysis of the Pu and Np concentration using AMS. The lower four samples served as background samples to characterize nuclear bomb fallout. B-10 denotes “bottom - 10m” and corresponds to 139 m depth.

4.2. Chemical Pu and Np extraction

On the one hand, it has been shown in Ch. 3.5 that for the identification of an entry of actinides into the Pacific Ocean emitted by the FDNPP, it is essential to detect ^{241}Pu and to determine the isotopic ratio $^{241}\text{Pu}/^{239}\text{Pu}$. On the other hand, the two isobars ^{241}Pu and its daughter nuclide ^{241}Am cannot be separated by AMS as explained in Ch. 6.4. To solve this problem, Am has to be efficiently separated by chemical means but with a high yield for Pu. This demand on the chemical sample preparation method developed within the scope of this thesis, had highest priority. Another aim was to extract Np to produce a separate AMS target to increase counting statistics both on Pu and Np.

Even though there are many different separation procedures for actinides already published, a modified procedure had to be developed in order to meet the requirements not only for AMS but also for α - and γ -spectrometry and ICP-MS. The latter three detection techniques were used to determine the chemical yield of the Pu and Np extraction method (see Ch. 5). Most of the published methods are adjusted to only two different detection techniques at maximum. Furthermore, the sample preparation was intended to be used in the laboratory of the MLL which is equipped with two exhaust hoods with certain restrictions. For this reason, the use of some chemicals such as HF and some other hydrohalic acids is off-limits which are frequently used for the Pu and Np extraction. Consequently,



Figure 4.2.: Map of the central part of Japan in which the location of FDNPP is indicated by the green arrow and the sampling stations BD02 and BD04 are marked in red. The white dashed circles represent an estimate of the distance to FDNPP. Map from [107], modified.

these reagents had to be eliminated from the separation method. Finally, the procedure should be kept simple, which means the separation itself should be performed within one day with as little rinsing steps and medium changes as possible.

For this purpose extraction chromatography was chosen which is introduced in this section. Two other techniques commonly used for actinide separation, i.e. solvent extraction and ion exchange chromatography are described in Appendix D. In addition, the final chemical procedure which was applied to the sea water samples to extract Pu and Np is presented. It is also shown, that extraction chromatography requires a defined solution and a low salt concentration. Therefore, the salt matrix has to be separated and the actinides concentrated before the chromatography. Concentration was done by evaporation and iron hydroxide co-precipitation which also serves to reduce the salt content. Both preparatory steps are also described in this section.

4. Ocean water samples and AMS sample preparation

4.2.1. Concentration using a rotary evaporator

In order to simplify the handling of the samples, the volume of 20 L was reduced to 5-6 L by evaporation using a rotary evaporator. The maximum volume which could be evaporated was limited by the precipitation of salts in the sample volume. This had to be avoided, because especially Pu(IV) and Np(IV) preferentially stick to solids as it was discussed in ch 2.2 which leads to the co-precipitation along with the salts. However, the additional aim of the pre-concentration was to separate the salt matrix present in the sea water. A RE-111 rotary evaporator purchased from Büchi Labortechnik AG was used to concentrate the samples. The oil filled heat bath was set up during this work. Both are shown in operation in Fig. 4.3.

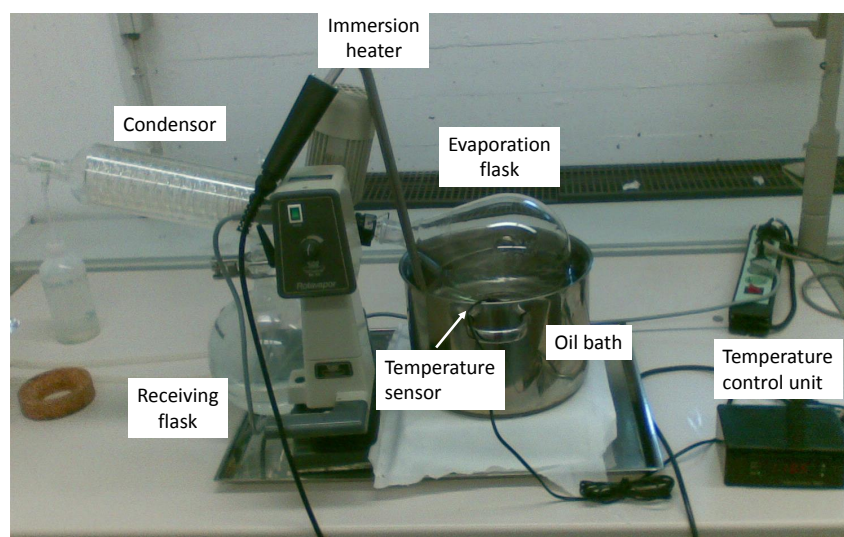


Figure 4.3.: Rotary evaporator and heat bath filled with oil used for the concentration of the Pacific Ocean water samples from 20 L to around 5 L.

The 3 L evaporation flask on the right side which dips into the oil bath was filled with maximum 1.75 L sample material and was set into rotation. The oil was heated to around 120 ° by a 2.0 kW immersion heater with a flat heating coil bought from Lükon AG. The immersion heater was controlled by a temperature switch which continuously monitored the temperature of the oil bath by a sensor. The rotation speed had to be chosen fast enough so that a thin warm water film forms on the inner side of the evaporation flask. Hence, the liquid can be very efficiently evaporated from a large surface, compared to which the direct evaporation from the horizontal surface of the water volume is negligible. In this way, the sample volume could be reduced by a factor of 5 in around 5 h. Special care had to be taken while setting the temperature of the oil bath, that the water did not start boiling or bumping which is a well known phenomenon for water. During boiling, Pu and Np can be dragged along with the water molecules and thus might be lost from the

sample volume. However, due to the rotation of the flask the risk for boiling, in general, is decreased compared to usual surface evaporation.

4.2.2. Spike material IRMM-085

The spike isotopic reference material IRMM-085 which contains a well-known concentration of ^{242}Pu , was purchased from the Institute for Reference Materials and Measurements (Geel, Belgium). The certificate can be found in Appendix G. ^{242}Pu was chosen as spike isotope as with its long half-life of $3.750 \cdot 10^5$ a [19] it is well suited for AMS and due to its low specific activity it can be also handled in a non-controlled area. Furthermore, the IRMM-085 has especially a much lower ^{241}Pu contamination than e.g. the ^{244}Pu spike solution IRMM-084 which was also considered regarding the half-life. However, by adding $5 \cdot 10^9$ ^{244}Pu , the sample would be contaminated also with $2 \cdot 10^6$ ^{241}Pu atoms, which is in the same order of magnitude as the expected amount in the Pacific Ocean water samples (see Ch. 2.5).

The mass concentration of the stock solution of $9.464(14)$ ng(^{242}Pu)/g(solution) which corresponds to $2.3552(35) \cdot 10^{16}$ ^{242}Pu atoms/kg(solution) is too high for the application in AMS measurements. Therefore, a dilution series was prepared with the final ^{242}Pu solution used to spike the samples having a concentration of $4.00(4) \cdot 10^9$ ^{242}Pu atoms/g(solution) (30.9.14). The spike solution was stored in PFA bottles in order to keep the attraction of Pu(IV) to the wall as small as possible. Furthermore, the bottle was weighed before and after the required solution was removed, to take a possible evaporation of the solution into account. Both effects might alter the concentration of ^{242}Pu in the solution.

The concentrated sample was transferred to a 5 L beaker or if necessary it was divided into two 5 L beakers. The canister which had contained the concentrated sample was washed three times with the distillate of the respective sample. The sample was then heated up to approximately 70°C to make sure that salts which might have precipitated, were redissolved again. The sample was spiked with around $(2-5) \cdot 10^9$ ^{242}Pu atoms taken from the IRMM-085 spike solution. To obtain an accurate number of the added ^{242}Pu atoms, the used spike solution was weighed before. Tab. 4.3 shows the corresponding contaminations of the interesting Pu isotopes in the added spike which have to be considered when calculating the final Pu concentrations in the samples. The sample was left stirring overnight to achieve an equilibrium and a homogeneous mixture between spike solution and the sample.

4. Ocean water samples and AMS sample preparation

| Isotope | Number of atoms |
|------------------------|----------------------|
| N(^{242}Pu) | $2.00 \cdot 10^9$ |
| N(^{239}Pu) | $1.64 \cdot 10^6$ |
| N(^{240}Pu) | $2.16 \cdot 10^5$ |
| N(^{241}Pu) | $5.07 \cdot 10^{3*}$ |

Table 4.3.: Contaminations of ^{239}Pu , ^{240}Pu , ^{241}Pu introduced into the sample by the spike solution when adding a spike of $5 \cdot 10^9$ ^{242}Pu . * decay corrected to 01/12/15.

4.2.3. $\text{Fe}(\text{OH})_3$ co-precipitation

Following the procedure described in [108], $\text{Fe}(\text{NO}_3)_3$ solution, which provides the Fe^{3+} ions for the co-precipitation, was added such that the overall concentration of Fe in the sample was larger than 12 mg/L. NH_4OH was slowly dropped into the sample at a temperature of 70° in order to increase the pH of the solution. At a pH of 7, $\text{Fe}(\text{OH})_3$ started precipitating which can be seen as red flocks in the rear beaker in Fig. 4.4 whereas the solution in the front beaker still is clearly acidic. The pH was not allowed to be raised above 8.5, because salts from the sea water already start precipitating leading to a poor separation between actinides and the salt matrix.

The efficiency of the co-precipitation crucially depends on the oxidation states of Pu and Np. As discussed in Ch. 2.2.1, the reduced species preferentially stick to particles whereas the oxidized species do not. Consequently, either one has to make sure that Pu and Np are present in oxidation state +III or +IV, respectively, by adding a reducing agent [109], e.g. NaHSO_3 [12], so that the co-precipitation can be performed with a small amount of Fe^{3+} , or a sufficiently large quantity of Fe^{3+} has to be added, i.e. > 10 mg/L, for the additional co-precipitation of the oxidized species [104]. The different behavior of Pu(IV) and Pu(V) is demonstrated in Fig. 4.5. This plot shows that during $\text{Fe}(\text{OH})_3$ co-precipitation almost 100% recovery can be obtained for Pu(IV) even at Fe^{3+} concentrations below 1 mg/L whereas the recovery for Pu(V) is well below 10% at this Fe^{3+} concentration. However, the Pu(V) recovery approaches 100% at Fe^{3+} concentrations larger than 10 mg/L. In first order, it can be assumed that Np behaves similarly and can be completely co-precipitated using insoluble metal-hydroxides [110]. The major difference to Pu is, that Np(V) is the dominating species in sea water, so that it can be expected that an efficient co-precipitation can only be obtained with significantly increased Fe^{3+} concentration. In this work, an excess of Fe^{3+} of a least 12 mg/L was added to the sample, as Fe^{3+} ions do not interfere during the separation process (see Ch. 4.2.4).

The sample was stirred for one further hour in order to increase the probability for adsorption of Pu and Np on the $\text{Fe}(\text{OH})_3$ cluster. Then the precipitate was left to settle for at



Figure 4.4.: Sample during the concentration step using $\text{Fe}(\text{OH})_3$ co-precipitation. In the rear beaker, the pH was adjusted to 8 leading to the precipitation of $\text{Fe}(\text{OH})_3$ whereas in the front beaker the Fe^{3+} ions are still in solution, causing the light yellow colour.

least 5 h or if possible overnight, then the supernatant was removed by a peristaltic pump. The precipitate was distributed over several 50 mL centrifuge tubes and the samples were centrifuged 20 min at around 3200 rpm (rounds per minute). Finally, the different parts of the precipitate were combined in one centrifuge tube and washed three times with diluted NH_4OH . The residue was dissolved in concentrated HNO_3 and evaporated to dryness. In this work, it was observed that in this way a salt is formed which can not be re-dissolved in concentrated HNO_3 . As this salt might interfere with the element separation process, it had to be filtered out of the sample solution. For this purpose, the dried precipitate was re-dissolved in 6 M HNO_3 and filtered through a $12\ \mu\text{m}$ filter and then evaporated to dryness. The filter was washed with 25 mL 6 M HNO_3 , which was added to the sample solution. An EDX (Energy Dispersive X-Ray) analysis of the salt identified silicon oxide as major constituent which is known to be insoluble in most solvents and which is present in natural waters.

4. Ocean water samples and AMS sample preparation

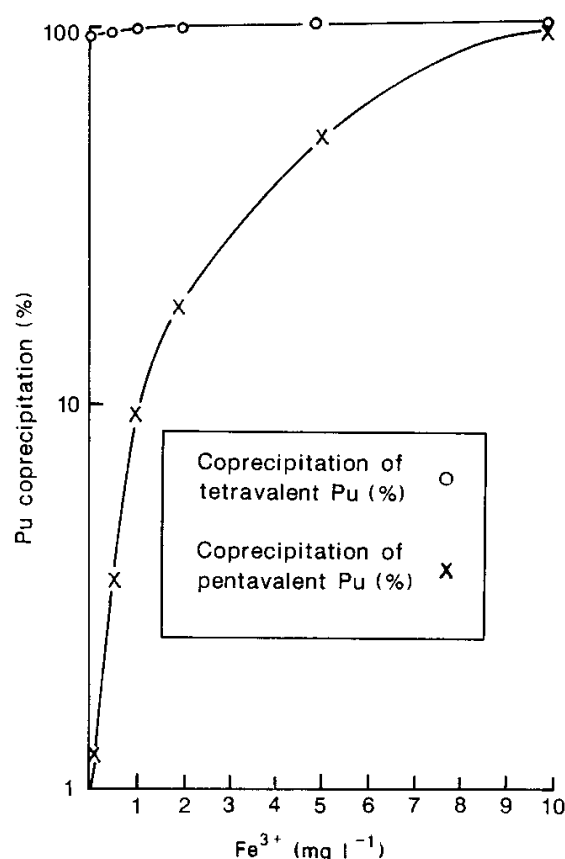


Figure 4.5.: Graph showing experimental values for the recovery of Pu(IV) and Pu(V) during Fe(OH)₃ cluster co-precipitation. Whereas Pu(IV) can be obtained with almost constantly high recovery of around 100%, the Fe³⁺ concentration has to be raised above 10 mg/L to obtain similar recoveries for Pu(V). Taken from [104].

4.2.4. Extraction chromatography using TEVA resin

In general, there are three techniques regularly used to separate actinides: solvent extraction, ion exchange chromatography and extraction chromatography. The latter was found to meet the requirements of the present study best and will be introduced in detail in the following. Information on solvent extraction and ion exchange chromatography can be found in Appendix D along with a discussion of the reasons why they were not chosen for the current application.

Extraction chromatography can be described as a combination of solvent extraction and ion exchange chromatography. For extraction chromatography, the organic phase of solvent extraction is made stationary by applying it to inert porous beads which forms the resin. Analog to ion exchange chromatography, the resin is filled in columns which is passed by usually acidic solutions, denoted as mobile phase, and which corresponds to the

aqueous phase of solvent extraction. Consequently, extraction chromatography shows the high elemental selectivity of solvent extraction but several columns with different resins can be easily combined forming a separation technique with several stages [111, 112]. Extraction chromatography was developed in the early 90's at Argonne National Laboratory and now is commonly used for the separation of actinides [111, 113]. The corresponding resins are commercially available from Eichrom Technologies, INC. and are distributed in Europe by TrisKem International.

Each of the resins is highly specialized for the separation of a specific group of radionuclides. Again, the retention of a radionuclide which is described by the resin capacity factor k' , strongly depends on its oxidation state in the column load solution. k' is defined as ratio of the number of free column volumes (FCV) and the maximum concentration of the respective ion in the eluate [114]. The FCV is the void space in the column and therefore can be used to quantify the volume of mobile phase which has passed through the column [115]. Hence, the larger the value for k' , the stronger the adsorption of the ion species on the resin. Fig. 4.6 shows the dependence of k' on the acid concentration of HNO_3 (left side) and HCl (right side) for the TEVATM (**T**etravalent actinides) resin. The chemically active substance of this resin is referred to as AliquatTM.336, which contains a quaternary amine as active component and thus is closely related with anion exchange resins. Similar as described in the section about anion exchange, TEVA preferentially adsorbs tetravalent ions. However, Fig. 4.6 clearly shows that a maximum adsorption on the resin is already achieved in 3 M HNO_3 compared to 8 M HNO_3 in the case of anion exchange chromatography. Furthermore, as the active compound is present as liquid and is not bound to the substrate, there is a higher flexibility in binding anions from the mobile phase. This leads to a large difference in take-up between Pu(IV) and Am(III) and thus, to a suppression of Am of around 5 orders of magnitude, which makes TEVA very well suited for the present application.

It has to be considered that salts which complex the radionuclides might have a significant influence on the retention on the column. This is especially relevant for sea water from coastal areas, where high concentrations of phosphates can be expected. A particularly strong effect can be observed for Np(+IV), which is presented in Fig. 4.7. When solutions with a high phosphate or oxalate concentration pass through the column, the Np retention drops several orders of magnitude if the HNO_3 concentration is kept constant (left side of Fig. 4.7). This effect can be attenuated by increasing the HNO_3 concentration and thus providing more NO_3^- ions (see right side of Fig 4.7 for the example of oxalates) or by adding for example Al^{3+} ions, which are able to bind present complexing agents. On the other hand, the strongly decreased adsorption of Np(IV) on the resin in the presence of oxalates can be exploited to elute Np(+IV) from the column by just rinsing the column with oxalic acid.

4. Ocean water samples and AMS sample preparation

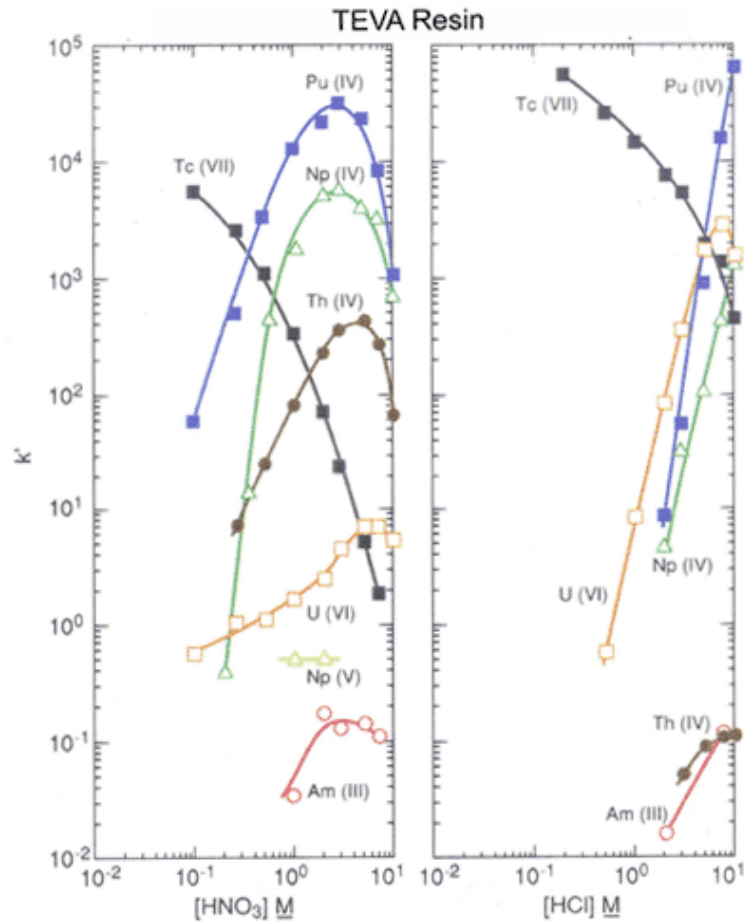


Figure 4.6.: Dependency of the adsorption onto the resin in terms of the k' -factor on the molarity of HNO_3 (left side) and HCl (right side) for the dominating oxidation states of different elements for the TEVA resin. The Am(III) adsorption on the resin in both media is suppressed by 5 orders of magnitude compared to Pu(IV). [10]

Regarding the simplicity of handling, ion exchange and extraction chromatography seemed to be most favorable for the present application. However, due to the chemicals required for the separation with ion exchange chromatography, this technique had to be abandoned for the use at the MLL (compare Appendix D). For this reason, a separation procedure based on the work of Maxwell [11] and Horwitz et al [10] was developed further to match the requirements of α -spectrometry, ICP-MS and AMS in addition to the specifications of the lab at the MLL. The resulting final procedure is described in the following section.

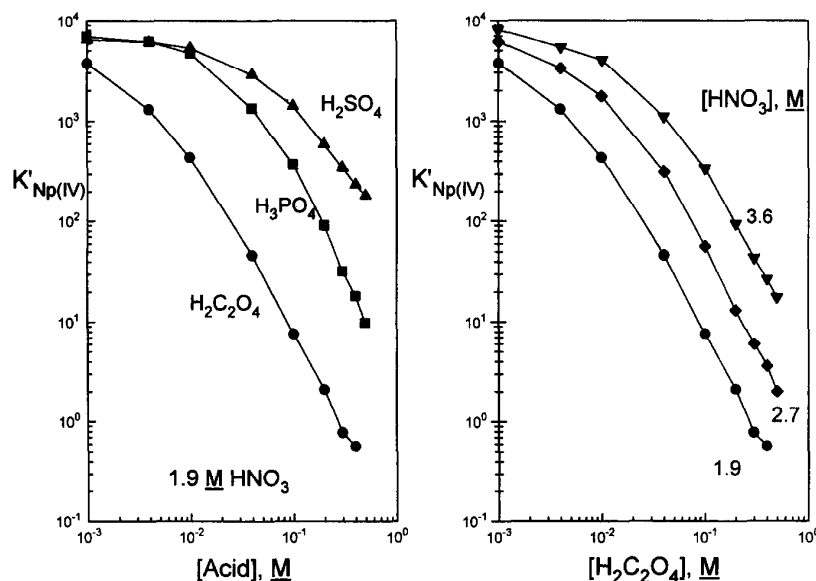


Figure 4.7.: Left side: Influence of the presence of different salts (sulfate, phosphate, oxalates) in 1.9 M HNO_3 load solution on the k' -factor of Np(IV). With increasing molarity of the salts the adsorption onto the resin drops by up to four orders of magnitude. Right side: Dependence of the k' -factor of Np(IV) on the concentration of oxalates and the HNO_3 concentration. Taken from [10].

The applied separation procedure

Starting from the dried iron hydroxide precipitate, this residue of the sample is redissolved in 12 ml 0.5 M $\text{Al}(\text{NO}_3)_3$ - 3 M HNO_3 . Al^{3+} ions are required to complex phosphates and oxalates which might be present in the sample and which limit especially the retention of Np on the column. However, $\text{Al}(\text{NO}_3)_3$ leads to a high salt content in the Am fraction which interferes with electro-deposition and very often shows elevated U concentrations. Therefore, we were aiming for low $\text{Al}(\text{NO}_3)_3$ concentrations. In the first test, $\text{Al}(\text{NO}_3)_3$ was completely eliminated from the procedure, but Np yields in sea water samples were not satisfactory.

Since TEVA is only selective for oxidation state +IV, the oxidation state of Pu and Np has to be adjusted to +IV, so that Pu and Np are retained on the TEVA column while Am +III and U +VI pass through the resin. According to the procedure described in [11], 0.5 ml 1.5 M sulfamic acid, 1.25 ml 1.5 M ascorbic acid and 1 ml 3.5 M sodium nitrite were added to the sample solution for this purpose. Sulfamic and ascorbic acid are required to reduce Pu, which can be present in different oxidation states, to +III. Afterwards Pu is oxidized again to +IV with NaNO_2 . Np is more effectively reduced by Fe +II ions, which are usually added as Fe +III and get reduced by the ascorbic acid. In this case, Fe +III

4. Ocean water samples and AMS sample preparation

ions were already present in the solution due to the initial $\text{Fe}(\text{OH})_3$ precipitation so that no additional Fe was required. The final load solution was left to be completely oxidized by NaNO_2 for 15 min [116].

The TEVA resin was washed with 3 M HNO_3 and 2-3 ml of the resin were transferred to the column after waiting for at least 15 min. The resin was rinsed with 5 ml 3 M HNO_3 and the sample solution was loaded on the column with a flow rate of around 0.5 ml/min which was controlled manually. The Am, Cm, U fraction, which passes through the column, was collected in a beaker and set aside for later analysis. The column was then rinsed with 20 Free Column Volumes (1 FCV = 1.3 ml) of 3 M HNO_3 which was collected in the same beaker. The Pu was eluted from the column by reducing Pu to +III with 20 FCV 4 M HNO_3 - 0.1 M rongalite (sodium hydroxymethanesulfinate). Finally, Np was eluted with 20 FCV 0.4 M oxalic acid - 0.1 M HNO_3 .

The applied pre-concentration and separation procedure is presented as a flow chart in Fig. 4.8. In this process nitric acid was chosen as aqueous phase in all separation steps, whereas it was pointed out before that HCl can also be used. Fig. 4.6 suggests an even better Pu / Am separation in HCl making this option more favorable. However, the separation in HCl was tested at the RCM showing a significantly lower recovery for Pu than for the procedure with HNO_3 (compare Ch. 5.3) and therefore was abandoned.

4.2.5. Combination with UTEVA resin for further U suppression

During the AMS measurements of the IAEA-443 sample at the MLL it became obvious that ^{239}Pu could not be clearly identified because of isotopic background from ^{238}U interfering with mass 239 (see Ch. 7.1). As ^{238}U is a primordial nuclide it is present in all environmental samples at a concentration on the ppm level. Concerning the suppression of U by the TEVA column, the retention of Uranium on the resin which is present in the column load solution as U(VI), is around four orders of magnitude lower than Pu(IV) (compare Fig. 4.6) which leads to a reasonable U(VI) suppression, but it does not seem to be sufficient if the difference in concentration between Pu and U is as large as in the sea water samples. In order to reduce the concentration of U in the Pu fraction further, the procedure using TEVA could be just repeated with the Pu fraction. However, this means that the oxidation state of Pu had to be adjusted to +IV again.

A more convenient method which was tested in this work, was to use a U/TEVATM (Uranium and tetravalent actinides) column in tandem with the TEVA column during Pu elution. U/TEVA binds tetravalent actinides as nitrate complex similar to TEVA but also U(VI) [117] resulting in a high uptake of U in total which is presented in terms of the capacity factor k' in Fig. 4.9. Different to TEVA which is closely related

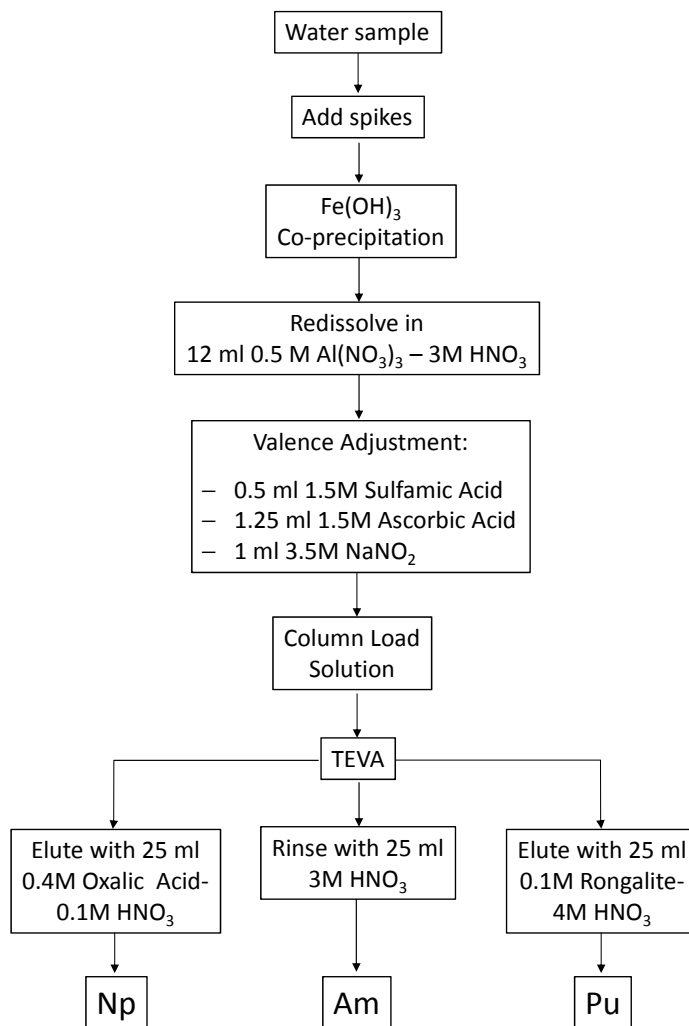


Figure 4.8.: Flow chart of the separation procedure for Am, Pu and Np using TEVA resin.

to a strong basic anion exchanger, the chemically active substance of U/TEVA is the organic extractant diamyl amyolphosphonate which is applied to the inert support Amberlite XAD-7. The retention of trivalent actinides on U/TEVA is suppressed by around three orders of magnitude compared to the oxidation states +IV and +VI as shown by Fig. 4.9 for Am(III). Pu which was eluted from the TEVA resin due to the reduction to +III using rongalite, also passed through the U/TEVA column which was placed directly below the TEVA column. U, whose dominating oxidation states are +IV and +VI, was retained on U/TEVA, so that U was further suppressed in the Pu fraction.

The flow chart of the separation procedure starting from the TEVA column, now with the U/TEVA column in addition, is presented in Fig. 4.10, which demonstrates that no

4. Ocean water samples and AMS sample preparation

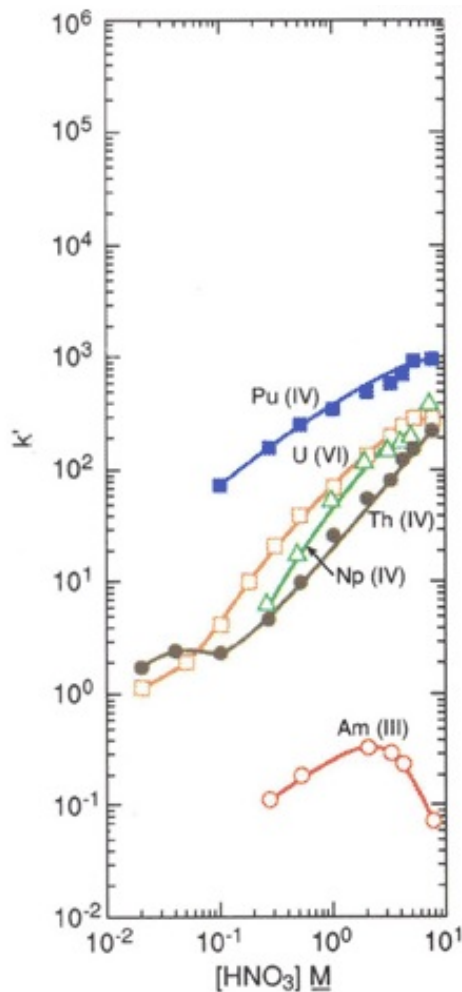


Figure 4.9.: Dependency of the k' -factor on the molarity of HNO_3 for the dominating oxidation states of different elements for the UTEVA resin. Both, U(+IV) and U(VI+) are retained on the U/TEVA resin whereas trivalent actinides (e.g. Am(III)) are suppressed by three orders of magnitude. [10].

changes to the overall method are required. The Pu eluate from the TEVA column directly passes on to the U/TEVA column which is then collected. Afterwards the two columns are separated again and the elution of Np from the TEVA column can be started. Hence, this method is very simple and does not need more time than the separation with TEVA column alone.

4.2.6. Final AMS sample

In order to obtain the AMS cathodes, first, the Pu and Np solutions were evaporated and redissolved with concentrated HNO_3 and 40% H_2O_2 and fumed three times to destroy organic compounds which might effect the following $\text{Fe}(\text{OH})_3$ co-precipitation. The dried

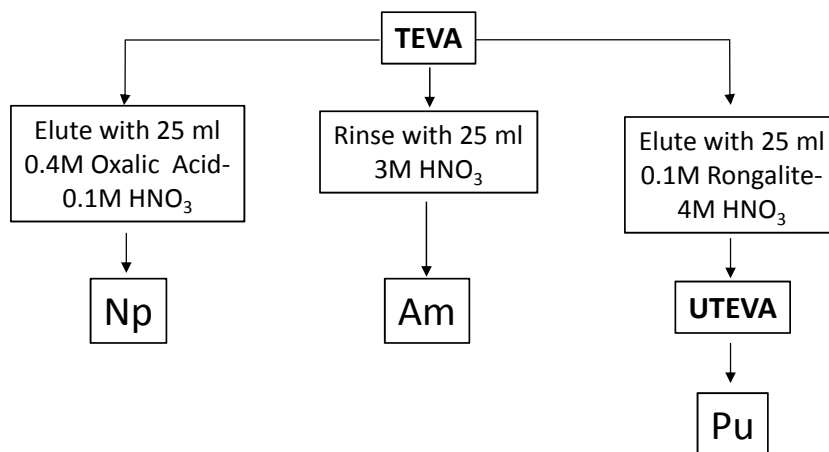


Figure 4.10.: Flow chart of the separation procedure using an additional U/TEVA column in tandem with the TEVA column during Pu elution for further U suppression. Preparation of the TEVA column load solution is identical to Fig 4.8 and therefore not presented again.

up samples were then dissolved in diluted HNO₃ and around 3 mg Fe³⁺ was added as iron nitrate solution. For the Pu fraction ultra pure Fe(NO₃)₃ was used to minimize an additional entry of U. The Np fraction was spiked with 2 - 5 · 10⁹ ²⁴²Pu atoms. By adding NH₄OH the actinides were co-precipitated with Fe(OH)₃ at approx. pH 9. The samples were centrifuged 20 min at approximately 3200 rpm and were washed two times with diluted NH₄OH (approx. pH 9). After drying the samples at 150 °C, they were ashed in an oven at 600 °C for 4 h to produce oxides of Pu and Np in an Fe₂O₃ matrix. The Fe₂O₃ was mixed with high purity silver powder (> 99.99%, Alfa Aesar) with a ratio 1:1 by volume then and pressed into a copper cathode for the measurements at the MLL. Silver is added to obtain better thermal and electrical conductivity of the sample material for a more efficient sputter process. Copper sample holders from the Physics Department (TUM) workshop were chosen since they have shown a high purity with regard to U in previous experiments [118]. For the detection of Pu and Np at VERA, the Fe₂O₃ was pressed directly without mixing into an Al cathode.

4.2.7. Blank samples

Blank samples are essential to correct the measured concentration for background introduced either during sample preparation or during the measurement itself. Background can be caused by a contamination in the laboratory or the chemicals itself. Provider for ultra pure reagents, for example, are only able to certify an uranium concentration below ppm, which is still a very high concentration compared to AMS levels. Background from

4. Ocean water samples and AMS sample preparation

the AMS measurement can be e.g. cross-talk in the ion source. Consequently, the blank sample should be chemically processed in the same way as the real samples, the starting material should consist of the same matrix and the concentration of the radionuclides of interest should be as low as possible. Especially, the last requirement is difficult to be met, as all surface waters and thus all oceans are contaminated with actinides due to nuclear weapon fallout. The best chance to find natural waters free from nuclear fallout are very old water layers located at great depths. In Munich, water originating from a water layer from the Tertiary Period, located at a depth of 240 m, is pumped to the surface by deep wells [119], which means that this water was not exposed to nuclear fallout. 1.6 L of this water was used as starting material, accepting that the matrix i.e. especially the salt content and composition is different to the real samples. The following sample preparation happened analogously to the Pacific Ocean water samples. Therefore, the contamination introduced by the IRMM-085 spike is taken into account by the blank sample. For the detection of $^{239-241}\text{Pu}$ and ^{237}Np in the IAEA-443 samples, ultra quality water purchased from Roth GmbH & Co KG was considered as adequate as blank material, since the concentrations were expected to be at least an order of magnitude higher than in the Pacific Ocean samples. The results of the blank measurements are discussed in Ch. 7.

4.3. Preparation of a $^{237}\text{Np}/^{242}\text{Pu}$ standard sample

It is pointed out in Ch. 6.4.1. that for the correct determination of an absolute ^{237}Np concentration in the ocean water samples, a sample with a well-known $^{237}\text{Np}/^{242}\text{Pu}$ ratio is required. This sample can be obtained by mixing a ^{242}Pu and a ^{237}Np spike solution, which are well described concerning the actual concentration of the spike radionuclide but also concerning possible impurities. In case of the IRMM-085 ^{242}Pu spike solution, this information is provided by the Institute for Reference Materials and Measurements (see Ch. 4.2.2). The purification and characterization of the ^{237}Np solution, obtained from the RCM, is described in Appendix E.

After mixing of the diluted ^{237}Np solution with the diluted IRMM-085 ^{242}Pu spike solution, 3 mg Fe^{3+} was added for the following $\text{Fe}(\text{OH})_3$ co-precipitation. The AMS sample preparation then happened similarly to the sea water samples which was described in Ch. 4.2.6. In that way, 5 standard samples for the measurement of the ocean water samples were prepared which are listed in Appendix F, where the used amount of spike material and the respective isotopic ratios are specified.

5. Chemical recovery of the separation procedure

The determination of the chemical yield was important especially for the detection of ^{237}Np , as this quantity directly enters into the final result of the ^{237}Np concentration in the ocean water samples (compare Ch. 6.4.4). However, the efficient suppression of Am was of primary importance, apart from a high chemical yield for Pu and Np. Differences in the chemical behaviour between macroscopic and trace amounts of TRU have been discussed in Ch. 2. In order to study the separation procedure under similar conditions as for the ocean water samples, only microscopic amounts of the tracer should be applied. In this case, ICP-MS would be the detection method of choice. However, due to the limited availability of ICP-MS, activity measurements have been performed to adjust the separation procedure to the defined objective. Consequently, the separation method had to fulfill the requirements of a comparatively large number of detection methods, which will be discussed in this chapter along with the obtained results for the chemical recovery.

5.1. Experimental settings

For the activity measurements, ^{243}Am ($T_{1/2} = 7.4 \cdot 10^3 \text{ a}$) and ^{242}Pu tracer solutions with a concentration of $18.38 \pm 0.55 \text{ Bq/g}$ and $21.28 \pm 0.64 \text{ Bq/g}$, respectively, were provided by the Radiochemie München (RCM). A contamination with ^{238}Pu (2.09 %) and $^{239+240}\text{Pu}$ (0.32 %) was present in the ^{242}Pu spike solutions. Using an ^{243}Am spike has the advantage, that both, the Am suppression and the Np yield can be determined simultaneously, as ^{243}Am decays into the short-lived ^{239}Np ($T_{1/2} = 2.25 \text{ d}$). Consequently, secular equilibrium between ^{239}Np and its mother nuclide can be assumed. When separating ^{239}Np completely from ^{243}Am , which is done by the applied chemical procedure, ^{239}Np decays with its characteristic half-life and can be detected by γ -spectrometry. Consequently, for the correct yield calculation, the time when Am separation was finished had to be documented. To make sure that there was no considerable build-up of ^{239}Np activity due to the presence of ^{243}Am , the α -activity in the Np fraction was determined in addition. The non-certified, but well characterized ^{237}Np solution, described in Appendix E and the ^{242}Pu isotopic

5. Chemical recovery of the separation procedure

standard IRMM-085 discussed in Ch. 4.2.2, were used as tracers for analysis with ICP-MS.

Apart from a general comparison of ion exchange using the anionic resin Dowex 1x-8 and extraction chromatography, different variations of the procedure proposed by Horwitz [10] and Maxwell [11] for the TEVA column were tested. No HF or other hydrohalic acids apart from HCl are allowed in the laboratory of the MLL and hence, alternatives had to be found e.g. for the very common elution of Np from the column with dilute HF. Furthermore, TrisKem International¹ proposed a change of media from HNO₃ to HCl for the elution of Pu and Np from the column to increase the overall recovery (see Ch. 4.2.4). In addition, for all applied detection techniques it is advantageous to keep the salt concentration in the final fractions low. Especially the Am fraction shows a very high salt load when Al(NO₃) is used, as Al³⁺ passes through the resin in the same way as Am³⁺. Therefore, separation processes without Al(NO₃) were also tested. To start with, fresh water was used as matrix material, to keep the influence of complexing agents on the recovery low (see Ch. 4.2.4). When the detected recoveries were satisfying, the matrix was switched to sea water collected from the Atlantic Ocean. Finally, also one of the Pacific Ocean water sample was used to obtain a Np recovery from a matrix material as close to the real samples as possible.

5.2. Applied detection methods

The relevant α - and γ energies emitted by the nuclides discussed in this chapter are listed in Appendix A.

5.2.1. α - and γ -spectrometry

Nuclide identification by α - and γ -spectrometry is based on the detection of the characteristic energy of the emitted α -particles and γ -rays, respectively. Both processes are very well understood from a nuclear physics point of view and are discussed e.g. in [120]. Most often semiconductor detectors, that is silicon (Si)-detectors for α - and germanium (Ge)-detectors for γ -spectrometry, are used. Both detector types and their applications are presented in more detail in [121]. Compared to the charged α -particles, energy loss of γ -rays in matter is very small. Consequently, γ 's have a long range, so that no specific sample preparation was required for the detection of ²³⁹Np after chemical separation. The beaker with the Np solution was put above a high purity Ge-detector (Canberra, FWHM

¹Provider for extraction chromatography resins

= 0.90 keV at 122 keV, relative efficiency: 91.5%) which had been calibrated to the required geometry before. The samples were measured for 17 h and all results were decay corrected to the end of the Am elution process. The interpretation of the spectra and the evaluation of the data was done by the RCM.

For α -source preparation, the respective fraction was fumed three times with concentrated HNO_3 and 40 % H_2O_2 in order to destroy organic compounds. Afterwards, it was redissolved in a electrolyte mixture of sodium hydrogensulfate and sulfuric acid and then electroplated on a steel plate for 3 hours using currents between 0.5 mA and 1.2 mA. A detailed description of the electroplating setup at the RCM and its working principle can be found in [122]. The samples were measured for about 240000 s in an Integrated Alpha Spectrometer from Canberra [123] equipped with Passivated Implanted Planar Silicon (PIPS) detectors with an active area of 100 mm^2 and 150 mm^2 respectively. The detection efficiency ϵ of the respective chamber is 0.036 and 0.023. Spectra were evaluated using the Genie 2000 Alpha Analysis software from Canberra. Fig. 5.1 shows an α spectrum of a Pu fraction obtained from a TEVA separation process where 550 mL Atlantic water was used as matrix material. $1.92 \text{ Bq } ^{242}\text{Pu}$ and $18.9 \text{ Bq } ^{243}\text{Am}$ had been added as tracer in this example.

In addition to the two most prominent emission lines of ^{242}Pu , several other peaks at higher energies with significantly lower intensity are visible in this spectrum. These can be identified as α -particles emitted by $^{239+240}\text{Pu}$ and ^{238}Pu , which were added to the sample as impurities of the tracer solution, but which are very well separated from the ^{242}Pu lines. On the left side of ^{242}Pu , i.e. at lower energies, a broad shoulder can be noticed, which is formed by α particles which lost some of their energy when passing through a layer of matter formed on the α source during electro-deposition. As this tailing represents a severe form of background and worsens the resolution drastically, α sources should be prepared as “mass-free”. However, the Pu fraction in this study contained an increased salt concentration forming a visible layer on the α -source due to the elution of Pu with rongalite, which could not be further reduced without decreasing the Pu recovery. In a few cases, the electro-deposition did not work correctly due to the salt concentration, so that no result for the ^{242}Pu recovery is available for these samples.

The activity of the α -source was calculated starting from the number of ^{242}Pu counts $N(^{242}\text{Pu})$ in a defined region of interest collected in time t by a detector with efficiency ϵ

$$A(^{242}\text{Pu}) = \frac{N(^{242}\text{Pu})}{t \cdot \epsilon} \quad (5.1)$$

From this value the corresponding activity derived from a background spectrum of a steel plate was subtracted and the result was divided by the initial tracer activity to obtain the recovery. No emission lines of ^{243}Am were noticed in any of the α spectra of the

5. Chemical recovery of the separation procedure

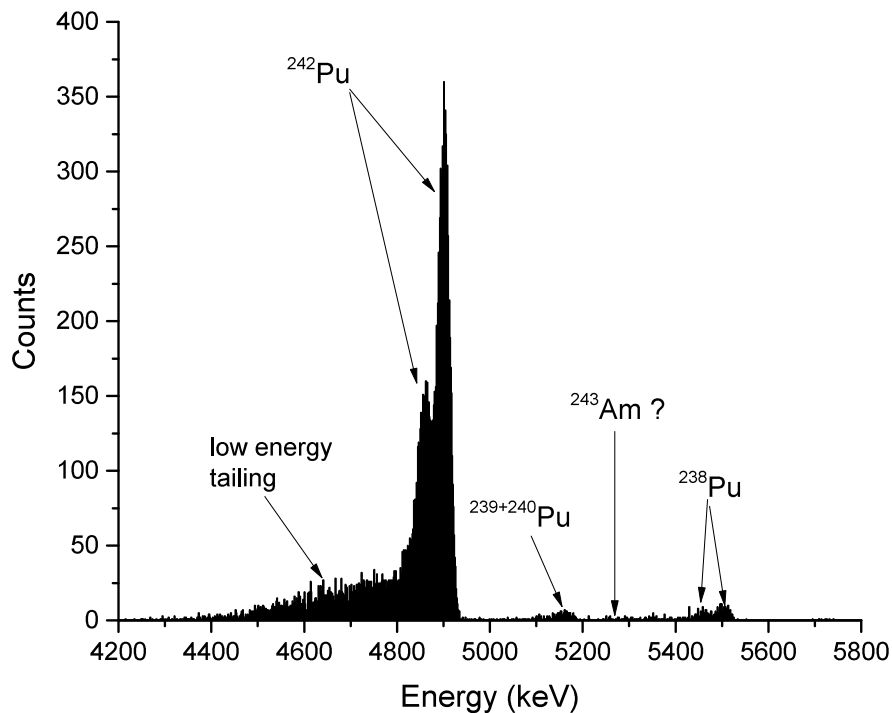


Figure 5.1.: α -spectrum of a sample with 550 mL Atlantic water as matrix material and 1.92 Bq ^{242}Pu added as tracer. Apart from ^{242}Pu also the ^{238}Pu and $^{239,240}\text{Pu}$ impurities of the tracer solution are visible. Tailing is caused energy loss in the material layer of the α source.

Pu fraction from the different separation processes. In two different measurements of sea water a conservative estimate on the Am suppression was made by assuming that all counts in the energy range of the two major emission lines of ^{243}Am were real events. In that way an Am suppression of around $1 \cdot 10^{-4}$ was obtained. This result compares well to a test measurement of one of the Atlantic water samples by AMS, which resulted in a similar value.

5.2.2. ICP-MS

There are several table-top mass spectrometry techniques available today, which basically differ by the applied method of ion formation and injection into the mass separator. For ICP-MS (Inductively Coupled Plasma Mass Spectrometry), usually liquid samples are transformed into an aerosol by a nebuliser. This is required to produce small droplets which can be then vaporized and finally ionized in the plasma torch at temperatures of

around 7000 °K [12]. In the torch, an argon plasma is ignited by a high-voltage spark and is stabilized by the magnetic field which is generated by an external radio-frequency (RF) load coil [124]. Consequently, the plasma is coupled to the power source by electromagnetic induction.

Fig. 5.2 presents a typical ICP-MS setup with its most important components, i.e. the sample injection system, the RF argon plasma source, ion beam optics, a quadrupole mass analyzer, and at the end a particle detector, e.g. an electron multiplier. The ICP-MS instruments used in this study, an ELAN 6100 (Perkin Elmer) of the Institute of Resource Ecology at HZDR (Helmholtz Zentrum Dresden-Rossendorf) and a 7500cx (Agilent) [125] of the division “Sicherheit und Umwelt” at KIT (Karlsruhe Institute of Technology), feature an identical setup. For more details on this type of ICP-MS instrument, its operation mode and performance, please refer to [124, 126].

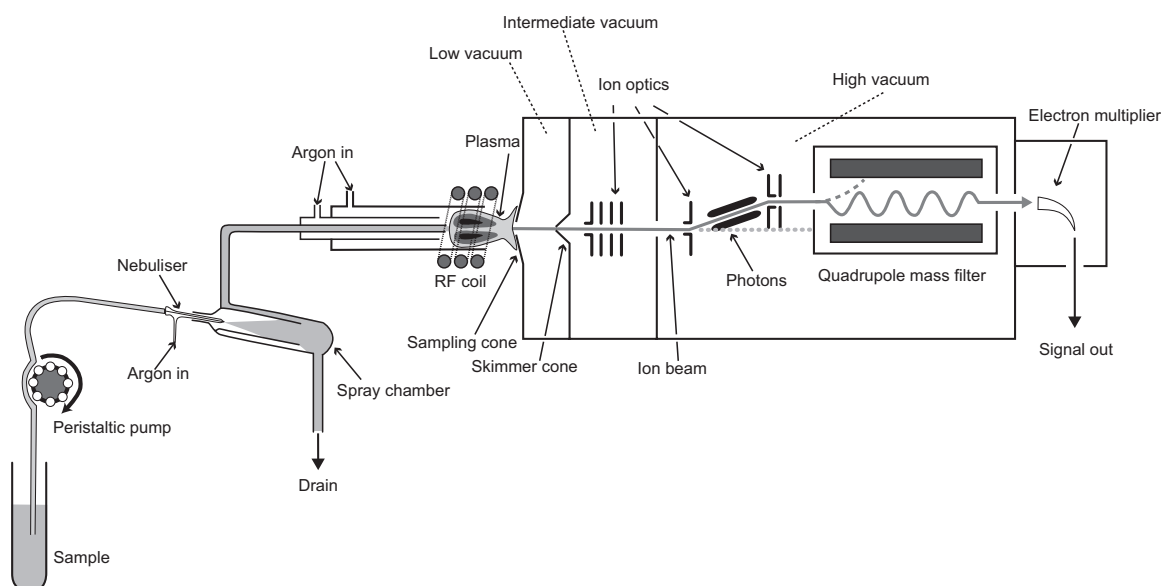


Figure 5.2.: Principal setup of an ICP-MS instrument using a quadrupole analyzer for mass selection. The liquid sample is transformed into a fine mist by the nebuliser, which is then positively ionized in the inductively coupled plasma ion source. After the quadrupole, ions are counted by an electron multiplier. Taken from [126].

The sensitivities for the detection of actinides given in Ch. 2.6, refer to a modified ICP-MS version, the so-called sector field ICP-MS, which uses a combination of a dipole magnet and an electrostatic analyzer (ESA) as mass filter. This results in a considerably better resolution compared to the usual ICP-MS using a quadrupole mass analyzer (ICP-QMS). ICP-QMS suffers from molecular background, like $^{238}\text{UH}^+$ interfering with ^{239}Pu detection. However, background due to tailing from ^{238}U is more severe on the low-mass

5. Chemical recovery of the separation procedure

side and hence, is a source for background on ^{237}Np . For the measurements at HZDR, ^{242}Pu and ^{237}Np solutions with three different concentrations (0.027 ug/L, 0.055 ug/L, 0.075 ug/L) were provided for calibration.

Sample preparation for ICP-MS comprised fuming of the respective fraction with concentrated HNO_3 and 40 % H_2O_2 and re-dissolution in 1% HNO_3 and hence, is only little elaborate. In order to account for drifts during the measurement, an internal standard is added to the sample. Rhodium (^{103}Rh) was used at HZDR, but the corresponding evaluation of the Pu data resulted in recoveries far more than 100 %, so that the internal standard was left out of the calculation. A test series with various internal standards, i.e. ^{232}Th , ^{236}U and ^{175}Lu at SUM, showed some inconsistencies in the final result of the same sample. Therefore, it was decided to conduct complementary measurements at the Institute of Nuclear Waste Disposal at KIT where ^{103}Rh was again used as internal standard.

5.3. Results for Pu and Np recovery

A rather low Np recovery of 48 % was detected and 29 % of the ^{242}Pu spike was found in the Np fraction, when using the ion exchange resin DOWEX 1-x8 and fresh water as matrix material. This is probably because the nitrate concentration for complexation of Pu(+IV) is too low during Np elution with dilute HNO_3 . Consequently, also a part of Pu is eluted from the column. To switch the Pu and Np elution step, however, did not seem feasible, as the resin was completely destroyed after the strong acid HI had passed through. Therefore, further development was focused on increasing the recovery for the procedure based on TEVA. The proposed change from HNO_3 to HCl did not seem promising, since only around 7% of ^{239}Np was found to have passed into the Np fraction, so that this approach was also discarded.

For each set of the most important parameters, which is sample volume and matrix, and the use of UTEVA and $\text{Al}(\text{NO}_3)_3$, selected results for the Np and Pu recovery with 1σ uncertainty are listed in Tab. 5.1. Results in the second half of the table were detected by ICP-MS. A complete list of all separation processes and the respective recoveries can be found in Appendix C. In the first place, these results suggest, that the use of $\text{Al}(\text{NO}_3)_3$ does not make a difference for small sample volumes (500 mL), but for larger volumes of sea water (3 L) the increasing salt concentration leads to a drop of the Np recovery as expected from Ch. 4.2.4. Therefore, the concentration of $\text{Al}(\text{NO}_3)_3$ proposed by Maxwell [11] had to be used for the Pacific Ocean samples, which means that an Al^{3+} separation is required before the Am fraction can be measured. Apart from a first set of measurements at HZDR, all ICP-MS show significantly lower yields for both Pu and Np. The reduced

| sample matrix | volume [ml] | method | Al(NO ₃) ₃ | ²⁴² Pu yield [%] | ^{239/237} Np yield [%] |
|---------------|-------------|------------|-----------------------------------|-----------------------------|---------------------------------|
| fresh water | 20 | TEVA | yes | 88.9 ± 2.8 | 107 ± 10 |
| sea water | 550 | TEVA | yes | 91.4 ± 4.3 | 82.9 ± 7.9 |
| sea water | 550 | TEVA | no | n.a. | 93.1 ± 9.0 |
| sea water | 3000 | TEVA | no | 88.8 ± 4.3 | 66.8 ± 5.9 |
| IAEA-443 | 600 | TEVA | no | 114 ± 12 | 96.9 ± 7.8 |
| sea water | 550 | TEVA+UTEVA | yes | 40.5 ± 4.5 | 49.0 ± 7.2 |
| Pacific Ocean | 2750 | TEVA+UTEVA | yes | 118 ± 8.5 | 50.9 ± 5.7 |

Table 5.1.: Chemical recoveries of Pu and Np tracer in different sample matrices with 1 sigma uncertainties detected by activity measurement (upper half) and ICP-MS (lower half), n.a.: not analyzed.

Pu yield could be explained by the use of the additional UTEVA column, whereas for Np there is no definite explanation at the moment. It is known that the choice of an inappropriate internal standard and a high salt content can lead to wrong ICP-MS results [126]. Problems with the salt content of the Pu fraction have been reported by the HZDR and might explain recoveries of more than 100% which have to be discarded. No such problems were evident for Np and also not for Pu during the measurements at KIT. From the current knowledge, variations in the recovery are interpreted as variations resulting from the chemical separation and not caused by the applied detection technique. Consequently, all processes listed in Appendix C using sea water were included in the calculation of a weighted average for Np and Pu recovery. A recovery of $70 \pm 9.2\%$ was obtained for Pu and $56 \pm 10\%$ for Np, which enters the final result of the Np concentrations in the ocean water.

6. AMS setup and measurements

This work was aiming for the optimization of the Accelerator Mass Spectrometry (AMS) setup and the measurement procedure at the Maier-Leibnitz-Laboratorium (MLL) for the detection of $^{239,240,241}\text{Pu}$ and ^{237}Np and the respective isotopic ratios using the reference material IAEA-443. For this reason, this setup is discussed more detailed in this chapter. The Pacific Ocean water samples, however, were measured at the VERA (Vienna Environmental Research Accelerator) laboratory due to an unexpected, temporary closure of the MLL. Differences between the two AMS setups at the MLL and VERA and differences in the detection method for actinides are presented in this chapter. Further information on AMS and its applications at VERA can be found in [127, 128, 129]. The general introduction to AMS is based on [130].

6.1. Introduction to AMS

AMS is the most sensitive detection method for long-lived radionuclides at present. Like other mass spectrometric techniques, the concentration of a certain radionuclide in a sample is determined by directly counting the ions, and is not based on the detection of the radioactive decay. This makes AMS especially interesting for the investigation of samples with low specific activity, i.e. small sample volumes and for radionuclides with very long half-lives in the order of 10^3 - 10^{10} years. In a very simplified view, a basic AMS setup can be represented by a negative ion source, two mass spectrometers for mass separation connected by a Tandem Accelerator and a particle detector in the end. The Tandem Accelerator which accelerates the ions to energies of up to several MeV/nucleon leads to the complete suppression of molecular background, so that AMS can reach significantly higher sensitivities than regular mass spectrometry. Molecular background is suppressed, because the ions have to pass through a stripping foil or gas at the high-voltage terminal of the accelerator where all the molecular bonds are destroyed. Due to the high energies, nuclear physics principles can be used to separate also stable isobaric background [131] and nuclear particle identification methods can be applied. In this way, concentrations of long-lived isotopes down to 10^{-17} , as in the case of $^{60}\text{Fe}/\text{Fe}$, can be detected [132].

6. AMS setup and measurements

In the beginning of AMS in the 70's, different accelerators than Tandem Accelerators, such as the Berkeley cyclotron, were also used for AMS. The development of AMS was strongly driven by the application to ^{14}C and ^{10}Be dating where the use of electrostatic accelerators was very successful. In the following years, the use of AMS was extended to many different, preferably long-lived, isotopes like ^{26}Al , ^{36}Cl , ^{41}Ca , ^{129}I , actinides as $^{239,240}\text{Pu}$, and ^{236}U but also stable isotopes [133]. The sensitivity of the application to stable isotopes, however, is limited due to their natural abundance in the environment. The determination of ultra low concentrations of long-lived isotopes is of interest in various fields of application, like oceanography (e.g. ^{129}I , ^{14}C), geology (e.g. ^{10}Be , ^{36}Cl), nuclear astrophysics (e.g. ^{53}Mn , ^{60}Fe), environmental science (e.g. $^{239,240}\text{Pu}$, ^{90}Sr) and also biomedicine (e.g. ^{14}C).

Today, AMS systems ranging from small table-top setups with an acceleration voltage of 200 kV (MICADAS) [134] to large facilities with voltages up to 14 MV exist, where many systems are dedicated to ^{14}C dating. The choice of the AMS system, but also the measurement procedure strongly depends on the radionuclide to be detected. ^{14}C is a prominent example for the application of the mentioned small MICADAS system, as its stable isobar ^{14}N does not form negative ions, so that a highly efficient isobar suppression is already achieved in the ion source. Furthermore, the routine AMS method to derive the concentration of a radionuclide with stable isotopes cannot be applied to actinides. The procedure usually used for actinides is presented in Ch. 6.4, to learn more about the detection method for radionuclides with stable isotopes, please refer to [132].

6.2. AMS setup for the detection of heavy nuclides ($m > 140$) at the MLL

A schematic drawing of the AMS setup at the MLL in Munich which features a 14 MV multi-purpose Tandem Accelerator is presented in Fig. 6.1. Negative ions are extracted from a Cesium-sputter ion source and have to pass a first mass separation stage (dipole magnet). The negative ions are injected into the Tandem accelerator and are attracted to the positive potential at the terminal where thin carbon foils are installed. When passing through the foil, electrons are stripped from the ions, resulting in a positive charge. Using the now repulsive potential, the ions are accelerated a second time. The ions are then guided to a second mass separation stage where only ions with the correct momentum/charge ratio are selected. There are two beam lines at the MLL dedicated to AMS: the lower one in Fig. 6.1 is equipped with a Time-of-Flight (ToF) path, a gas-filled analyzing Magnet and a ionization chamber as detection system (GAMS), the upper beam line uses a combination of a Time-of-Flight path with a silicon detector for particle identification. The GAMS beam line is usually chosen for the detection of radionuclides

6.2. AMS setup for the detection of heavy nuclides ($m > 140$) at the MLL

with background from stable isobars, e.g. ^{60}Fe , ^{53}Mn or ^{41}Ca . For a detailed description of this beam line and its application, please refer to [131, 132, 135]. In general, the second beam line (ToF beam line) is used for isotopes without stable isobars, like different actinides [118] or for the search for superheavy elements on earth [8]. Recently, however, the detection of ^{93}Zr by separating it from its stable isobar ^{93}Nb using a passive absorber, has shown promising results [136].

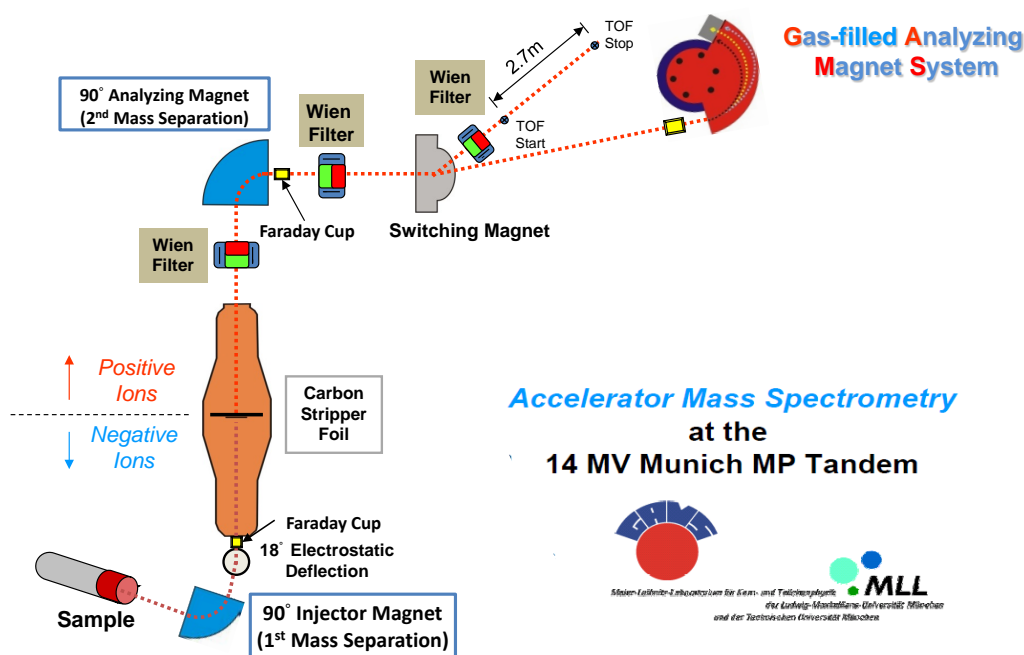


Figure 6.1.: Schematical drawing of the AMS setup at the MLL in Munich.

The experiments for the detection of $^{239,240,241}\text{Pu}$ and ^{237}Np in sea water samples were performed at the ToF beamline, which is therefore presented in more detail in the next subsections along with the other components which are essential for the high selectivity of the AMS setup at the MLL.

6.2.1. AMS injector

The use of a Tandem Accelerator requires the injection of negative ions which are produced in a modified Middleton-type single cathode cesium-sputter ion source [137]. The technical drawing in Fig. 6.2 shows a cross-section of the ion source, of which the general working principle has been reported several times before [132, 135, 138]. Only negatively charged ions are then extracted from the ion source by applying a voltage of 23 kV on the so-called extraction lens which is located directly behind the ion source. In total, the ions enter the first mass separation stage, the injector magnet, with an energy of 28 keV after passing through a pair of electrostatic lenses.

6. AMS setup and measurements

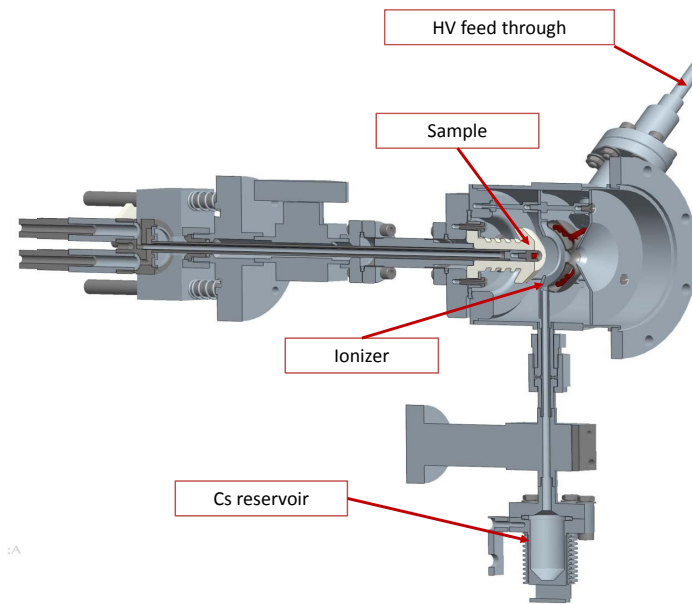


Figure 6.2.: Technical drawing of the single-cathode Cs-sputter ion source. Courtesy of P. Hartung, modified.

The injector magnet is a double focusing 90° dipole magnet with a maximum field strength of 1.2 T and a mass resolution of $\Delta m/m = 2 \cdot \Delta B/B \approx 1/400$ if the 2 mm aperture at the exit of the magnet is used. The ions with selected mass are then pre-accelerated by a voltage of 150 kV, so that they enter the Tandem Accelerator with a total energy of 178 keV.

6.2.2. Tandem accelerator

The Tandem Accelerator, which uses chains for charging, can reach voltages up to 14 MV. The negatively charged ions are accelerated by the positive potential towards the terminal, where a thin carbon foil with a areal density of $4 \mu\text{g}/\text{cm}^2$ is located. When passing through the foil, electrons are stripped from the ions according to Bohr's criterion [139] which leads also to the break-up of molecular bonds and the complete suppression of molecular background. The ions emitted from the foil now have a positive charge distribution, and hence are accelerated a second time by the same terminal voltage which now acts repulsive. Starting from the general case of a singly negative molecular ion which enters the accelerator, the final energy of the ions is given by

$$E_f = \frac{m_{ion}}{m_{molecule}} \cdot E_{PA} + \left(\frac{m_{ion}}{m_{molecule}} + q \right) \cdot e \cdot U_T \quad (6.1)$$

with U_T : terminal voltage, E_{PA} : energy after the pre-acceleration, and q : charge state. For the detection of actinides, a typical terminal voltage of 9 - 10 MV and a charge state

10^+ was used which corresponds to an energy of around 117 MeV.

6.2.3. Beam transport

The chargestate, ore more precisely the $m \cdot v/q$ ratio of the ions to be guided to the detection system is selected by another 90° dipole magnet, called the Analyzing Magnet in Fig. 6.1. For this purpose, the magnet was set to a fixed magnetic rigidity $B \cdot r$ using the maximum magnetic field strength of 1.45 T for actinides. The bending radius of this magnet is $r = 1.6674$ m [140]. Considering the dependency of the magnetic field on the energy and the mass of the ions

$$B \cdot r = \frac{\sqrt{2mE}}{q} \quad (6.2)$$

it is evident, that the energy of the ions and hence, the terminal voltage had to be adjusted when changing between the different isotopes. However, also background ions with a different q and a different E given by eq. (6.1) can pass through the Analyzing Magnet if the mass scales accordingly. In order to suppress isotopic background further, three Wien filter are available. The first one with a mass resolution $\Delta m/m \approx 1/60$ is located between accelerator and Analyzing Magnet, the second ($\Delta m/m \approx 1/20$) behind the Analyzing Magnet and the third one ($\Delta m/m \approx 1/110$) is installed in the ToF beam line. However, the most selective third Wien filter, was out of service during these experiments. To be able to reduce the count rate at the final detection system in order to protect rate sensitive detectors like silicon detectors, three different attenuators can be inserted into the beam line. The attenuators are steel plates with different densities of small holes which define the attenuation factor which is about 1000 for 2 attenuators and 33 for the third one.

6.2.4. Detection system

For the final identification of the ions, which have passed the Analyzing Magnet and also the Wien filters, a Time-of-Flight (ToF) path with a length of $L = 2.7$ m is used, which is shown on the photography of Fig. 6.3. The ions arriving at the start detector of the ToF path have all the same magnetic rigidity, so that the ToF can be expressed in terms of ($B \cdot r$) as

$$ToF = \frac{L \cdot m}{(B \cdot r) \cdot q}. \quad (6.3)$$

Consequently, ions with different mass can be distinguished for a fixed charge q . In order to separate background ions with the same m/q ratio, which leads to an identical ToF,

6. AMS setup and measurements

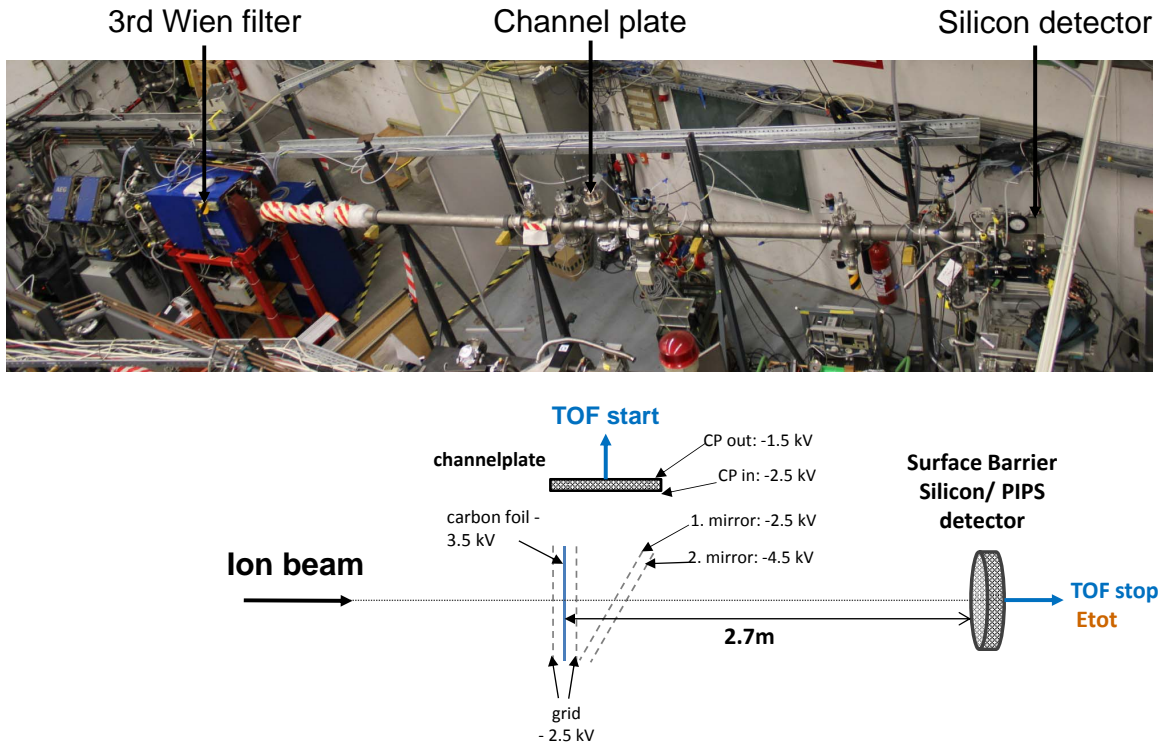


Figure 6.3.: Top: Photograph of the ToF beam line. Bottom: Schematic drawing of the ToF path using a Micro Channel Plate (MCP) to generate the start signal and a silicon detector as stop detector.

an additional energy measurement is required. As shown by eq. (6.1), the energy from the accelerator depends on the charge state.

The start signal is generated by a Micro Channel Plate (MCP) detector. The setup of the detection system, including the MCP and the electron production, is presented schematically in the lower picture of Fig. 6.3. The ions have to pass through a homogeneous carbon foil with a areal thickness of $7 \mu\text{g}/\text{cm}^2$ which causes the emission of secondary electrons from the foil. The electrons are accelerated and then deflected by electric potentials applied to thin grids. The mirror grid, which is installed at an angle of 45° to the carbon foil deflects the electrons into the MCP, where the signal is amplified by electron multiplication. Energy straggling in the carbon foil of the start detector decreases the ToF resolution, but tests with thinner foils were not successful as they were produced less homogeneously and easily broke.

Several modifications of the stop detector, i.e. the energy measurement, have been carried out in this project. In a first step, the ionization chamber with a segmented anode for energy loss measurements was removed. The ionization chamber served as a possibility to separate isobars due to their difference in their atomic number and hence, in the stopping

power. If actinides are considered, the relative difference in the atomic number is around $1/94 \approx 0.01$. The corresponding difference in energy loss at the energies available is hardly detectable by this type of ionization chamber. However, the gas (2 - 7 mbar isobutane) causes energy straggling which then leads to an additional broadening of the ToF signal and hence, worsens the isotopic resolution. The primary aim was to improve the separation between ^{239}Pu and ^{238}U (compare Ch. 6.4.1), so that for this project the silicon surface barrier detector was used as stop detector and for the energy measurement. A ToF resolution of around 0.62 ns FWHM for $^{238}\text{U}^{10+}$ was obtained with this setup. A further improvement (0.41 ns FWHM for $^{238}\text{U}^{10+}$) was achieved by replacing the surface barrier detector by a PIPS (Passivated Implanted Planar Silicon) detector from Canberra [141] coated with a 25 - 35 nm thick aluminum layer for better timing performance and an active area of 450 mm². Naturally, the aluminum layer leads to a worse energy resolution, which is not a problem, as the different charge states are well separated in energy. A description of the electronics and the data acquisition for the TOF beam line in general can be found in [142]. Only the signals of the MCP and the silicon detector were processed further in this project.

6.3. AMS setup at VERA laboratory

In contrast to the MLL, the Vienna Environmental Research Accelerator (VERA) which was built up in the late 1990's, is exclusively dedicated to AMS. The layout of the facility is presented in Fig. 6.4, where also the resolutions of the different separation devices are given. The central elements are a 3 MV Pelletron tandem accelerator produced by National Electrostatic Cooperation (NEC) as well as a multi-cathode Cs sputter ion source. This ion source contains a target wheel with 40 sample positions, so that samples can be changed automatically during the measurement. In Fig. 6.4 off-set Faraday cups for beam current measurement are marked behind the Injector Magnet and the Analyzing Magnet. Both magnets can be operated in bouncing mode, which enables the sequential injection of a stable isotope measured in the off-set cup and the radioisotope which is transmitted to the particle detector. Thus, the precision of the measurements is improved, as this fast cycling system enables measurement durations of only ms. However, the off-set cups are not of further interest for the detection of actinides, as there are no stable isotopes.

The tandem accelerator was operated at a terminal voltage of 1.7 MV with He as stripper gas ($\cong 1 \mu\text{g}/\text{cm}^2$) and using charge state 3+ during this project as an enhancement of the detection efficiency compared to the previously used charge state 5+ had been observed in previous studies [143]. Another major difference to the setup at the MLL is the electrostatic analyzer (ESA) which is located after the Analyzing Magnet and which

6. AMS setup and measurements

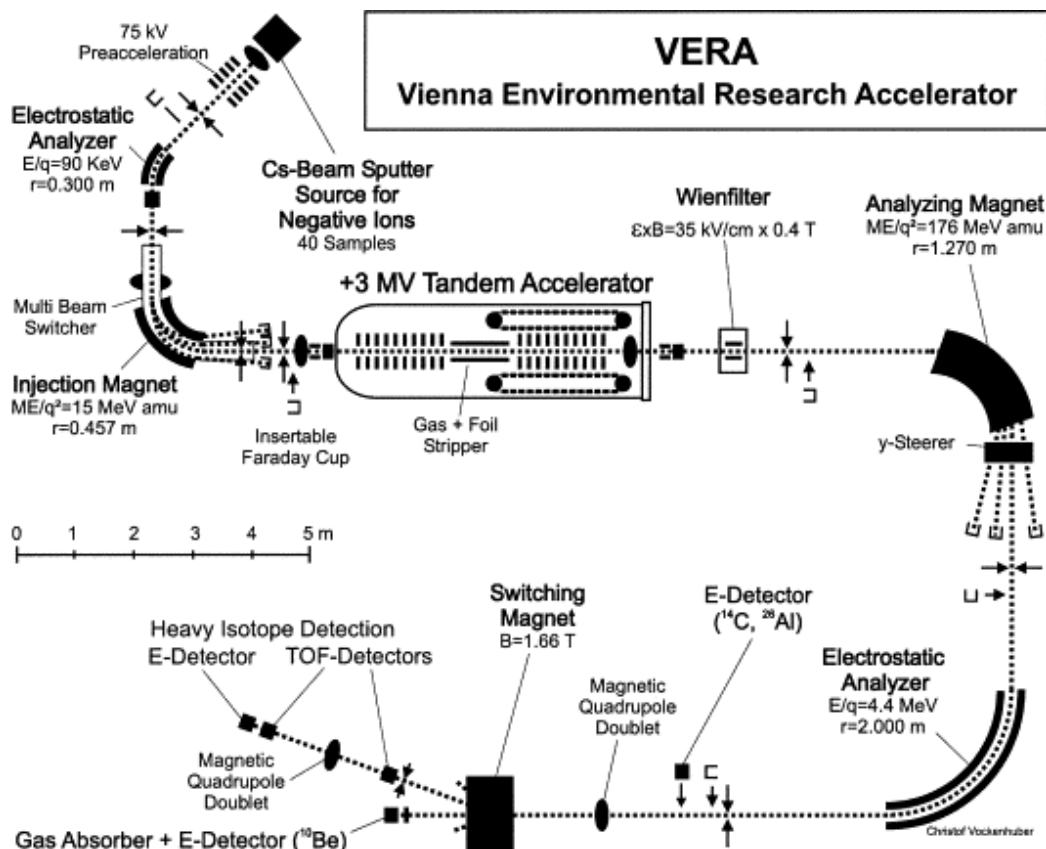


Figure 6.4.: Layout of the AMS set-up at VERA after the upgrade in 2004 for the detection of nuclides with masses larger than 150 amu. The ion source is shown in the left upper corner, the detector in the lower left corner of the drawing. Taken from [129].

was operated at ± 50 kV. From the equilibrium of electrical and centrifugal force, it can be derived that the ESA selects a specific energy E

$$E = \frac{1}{2} \cdot q \cdot E_{el} \cdot r \quad (6.4)$$

with

r : radius of the ESA

E_{el} : electrical field of the ESA

with a resolution of ΔE (FWHM)/ $E = 1/670$. As the m/q ratio is fixed by the Analyzing Magnet, the ESA acts as a high-resolution velocity filter in addition to the Wien filter at the exit of the accelerator. Recently (in 2015), another 90° magnet was installed after the switching magnet (not shown in Fig. 6.4) which efficiently suppresses background with deviating momenta. The ions which remain after the different separation steps are detected in a Bragg-type ionization chamber where the energy of the ions is measured.

The ToF path which is available in this beam line as marked in Fig. 6.4 was not required for the actinide measurements in this project.

6.4. Measurement procedure for Pu and Np

An AMS measurement of actinides differs significantly from standard AMS isotopes like ^{14}C , ^{10}Be or ^{26}Al . As there are no stable isotopes to produce a macroscopic beam, the tuning of the beam and hence, the transmission through the setup cannot be continuously monitored by reading the beam current using Faraday cups. For the same reason, the sample has to be spiked with another, appropriate long-lived isotope, to be able to determine the concentration of the isotope of interest in the initial sample taking into account the detection efficiency of the respective setup. Whereas actinides, especially ^{236}U but also $^{239,240}\text{Pu}$ are routinely measured at VERA, this was not the case for the AMS at the MLL, so that a measurement routine first had to be established. The specific requirements of the different isotopes are discussed in the following.

6.4.1. Challenges of measuring $^{239-241}\text{Pu}$ and ^{237}Np

Interfering ^{238}U , which is injected into the tandem accelerator as a $^{238}\text{UH}^-$ compound, can lead to background at mass 239 and hence, deteriorates the detection of ^{239}Pu . Especially scattered ^{238}U particles form a low energy tail resulting in a longer ToF which may overlap with the ^{239}Pu signal. As explained before, at the MLL, the $^{238}\text{UH}^-$ compound is broken up at the terminal of the accelerator and the resulting $^{238}\text{U}^{10+}$ is suppressed by the subsequent mass separation stages according to their mass resolution. However, it has to be considered, that the primordial nuclide ^{238}U is present in the Pacific Ocean at a concentration of $3.3 \mu\text{g/L}$ [144], which is 9 orders of magnitudes higher than the expected ^{239}Pu concentration. With the third Wien filter not working, the setup was able to suppress ^{238}U by around 5 orders of magnitude, so that the remaining ^{238}U still causes strong isotopic interference on mass 239 (see Fig. 6.6 (a)). Therefore, several measures were taken to decrease the U concentration already during sample preparation, like the use of supra- or even ultra-pure reagents and the additional U/TEVA column for U separation (compare Ch. 4.2.5). Furthermore, the resolution of the ToF was enhanced by the PIPS detector as stop detector. The results were very satisfying (compare Fig. 6.7 (b) and Ch. 7.1) and this modified procedure was then applied to the ocean water samples. At VERA, charge state 3+ is chosen for detection of actinides, to profit from a higher stripping yield. However, it was shown by Lachner et al [145], that actinide-hydride molecules in charge state 3+ do exist, i.e. $(^{238}\text{UH})^{3+}$ can cause isobaric background at

6. AMS setup and measurements

mass 239. To estimate the background from $(^{238}\text{UH})^{3+}$, a run on mass 239 in a pure Uranium sample (Vienna-US8 with $^{236}\text{U}/^{238}\text{U} = 1.03(7)\cdot 10^{-8}$) was performed, where 0 counts were detected which corresponds to an upper sensitivity level of $^{238}\text{UH}^+/^{238}\text{U} = 8.9\cdot 10^{-11}$. Then, in the Pacific Ocean water samples, the rate of ^{234}U was measured to scale the background level on mass 239 to the Uranium concentration in the ocean sample. This leads to an upper limit for the number of background counts due to $(^{238}\text{UH})^{3+}$ between $5\cdot 10^{-5}$ and 10^{-3} during one run which is negligible compared to a minimum number of $m = 239$ counts per run of 10. Due to high-resolution ESA and the second 90° magnet on the high energy side, $^{238}\text{U}^{3+}$ is efficiently filtered out before it can reach the ionization chamber. ^{240}Pu can be very well separated from ^{238}U by the AMS setup at the MLL as well as at VERA, due to the larger difference in mass.

A separation of ^{241}Pu from its isobar ^{241}Am by means of usual AMS is not possible. The isobar is present in the sample as it is continuously produced by the β^- decay of ^{241}Pu . The dipole magnets, the Wien filter but also the ESA are mass selective. As discussed with respect to the ionization chamber, the relative difference in atomic number is too small to obtain a measurable difference in energy even after the passage through solid matter like SiN foils. At sufficiently high energies, isobar separation is possible by a strong gas-filled magnet or complete stripping of the electrons. As both techniques cannot be applied at the MLL or VERA, the isobar has to be separated very efficiently by the chemical Pu extraction method presented in Ch. 4.2.4.

The detection of ^{237}Np by mass spectrometry in general is difficult, not because of the background situation, but due to the lack of commercially available, suitable spike material. With a half-life of $1.54\cdot 10^5$ a, ^{236}Np would be a candidate spike material for an AMS measurement. But the production rates of ^{236}Np in a cyclotron via $^{235}\text{U}(\text{d},\text{n})^{236}\text{Np}$ or $^{238}\text{U}(\text{p},3\text{n})^{236}\text{Np}$ are low and depending on the p energy, also considerable amounts of ^{237}Np are produced [12]. The second nuclide which has been already discussed as spike material and which can be produced with a lower ^{237}Np contamination, is ^{235}Np ($T_{1/2} = 396$ d) [146]. Apart from the production by proton bombardment on an U target, ^{235}Np could be also produced via $^{232}\text{Th}(\text{}^6\text{Li},3\text{n})^{235}\text{Np}$ using a large tandem accelerator, e.g. at the MLL. The irradiated material needs to be purified from radioactive co-products and the target material ^{232}Th . Furthermore, a careful characterization regarding the produced concentration of ^{235}Np and possible ^{237}Np contamination has to be done before it can be used as spike for ^{237}Np detection. Both possible spike materials were not available during this project.

6.4.2. Injector and beam tuning

In general, actinides are extracted from the ion source as a single oxygen compound AcO^- [147, 148] but show rather low negative ion yields of around 0.6% [7]. Since a higher current of ThO_2^- (~ 20 nA) extracted from a ThO_2 sputter cathode was measured at the Faraday Cup in front of the accelerator compared to ThO^- (nA), several Pu compounds (PuO^- , PuO_2^- , PuO_3^- , PuF^- , PuCu^-) were tested in this study at the MLL. No stable beam can be produced out of the mentioned Pu compounds as even the ^{242}Pu spike is present only in microscopic amounts so that a beam current measurement is not possible. Therefore, event rates of ^{242}Pu relative to ^{242}Pu extracted as PuO^- in the detector were compared. The event rates from all tested compounds were lower than for PuO^- . Consequently, Pu and Np were extracted from the sea water samples as PuO^- and NpO^- , respectively, also at VERA.

For beam tuning, a $^{209}\text{BiO}^-$ beam (~ 40 nA on cup in front of accelerator) was extracted from a Bi cathode. Since the magnetic components after the accelerator are mass dependent, the mass of the beam used for tuning has to be as close as possible to the actinides. A U sputter target was not used for this purpose, to avoid a macroscopic contamination of the ion source with U. With the Analyzing Magnet fixed to its maximum value of 1450 mT, charge state 9+ at a terminal voltage of 11.0 MV was chosen. This magnetic rigidity corresponds to charge state 10+ using a terminal voltage of 10.8 MV with a stripping yield of 18% for ^{239}Pu . Charge state 10+ was chosen because of a favourable background situation with respect to lower charge states (see Fig. 6.6 (a)-(c)). A $^{232}\text{Th}^{10+}$ beam extracted as ThO_2^- from a ThO_2 sputter cathode was used to correct the tuning for higher masses than ^{209}Bi . The magnetic field of the Wien filter is set to a fixed value, whereas the electric field is optimized on the beam current like all the other electrical and magnetic lenses. When changing between isotopes or charge states, the electric field of the Wien filter has to be scaled accordingly.

At VERA, an $^{238}\text{U}^{3+}$ beam extracted as $^{238}\text{UO}^-$ from a U target (Vienna-KkU with $^{236}\text{U}/^{238}\text{U} = (6.98 \pm 0.32) \cdot 10^{-11}$) was used for tuning. At a terminal voltage of 1.65 MV, the ions are accelerated to an energy of 6.7 MeV with a stripping yield of 42-50% [143].

6.4.3. Detector calibration

To be able to identify the counts measured by the detector, the signals from the particle detection system at the MLL had to be calibrated in terms of time and energy, respectively. For this purpose, different stable beams, like $^{197}\text{Au}^{7,8+}$, $^{209}\text{Bi}^{8,9+}$ and $^{232}\text{Th}^{10+}$ were attenuated if necessary and guided into the detector. The energy and the ToF can

6. AMS setup and measurements

be calculated with eq. (6.1) and (6.3), respectively. Additionally, the results from these equations have to be corrected by the energy loss of the ions in the carbon foil of the start detector. The relative energy loss was determined to be 0.3% by detecting the energy of $^{238}\text{U}^{10+}$ extracted from a ThO_2 sample, first with the start detector inserted into the beam line and then, without detector. The measurement without start detector could not be done with a stable beam, as the attenuators form a heterogeneous beam with spots of increased dose rate on the silicon detector which seems to be locally damaged, as a decrease of energy resolution and an increase of leakage current was observed. The position of the different ion species in the E-ToF-spectrum, which is shown in Fig. 6.5 as a superimposition, can be assigned to the calculated energy and ToF so that both axes can be calibrated by linear interpolation.

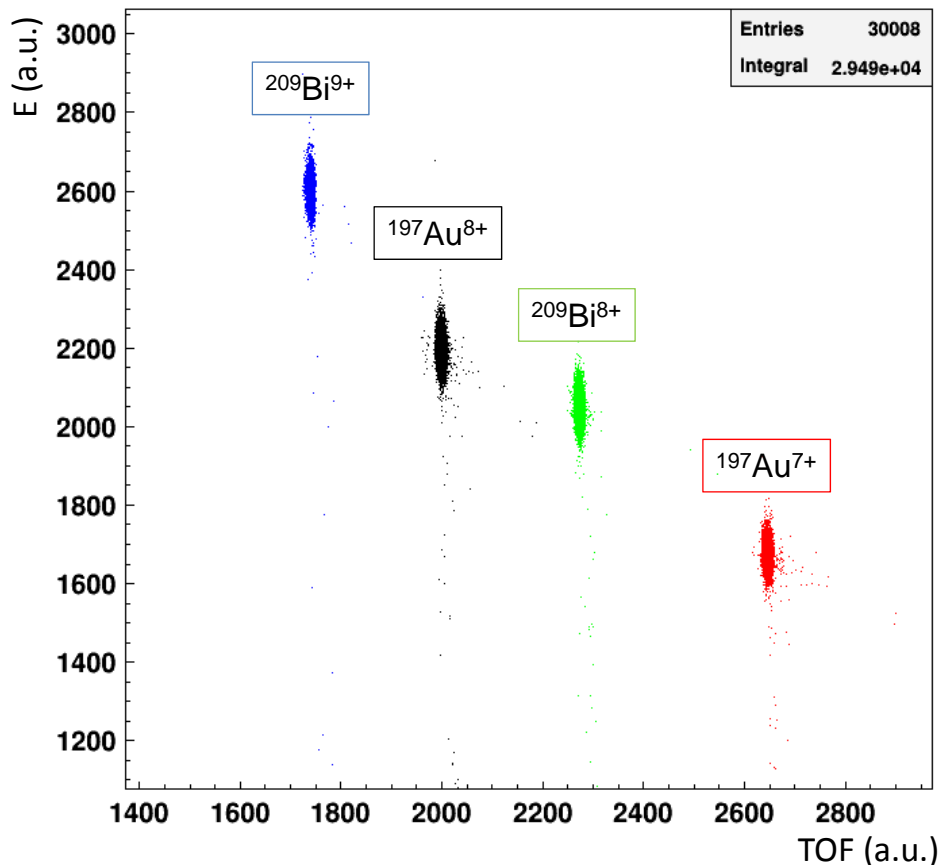


Figure 6.5.: Measurements with different stable beams presented in different colours, superimposed on each other. The position in the spectrum can be used to calibrate the axes, as energy and ToF are known.

For ion identification with the Bragg-detector of VERA, a pulse width at constant height versus pulse height spectrum is used, which has proven to be very efficient to distinguish pile-up from real events [149]. A calibration of this spectrum in eV is not required, as

6.4. Measurement procedure for Pu and Np

actinides in charge state 3+ arrive at approximately the same position in the spectrum, as demonstrated by Fig. 6.6 (d) where two measurements with $^{236}\text{U}^{3+}$ (red) and $^{234}\text{U}^{3+}$ (blue) settings are shown superimposed. As differences in energy are very small between the masses to be detected, a general Region of Interest (ROI) can be defined for all actinides in charge state 3+ using the example of $^{236}\text{U}^{3+}$ (red square in Fig. 6.6 (d)). If nuclides with higher count rates are considered, like ^{234}U which has an isotopic abundance of 0.0054 %, the ROI has to be extended to lower pulse widths (blue square). Although, background with differing m/q are suppressed efficiently by the dipole magnets, nuclides with lower q and m forming the same m/q ratio, and which are not filtered out by the ESA, might arrive at the detector and show up in the low energy tail in the lower left corner of the spectrum (compare Fig. 6.6 (e) and (f)). Pile-up of these background events appear as a back-bending belt parallel to that of the 3+ pile-up events shown in Fig. 6.6 (d) but on its left side. Consequently, the left and right borders of the ROI have to be carefully set. The red square was considered to fulfill these requirements and hence, was used for the evaluation of the data.

6. AMS setup and measurements

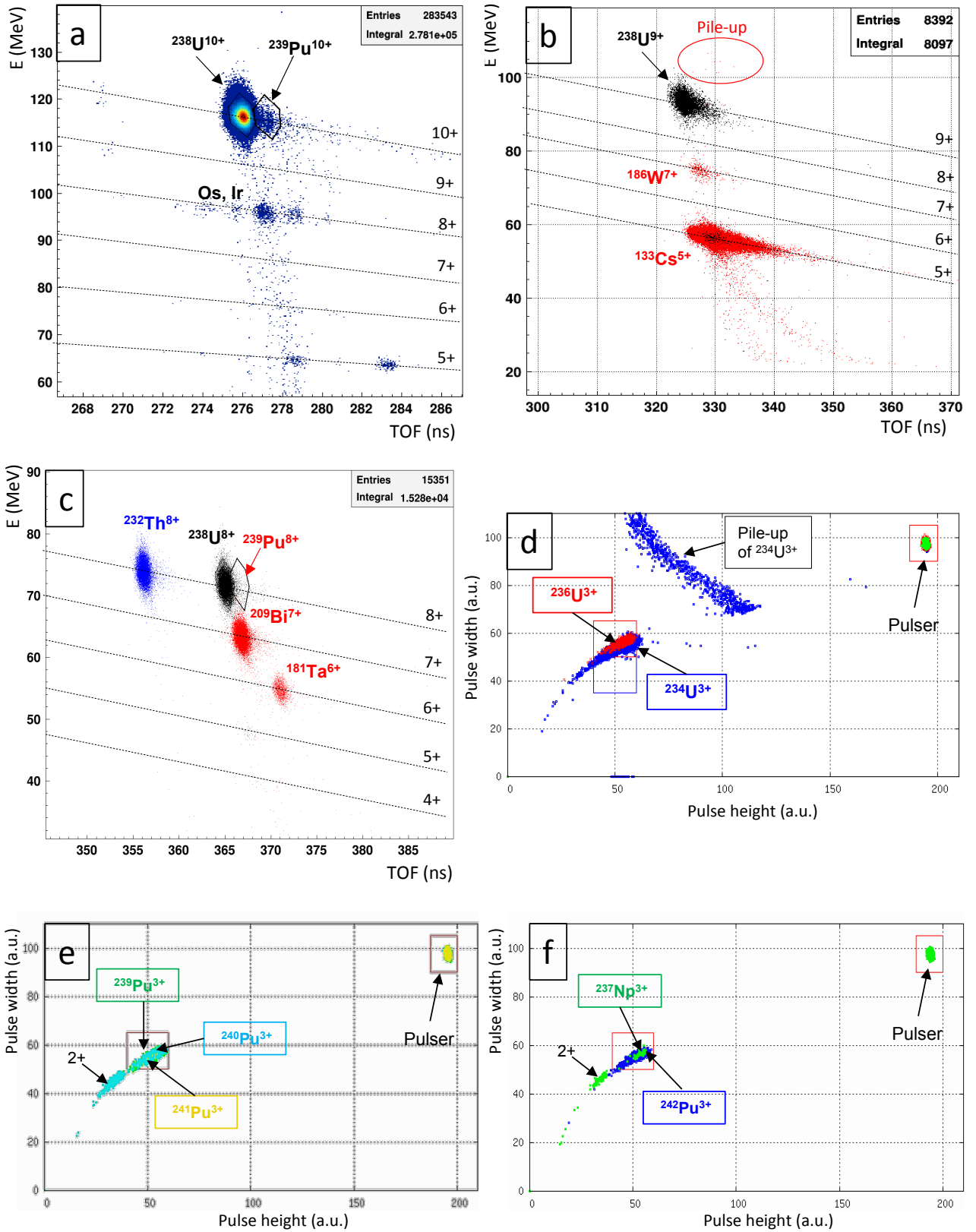


Figure 6.6.: Examples of some typical AMS spectra obtained at the MLL (a)-(c) and at VERA (d)-(f). Apart from figure (a), the figures are overlays of two or more separate spectra measured with different settings. (a) IAEA-443 sample with settings on $m = 239$ suffering from a strong ^{238}U background. (b) ThO_2 sample with settings on $m = 238$ (black) and $m = 239$ (red). For $m/q = 239/9$, Cs, probably from the ion source, caused a count rate, which was too high for the Si detector. (c) ThO_2 sample with settings on $m = 232$ (blue), $m = 238$ (black) and $m = 239$ (red). ^{209}Bi , used for beam tuning, interferes with the $^{239}\text{Pu}^{8+}$ measurement. (d) Vienna-US8 sample with settings on $m = 234$, $q = 3+$ (blue) and $m = 236$, $q = 3+$ (red), with the red square representing the ROI for actinides with $q = 3+$ at microscopic amounts and the blue square for macroscopic amounts with high count rates. (e) Pacific Ocean water sample with settings on $m = 239$ (green), $m = 240$ (light blue) and $m = 241$ (yellow) with $q = 3+$. For $m = 240$, background from charge state $2+$ is visible. (f) Pacific Ocean water sample with settings on $m = 237$ (green), $m = 242$ (blue) with $q = 3+$. For $m = 237$, background from charge state $2+$ is visible.

6.4.4. Measurement principle

In general, the measurement procedure for $^{239-241}\text{Pu}$ and ^{237}Np at the MLL and VERA was similar. But because of the fast cycling system and the higher detection efficiency (see Ch. 6.4.4) at VERA, the typical measurement durations were kept shorter but were repeated more often, to increase the precision of the measurements. Because of the specific detection systems of the two AMS setups, the data evaluation had to be adjusted accordingly. The discussion of the measurement principle in this section focuses on the procedure for VERA, which applies to the Pacific Ocean samples.

Plutonium

As explained before, $^{239-241}\text{Pu}$ has to be measured relative to the ^{242}Pu spike, in order to take possible transmission losses and variations of the ion yield into account. In a first set of experiments with background samples at VERA, the ^{242}Pu spike was measured before and after the actual $^{239-241}\text{Pu}$ measurements. However, the output of the ion source seemed to increase strongly during the $^{239-241}\text{Pu}$ runs, as unexpectedly high $^{240}\text{Pu}/^{239}\text{Pu}$ ratios were observed. Consequently, in the following beam time, Pu was measured in the order ^{242}Pu , ^{239}Pu , ^{242}Pu , ^{240}Pu , ^{242}Pu , ^{241}Pu , ^{242}Pu , which is named a sequence. The measurement of an individual isotope is denoted by “run” in the following. The detected events N in each run were divided by the run time t to obtain the event rate R , e.g. for

6. AMS setup and measurements

^{239}Pu

$$R(^{239}\text{Pu}) = \frac{N(^{239}\text{Pu})}{t} \quad (6.5)$$

where the detected events N correspond to the number of events located in the ROI defined in Ch. 6.3.3. The run time was chosen according to the expected concentration of the respective isotopes and then fixed for all measurements. For the measurement of the Pacific Ocean water samples, run times were set to 30 s for ^{242}Pu , 100 s for ^{239}Pu , 250 s for ^{240}Pu and 300 s for ^{241}Pu . To calculate the number of ^{239}Pu atoms in the sample, $R(^{239}\text{Pu})$ was normalized to the average rate of ^{242}Pu , $R_{av}(^{242}\text{Pu})$ obtained from the ^{242}Pu run before and after the ^{239}Pu run. The number of ^{239}Pu atoms in the sample $N_0(^{239}\text{Pu})$, was obtained by multiplying the ratio of $R(^{239}\text{Pu})/R_{av}(^{242}\text{Pu})$ with the initial ^{242}Pu spike, $N_0(^{242}\text{Pu})$, which was added before the chemical element separation

$$N_0(^{239}\text{Pu}) = \frac{R(^{239}\text{Pu})}{R_{av}(^{242}\text{Pu})} \cdot N_0(^{242}\text{Pu}) \quad (6.6)$$

In this way, also losses during the chemical sample preparation were included in the result for $N_0(^{239}\text{Pu})$. The number of $^{240,241}\text{Pu}$ was calculated similarly. Naturally, for a correct result, the ROI had to be applied in the same way to the ^{242}Pu spike as to the $^{239-241}\text{Pu}$ isotopes. The described sequence was measured three times, before switching to the next sample holder. After each sample on the target wheel was measured in this way (one turn of the sample wheel), the described measurement procedure was repeated. For the Pacific Ocean water samples, between 3 and 4 turns of the target wheel were performed. The final result for the number of atoms of the respective isotope was obtained by calculating the arithmetic mean from the results of the individual runs.

At the MLL the general measurement sequence was the same, but the Ag-current on the cup before ($I_1(\text{Ag})$) and after ($I_2(\text{Ag})$) the radioisotope run was read in addition to take variations in the output of the ion source into account. Therefore, the events in the detector were normalized to an effective charge

$$Q_{eff} = \frac{I_1(\text{Ag}) + I_2(\text{Ag})}{2} \cdot t \quad (6.7)$$

to obtain the event rate R . The following calculation of N_0 was the same as for VERA. Due to the ToF measurement, the evaluation of the data to determine the number of counts of the respective isotope was different. A cut (2-dimensional window) was drawn around the $^{242}\text{Pu}^{10+}$ events as shown by the solid black line in Fig. 6.7 (a). This cut defined the number of ^{242}Pu events, $N(^{242}\text{Pu})$ used in the data analysis. In the run on mass 239 measured in between the two corresponding ^{242}Pu runs, the ^{242}Pu cut was then moved to the position of $^{239}\text{Pu}^{10+}$ in the spectrum according to its calculated energy and ToF (see Fig 6.7 b). The counts located in this cut were used as number of ^{239}Pu events, $N(^{239}\text{Pu})$. This method was also applied similarly to ^{240}Pu and ^{241}Pu . The initial number of atoms in the sample, was calculated as described before for VERA.

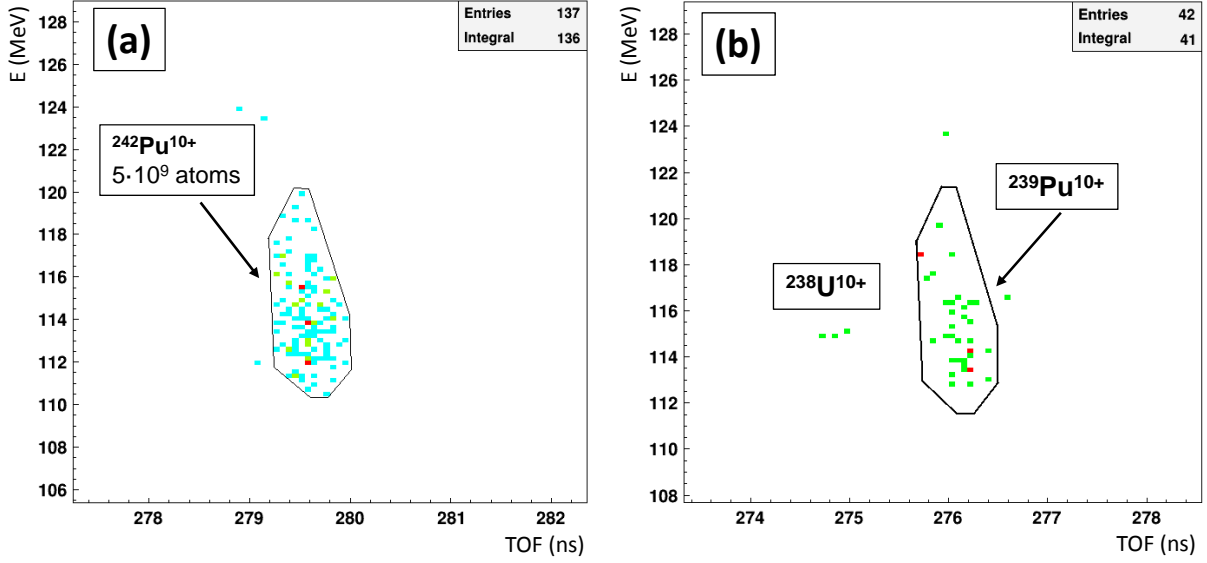


Figure 6.7.: E versus ToF spectrum of $^{242}\text{Pu}^{10+}$ spike (a) and $^{239}\text{Pu}^{10+}$ (b) in a sea water sample (IAEA-443) measured at the MLL. The solid black line represents a cut on the $^{242}\text{Pu}^{10+}$ events, which is shifted according to the calculated ToF and E of $^{239}\text{Pu}^{10+}$ to evaluate the number of counts.

Neptunium

Because of the lack of a suitable spike material for ^{237}Np , the detection method proposed by Fifield et al [150] was applied. A ^{242}Pu spike added to the Np fraction after the chemical separation is used to monitor the transmission through the AMS setup. The yield of negative ion formation for Np is determined relative to Pu with a sample of known $^{237}\text{Np}/^{242}\text{Pu}$ ratio (compare Ch. 4.3). In contrast to [150], ^{239}Np could not be used as chemical yield monitor in this study, as it decays to ^{239}Pu , which might lead to a contamination in the Pu fraction which cannot be characterized. For this reason, a constant correction factor for the chemical Np recovery $\epsilon = 0.56 \pm 0.10$ was assumed, which was calculated as weighted average from the results presented in Ch. 5.3.

A usual sequence for the ^{237}Np determination in a sample at VERA and the MLL contained three runs in the order ^{242}Pu , ^{237}Np , ^{242}Pu . Similar to the Pu measurements, the number of ^{237}Np atoms extracted from the cathode, $n(^{237}\text{Np})$, can be obtained by putting the ^{237}Np and ^{242}Pu rates in relation

$$n(^{237}\text{Np}) = \frac{R(^{237}\text{Np})}{R_{av}(^{242}\text{Pu})} \cdot N_0(^{242}\text{Pu}) \quad (6.8)$$

For the initial number of atoms in the sea water sample, the chemical Np recovery and the negative ion yield correction factors ϵ and η , respectively, have to be taken into account:

$$N_0(^{237}\text{Np}) = \frac{R(^{237}\text{Np})}{R_{av}(^{242}\text{Pu}) \cdot \epsilon \cdot \eta} \cdot N_0(^{242}\text{Pu}) \quad (6.9)$$

6. AMS setup and measurements

At VERA, this sequence was repeated three times, before switching to the next sample holder. The same sequence as for the Np cathodes was applied to the Np/Pu standards three times in a turn of the wheel, so that an experimental value for the $^{237}\text{Np}/^{242}\text{Pu}$ ratio was determined by using the mean of the three sequences. In total, three standard samples had been placed on the target wheel, so that always two different standards were measured before and after a number of ocean water samples. Normalizing the experimental ratio to the initially applied spike ratio $(^{237}\text{Np}/^{242}\text{Pu})_0$ gives the negative ion yield correction factor η

$$\eta = \frac{^{237}\text{Np}/^{242}\text{Pu}}{(^{237}\text{Np}/^{242}\text{Pu})_0} \quad (6.10)$$

An overall relative negative ion yield of 1.3 ± 0.6 was determined in a beam time at VERA which is in agreement with the value of 0.77 ± 0.03 measured by Fifield et al [150]. However, the very large error of almost 50% accounts for large fluctuations in the individual results, in particular between different standard samples. This demonstrates the urgent need for a spike material which serves as a chemical yield monitor as well as a spike for the AMS measurement, in order to obtain reliable results for the ^{237}Np concentration. The data evaluation and analysis happened analogue as for Pu.

6.4.5. Detection efficiency

The detection efficiency was not explicitly determined in this project, as it is already taken into account by the detection of the ^{242}Pu spike. However, previous experiments determined a detection efficiency at VERA for $^{236}\text{U}^{3+}$ in the order of $5 \cdot 10^{-4}$ using He as stripper gas [143]. The detection efficiency at the MLL can be roughly estimated by using the transmission of the ^{209}Bi beam from one Faraday cup to the next. Here, the dominating factor is the very low negative ion yield for actinides of only 0.6% as already stated before. Usually, the $^{209}\text{BiO}^-$ beam can be tuned to the cup at the entrance of the accelerator with a transmission of around 30%. The transmission through the accelerator until the cup behind the Analyzing Magnet (Cup 5) for $^{209}\text{Bi}^{9+}$ is approximately 20%. The stripping yield of actinides in charge state 10+ with the same magnetic rigidity as $^{209}\text{Bi}^{9+}$ is approximately the same or even higher. The beam on the cup after the switching magnet, which is the last cup for current measurement during a run, can be tuned to 70% of the current at Cup 5. An detection efficiency of the detector of around 30% with MCP inserted into the beam line, was determined by using an attenuated $^{209}\text{Bi}^{9+}$ beam. That gives an overall detection efficiency for very heavy ions of roughly $7 \cdot 10^{-5}$.

6.5. Analysis of uncertainties

Spike solutions and measurement

The uncertainty of the ^{242}Pu concentration in the IRMM085 spike solution is stated as 0.148 % in the certificate (see Appendix F). During the dilution series an additional uncertainty is introduced by the weighing of the solution. A conservative estimate of 0.0005 g for the uncertainty of the balance was made. The uncertainty of the spike and the balance were quadratically added. The resulting uncertainty of the dilutions and finally also the spike added to the sample was calculated by Gaussian error propagation. The uncertainty introduced by the spike was calculated to be 1.0 %. The uncertainty of the ^{237}Np solution was discussed already in Ch. 4.3.2 and the resulting error of the spike added to the sample of up to 10 %, was calculated in the same way as for the ^{242}Pu spike. The ^{242}Pu spike count rate was calculated as a mean value of the measurements before and after the respective run of $^{239-241}\text{Pu}$. As the number of events of the individual ^{242}Pu runs was generally higher than 50 events, a normal distribution with an uncertainty of \sqrt{N} was assumed. However, the error of the mean ^{242}Pu count rate $\Delta\bar{R}$

$$\Delta\bar{R} = \left(\frac{1}{n(n-1)} \sum_i^n (R_i - \bar{R})^2 \right)^{1/2} \quad (6.11)$$

with n : number of runs, here $n = 2$

was usually larger than the propagated statistical uncertainty. This can be explained by variations in the output of the ion source. As the two errors are correlated, because the number of detected ^{242}Pu increases with the output of the ion source, they were added linearly.

Statistical uncertainty at low count rates

For very low numbers of counts, i.e. below 20 events, confidence intervals as proposed by Feldman and Cousins [151] were used, which result in an asymmetric negative and positive error. For example, the detection of zero events corresponds to a 1σ interval from 0.00 to 1.29 events. For larger N , the interval approaches the results of a symmetrical distribution. The error for the initial number of atoms in the sample of the individual runs was calculated by Gaussian error propagation including also the error of the ^{242}Pu spike and of the spike measurement.

Final result for the concentration

A χ^2 -test as proposed by the Particle Data Group [152] was applied to the results of the individual runs, to check whether the deviation from the mean value \bar{N}_0 is due to

6. AMS setup and measurements

statistical fluctuations. χ^2 was calculated for i measurements as

$$\chi^2 = \sum w_i (N_{0i} - \bar{N}_0)^2 \quad (6.12)$$

with $w_i = 1/(\Delta N_{0i})^2$

For measurements with $\chi^2/(N-1) \leq 1$, the error of the mean number of atoms in the initial sample was simply calculated by Gaussian error propagation. For measurements with $\chi^2/(N-1) > 1$ the error was scaled up by the factor

$$S = (\chi^2/(n-1))^{1/2} \quad (6.13)$$

with n : number of runs.

Only for measurements with large count rates, a χ^2 larger than one was obtained, as the corresponding statistical errors were correspondingly small. For those measurements the error is dominated by variations in the setting of the instrument, e.g. the output of the ion source or beam stability, which is taken into account in the final result by the scaling factor. For two measurements the χ^2 was calculated to be even larger than 5.

Negative ion yield correction factor η

In general, the error analysis for the Np measurements worked similar to the Pu measurements. However, the error of the negative ion yield correction factor η had to be also included. In a first step, the error of η obtained from the individual sequences was calculated by Gaussian error propagation including the statistical error of both, the ^{242}Pu and the ^{237}Np , with an uncertainty of \sqrt{N} , and the uncertainty of the added spike solution which was already discussed before. The error of the mean value of three subsequent sequences was calculated in an analogous way to the mean ^{242}Pu rate of the ^{242}Pu spike measurement. The same approach was applied, to obtain the resulting error of the average η calculated from the measurements of two different standards measured before and after the ocean water samples.

7. Results and Discussion of the Ocean Water Samples

The quantity obtained by an AMS measurement of actinides is the number of atoms in the respective sample which was used for the calculation of the isotopic ratios. For the discussion of the concentrations in the Pacific Ocean, the number of atoms was normalized to the sample mass, which was measured before evaporation with an uncertainty of 0.1 kg. For three sample, the volume was determined instead, which leads to a higher uncertainty of 0.5 L. To compare the results of this work directly with previously published data, all concentrations of Pu in Pacific Ocean water were additionally converted into mBq/m³. For this purpose, a density of sea water of 1026.4 kg/m³ was assumed, using the average measured salinity of the samples of 34.25 in terms of PSU (Practical Salinity Unit) and a mean temperature of 10° C at longitude 50° North [153].

7.1. IAEA-443

298 g of the reference material IAEA-443 were prepared as described in Ch. 4.2 for ^{239,240}Pu and ²³⁷Np analysis and additional 500 g were processed for ²⁴¹Pu detection, to obtain good statistics. From the specific activity of the respective isotopes given in [103], the number of atoms per kg sample material was calculated. The value for ²⁴¹Pu was decay corrected to 01.12.14, the date when Pu and Am were separated. These values are referred to as literature values in the following. A spike of $2.8 \cdot 10^9$ ²⁴²Pu atoms was added to the smaller sample and $7.2 \cdot 10^9$ ²⁴²Pu to the larger sample. A relative negative ion yield with respect to ²⁴²Pu for ²³⁷Np of 0.5 ± 0.3 was measured in this experiment. Fig. 7.1 presents the results for the concentration of the respective isotopes detected by AMS in comparison with the literature values, which show a very good agreement within the error bars. The 1σ error of the AMS measurements was calculated as explained in Ch. 6.5 and the error of the literature value was derived from the expanded uncertainty with a coverage factor of $k = 2$ as stated in [103] by Gaussian error propagation. The respective blank level is shown in blue, which is already subtracted from the AMS results. No counts were detected on mass 241 in the blank, which means that the upper limit for the detection sensitivity could be decreased further by increasing the measuring time and the transmission through the

7. Results and Discussion of the Ocean Water Samples

set-up. It should be noticed that the blank level for ^{241}Pu only takes machine background into account and not a possible contamination from the chemistry as it did not pass through the whole separation chemistry.

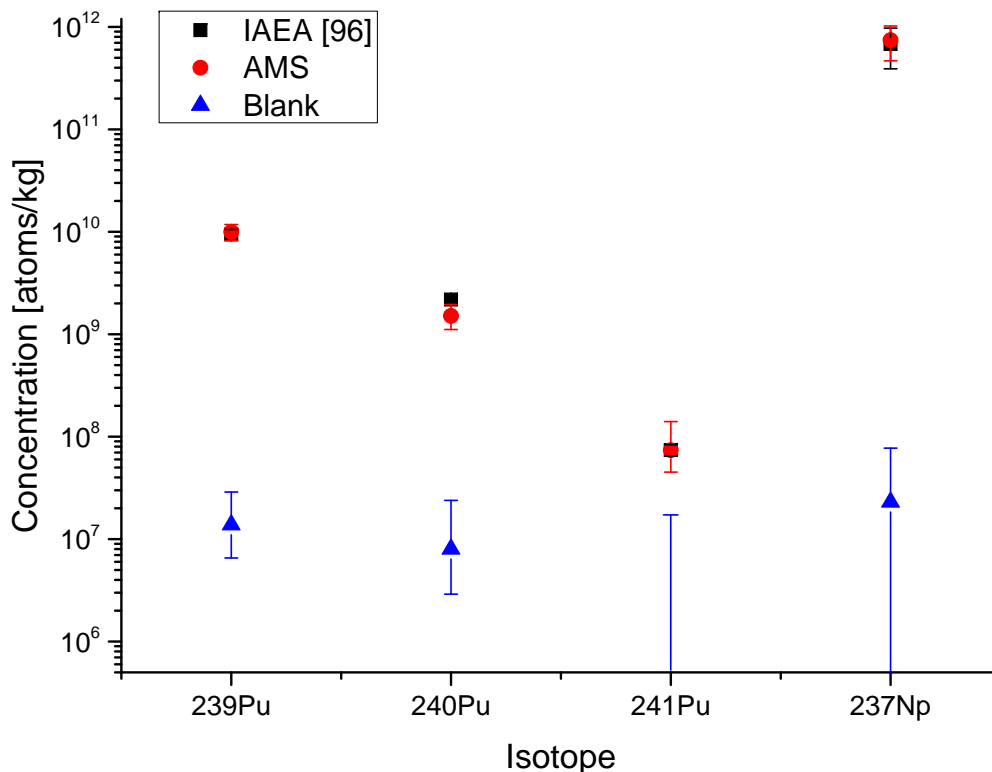


Figure 7.1.: Concentration of $^{239-241}\text{Pu}$ and ^{237}Np in the IAEA-443 reference material detected by AMS at the MLL (red dots) in comparison with the literature values (black squares) [103] and the respective blank levels (blue triangles).

The measured values are listed in Tab. 7.1 for direct comparison along with the literature values, the blank levels and the contamination of the samples by the addition of the spike. Due to the high concentration of Pu and in particular Np isotopes in the Irish Sea from the reprocessing plant Sellafield, the contribution of the spike is around three orders of magnitude lower than the measured concentration in the sea water and thus, can be neglected. Taking into account the in-growth of ^{241}Am from ^{241}Pu , an ^{241}Am concentration of $(4.2 \pm 0.5) \cdot 10^8$ atoms/kg was calculated from the value given in the reference sheet. This is significantly higher, than the positive error of the ^{241}Pu measurement, which demonstrates the good performance of the chemical Am and Pu separation. In general, the very good agreement between the experimental and the literature values proves not only the applicability of the sample preparation method but also the measuring principle to sea water samples.

| Isotope | This work [atoms/kg] | Literature value [atoms/kg] [103] | Blank level [atoms/kg] | contamination spike [atoms/kg] |
|---------------------|-------------------------------|---|----------------------------------|--------------------------------------|
| ^{239}Pu | $(10.0 \pm 1.8) \cdot 10^9$ | $(9.4 \pm 1.1) \cdot 10^9$ | $(1.4_{-0.7}^{+1.5}) \cdot 10^7$ | $7.7 \cdot 10^6$ |
| ^{240}Pu | $(1.5 \pm 0.4) \cdot 10^9$ | $(2.2 \pm 0.2) \cdot 10^9$ | $(0.8_{-0.5}^{+1.6}) \cdot 10^7$ | $1.0 \cdot 10^6$ |
| $^{241}\text{Pu}^*$ | $(7_{-3}^{+7}) \cdot 10^7$ | $(7.4 \pm 0.9) \cdot 10^7$ | $< 1.7 \cdot 10^7$ ° | $4.9 \cdot 10^4$ |
| ^{237}Np | $(7.4 \pm 2.8) \cdot 10^{11}$ | $(7 \pm 3) \cdot 10^{11}$ | $< 7.7 \cdot 10^7$ | - |

Table 7.1.: Comparison of ^{239}Pu , ^{240}Pu , ^{241}Pu and ^{237}Np concentrations detected by AMS with literature values with 1 sigma uncertainties for IAEA-443 Atlantic water.

*Decay corrected to 01/12/14, ° Machine Blank.

7.2. Pu in Pacific Ocean Water

The samples BD07-100m and BD11-4000m showed a very low ^{242}Pu count rate of less than 0.07 Hz compared to around 20 Hz obtained from the other samples, which indicates a low chemical recovery of Pu. This matches the observation of unexpected gas formation on the TEVA and UTEVA column during the separation process of these two samples, which seem to influence significantly the Pu recovery. This problem could be eliminated for the remaining samples by thorough mixing of the column load solution to remove nitrogen oxides. The measurement of BD07-100m and BD11-4000m was stopped after the first turn, as no counts were detected for $^{239-241}\text{Pu}$, so that results are not available and hence, those two samples are discarded from the following discussion. The individual sample results of all sample are listed in Appendix B.

7.2.1. Concentration

The concentrations in atoms/ m^3 of ^{239}Pu , ^{240}Pu and ^{241}Pu detected by AMS are plotted in Fig. 7.2 with 1σ error bars. The blank level of BLKP and BLKA is around one order of magnitude lower than the measured concentrations in the samples and is largely dominated by the impurities of the ^{242}Pu spike material (compare Ch. 4.2.2). The concentrations of both blanks are comparable, whereas a larger error of BLKA can be noticed, due to lower statistics caused by a lower chemical recovery. In general, the large error bars of the ^{241}Pu measurement are also governed by low statistics, due to the expected low atomic concentration in the sea water. Although for BD02 B-10 high count rates were measured and a correspondingly increased concentration was obtained, the ^{239}Pu measurement shows a significantly elevated error. This is due to systematic variations between different runs probably caused by fluctuations in the ion source output. For BD02-50m and BD04-500m, the results of two parts of each sample are plotted which were obtained

7. Results and Discussion of the Ocean Water Samples

during sample preparation, as the $\text{Fe}(\text{OH})_3$ co-precipitation did not seem complete. For this reason, the solution was separated from the precipitate, and after acidification, the co-precipitation was conducted a second time, leading to the AMS samples BD02-50mII and BD04-500mII. Since the results from both parts of the respective sample agree well within 2σ uncertainty, a weighted average was calculate for the final concentration of sample BD02-50m and BD04-500m, presented in Fig. 7.3 in units of mBq/m^3 .

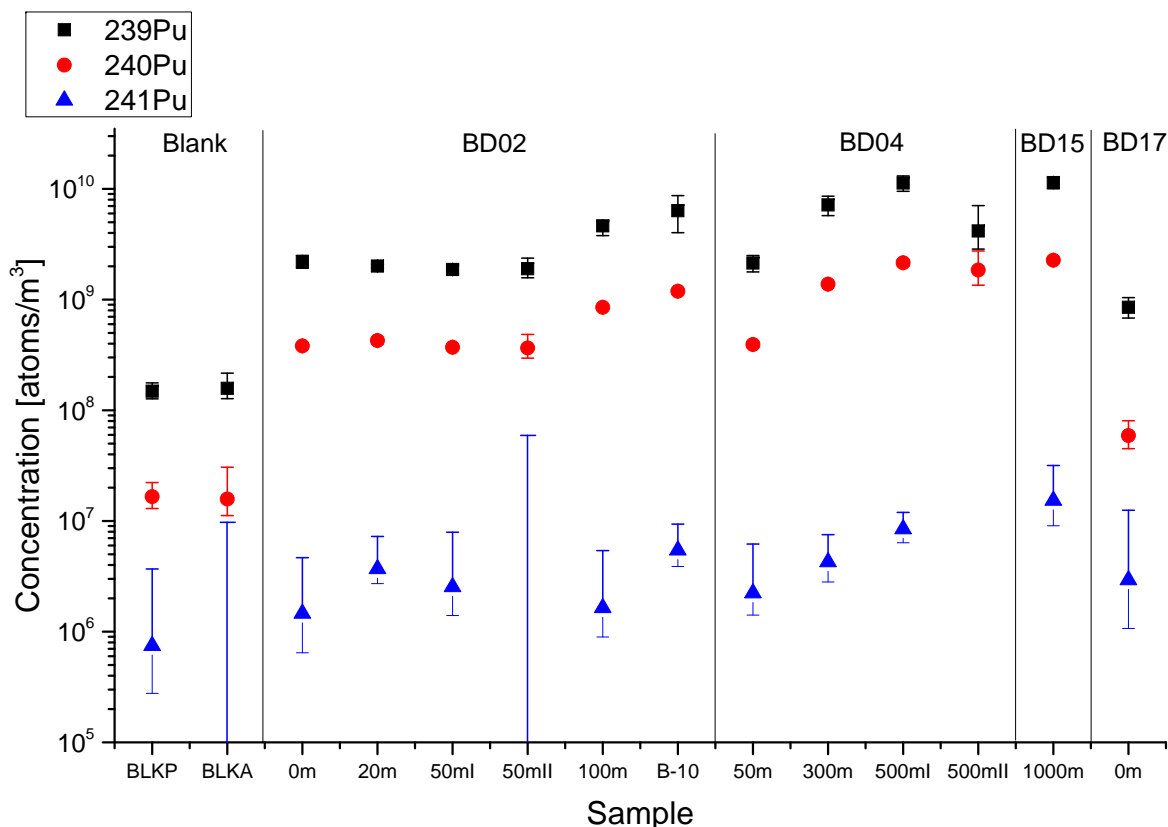


Figure 7.2.: ^{239}Pu (black squares), ^{240}Pu (red dots) and ^{241}Pu (blue triangles) concentrations in $[\text{atoms}/\text{m}^3]$ measured by AMS with 1σ uncertainties. No ^{241}Pu counts were detected for BLKA and BD02-50mII, so that only the upper limit of the positive error is plotted. For a clear presentation, the large positive error of ^{241}Pu in BD04-500mII is not shown.

The concentrations in Fig 7.3 were calculated by subtracting the blank level of BLKP and by correcting the results with respect to the difference in the added ^{241}Pu spike. The overall combined specific activity of $^{239+240}\text{Pu}$ in BD02 and BD04 shown in Fig. 7.3 [a] compares well to the concentrations of around $10 \text{ mBq}/\text{m}^3$ found in previous studies in the NW Pacific Ocean due to nuclear weapon fallout. Also the depth profile of BD02 and to some extent also BD04 featuring a low concentration in surface waters and a noticeable increase starting at a depth of around 100 m is in good agreement with the available data

(compare Ch. 2.6). The sampling depth of the background sample BD15-1000m is close to the subsurface maximum and accordingly shows the highest concentration detected in this study. Compared to the surface water sample at BD02, the concentration of ^{239}Pu and ^{240}Pu at BD17 is remarkably low. In general, even recent publications hardly ever reported on surface water concentrations of $^{239+240}\text{Pu}$ below 1 mBq/m^3 in the North Pacific Ocean [40, 57, 102, 154]. A detailed discussion of the BD17-0m sample can be found in Ch. 7.9. The distribution of the ^{241}Pu shown in Fig. 7.3 [b] in general follows the trend of ^{239}Pu and ^{240}Pu , but a detailed interpretation is not possible, due to the large statistical uncertainties at low count rates.

7. Results and Discussion of the Ocean Water Samples

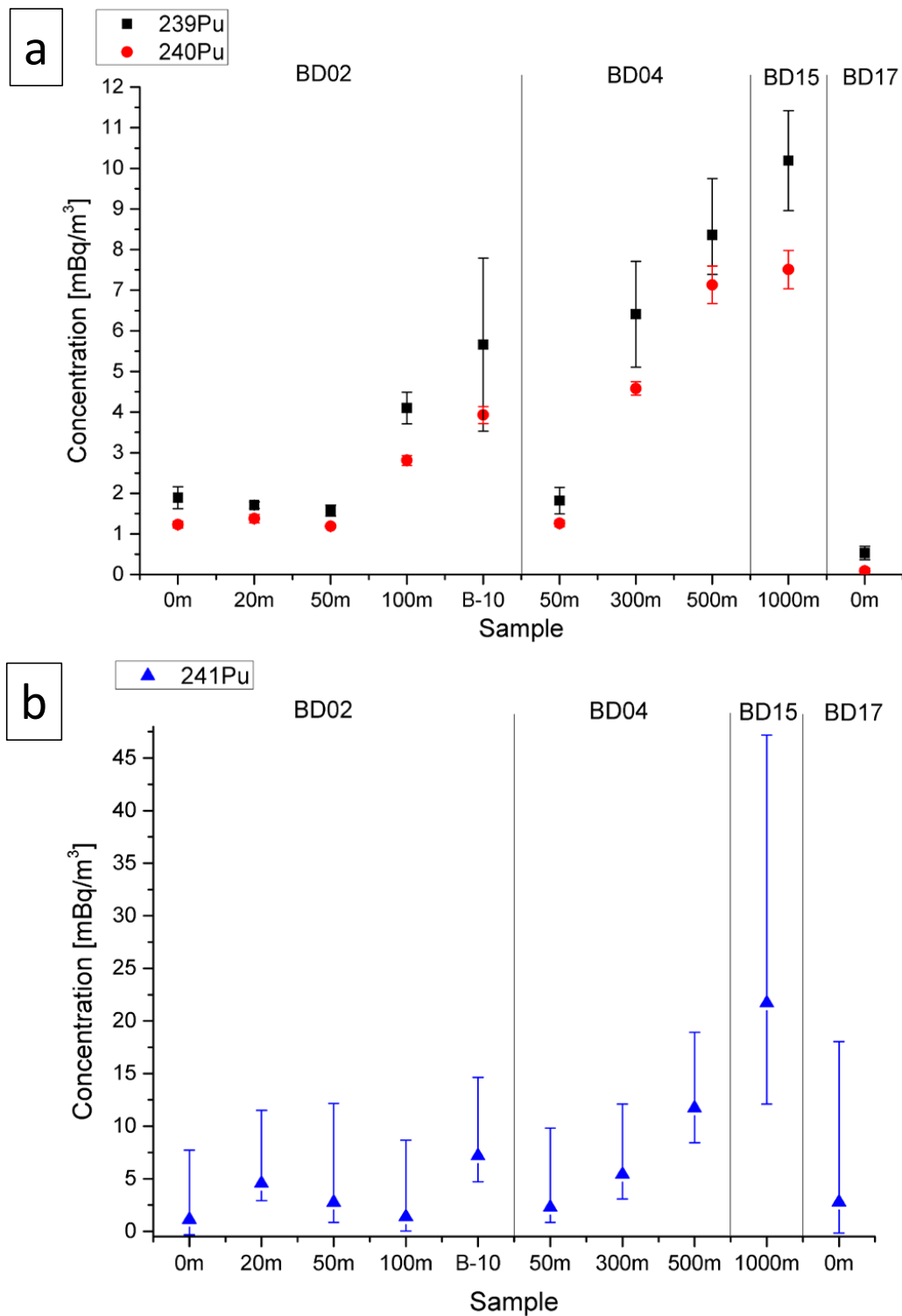


Figure 7.3.: Concentrations of $^{239,240}\text{Pu}$ (a) and ^{241}Pu (b) in Pacific Ocean water samples in units of specific activity after subtraction of the blank level and correction for the contaminants of the ^{242}Pu spike.

7.2.2. Isotopic ratios

The atomic Pu ratios $^{240}\text{Pu}/^{239}\text{Pu}$ and $^{241}\text{Pu}/^{239}\text{Pu}$ are presented in Fig. 7.4 (a) and (b), respectively. The ratios of the most prominent Pu sources in the Pacific Ocean as discussed in Ch. 2.5 and 2.6 are marked by horizontal lines. The green line indicates global fallout with its uncertainty (dashed green lines) as given by Kelley et al [51], the two blue lines represent the range of detected ratios at the Pacific Proving Grounds (PPG) altered by tropospheric close-in fallout [2, 53] and the red line shows the average ratio detected in litter samples attributed to the FDNPP accident, with the dashed lines indicating the minimum and maximum detected value [3]. $^{241}\text{Pu}/^{239}\text{Pu}$ ratios were decay corrected to the date of the measurement 12/15. Most of the samples can be clearly assigned to global fallout within 1σ uncertainty, considering just the $^{240}\text{Pu}/^{239}\text{Pu}$ ratio. However, there are two samples of the relevant sampling station BD02 and one at BD04 which show an elevated $^{240}\text{Pu}/^{239}\text{Pu}$, these are BD02-20m, BD02-50m and BD04-500m. This may be due to statistical fluctuations but could also be explained by mixing of water masses showing a global fallout Pu signature with water either originating from the PPG or which is contaminated by the FDNPP accident. A definitive statement is not possible, which also holds for sample BD02 B-10 due to its large uncertainty. The $^{240}\text{Pu}/^{239}\text{Pu}$ ratio of sample BD17-0m is unexpectedly low and cannot be assigned to any of the three mentioned sources of Pu in the Pacific Ocean. BD17-0m is discussed in detail in Ch. 7.9. With respect to the $^{241}\text{Pu}/^{239}\text{Pu}$ ratio, all samples are clearly consistent with nuclear weapon fallout and a contribution from the FDNPP accident can be certainly considered as negligible. The average measured $^{241}\text{Pu}/^{239}\text{Pu}$ ratio of $6.5_{-1.1}^{+3.0} \cdot 10^{-4}$ is two orders of magnitude lower than the ratio expected for the FDNPP. Using the inventory of $^{239+240}\text{Pu}$ in the water column at sampling station BD02, an upper limit of the dissolved Pu fraction released by the accident can be estimated (see Ch. 7.4).

7. Results and Discussion of the Ocean Water Samples

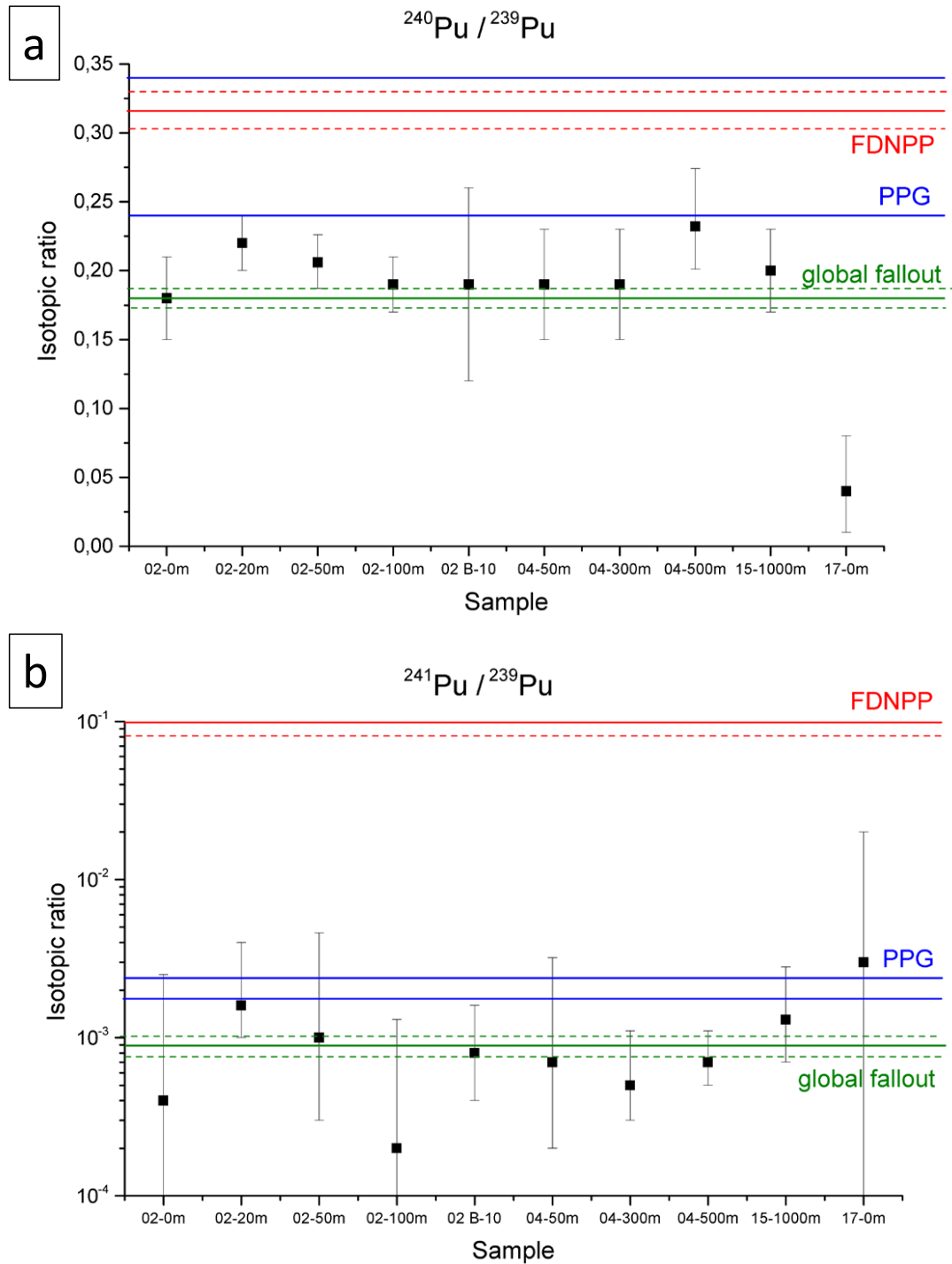


Figure 7.4.: Isotopic ratios $^{240}\text{Pu}/^{239}\text{Pu}$ (a) and $^{241}\text{Pu}/^{239}\text{Pu}$ (b) of the Pacific Ocean water samples. Horizontal lines mark the characteristic isotopic ratio of the respective emission sources, i.e. red: FDNPP [3], green: global fallout [51], blue: range of values measured for tropospheric close-in fallout at the PPG [2]. The $^{241}\text{Pu}/^{239}\text{Pu}$ ratios clearly show no contribution of Fukushima-driven Pu.

7.3. Np in Pacific Ocean Water

Because of the long half-life of ^{237}Np , a conversion of the atomic concentration to a specific activity was not considered, as it is more expedient to discuss the ^{237}Np concentrations in the ocean water in terms of atoms/m³ only.

7.3.1. Concentration

In Fig. 7.5 the results for the ^{237}Np concentration in comparison to ^{239}Pu of each measured sample are presented, including also BD07-100m and BD11-4000m as count rates for Np were reasonable high. Errors are quoted as 1σ uncertainty. Obviously, Np recovery was less influenced by the gas formation on the TEVA resin than Pu, where the additional gas formation on the U/TEVA resin might have reduced the yield even further. However, it is not known to which extent the Np recovery was altered, so that in the case of those two samples an error for the chemical recovery of $\pm 50\%$ was assumed, leading to significantly larger error bars in the concentration. In addition, three runs of BD07-100m had to be discarded causing an even larger error due to low statistics. The pulser rate for these runs was considerably decreased indicating problems with the electronics of the data acquisition. Part I and II of BD02-50m were obtained similarly as explained for Pu, but the Np concentration obtained from the first $\text{Fe}(\text{OH})_3$ co-precipitation is much lower than from the second co-precipitation and even compatible with the level of the process blanks BLKP and BLKA. This indicates a considerably different behaviour of Np compared to Pu during the $\text{Fe}(\text{OH})_3$ co-precipitation. As the ^{242}Pu spike was added after the separation chemistry, the number of ^{237}Np atoms measured in the individual parts can be added up and by applying the average chemical yield the initial ^{237}Np concentration in the sample can be calculated. The errors of the individual measurements were added linearly, as the results of the two parts depend on each other. The resulting concentration for BD02-50m is presented in Fig. 7.6. The two parts of BD04-500m were directly mixed after the final co-precipitation, so that one AMS cathode was produced and the overall concentration was directly obtained.

The final results after blank subtraction for the ^{237}Np and the ^{239}Pu concentrations are plotted in Fig. 7.6. The fact that only little data on the Np distribution in the Pacific Ocean water is known and that to my knowledge, the presented depth profile for BD02 is the first one to be published, makes the interpretation of the data quite difficult. Furthermore, due to the large fluctuations in the Np yield relative to Pu during the AMS measurement, which are not completely understood, the data are supposed to show the order of magnitude only. The general trend which can be observed from the presented data is that the Np distribution follows that of Pu to a large extent, with an increase below the water surface and the lowest concentration at great depth, i.e. 4000 m. From

7. Results and Discussion of the Ocean Water Samples

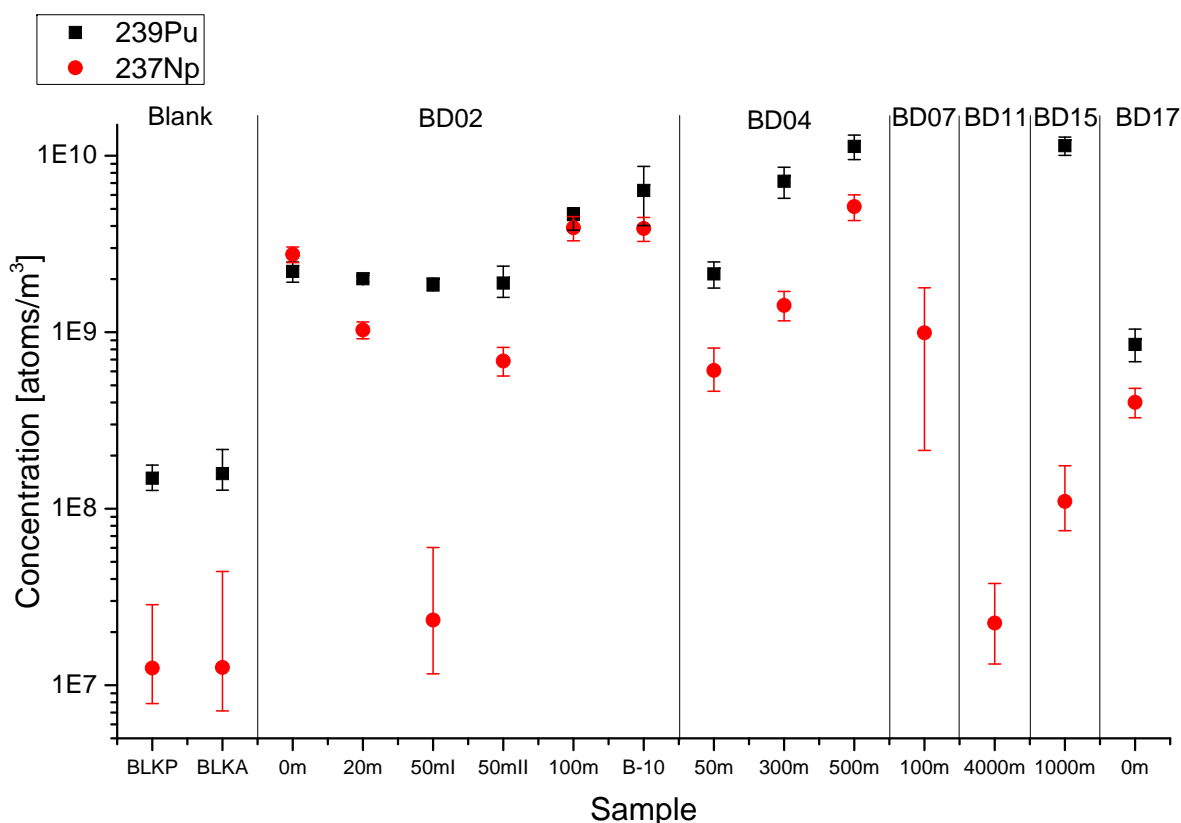


Figure 7.5.: ^{237}Np (red dots) and ^{239}Pu (black squares) concentrations measured by AMS with 1σ uncertainties. The errors of BD07 and BD11 are dominated by the unknown chemical recovery, so that an uncertainty of 50% was assumed for these two separation processes.

this data set the position and the width of the subsurface maximum cannot be exactly deduced. But considering the significantly lower concentration of Np compared to Pu at a depth of 1000 m of BD15, it can be assumed that this sample is already located on the falling edge of the maximum, whereas for Pu this is approximately the maximum of the distribution (compare Ch. 7.2.1 and 2.6). This can be interpreted as a more narrow distribution of Np compared to Pu. This would fit to the picture of Np being present in oxidation state +V in the ocean water, leading to a behaviour similar to more soluble species like ^{90}Sr . As discussed in [32], only the amplitude of the subsurface maximum of ^{90}Sr changes with time, but not its width and it is not shifted to greater depths. For a definitive statement more data are required.

7.3.2. Isotopic ratios

The measured values of the $^{237}\text{Np}/^{239}\text{Pu}$ ratio plotted in Fig. 7.7 scatter much more strongly than the Pu ratios (Fig. 7.4) and a clear assignment to one of the possible emis-

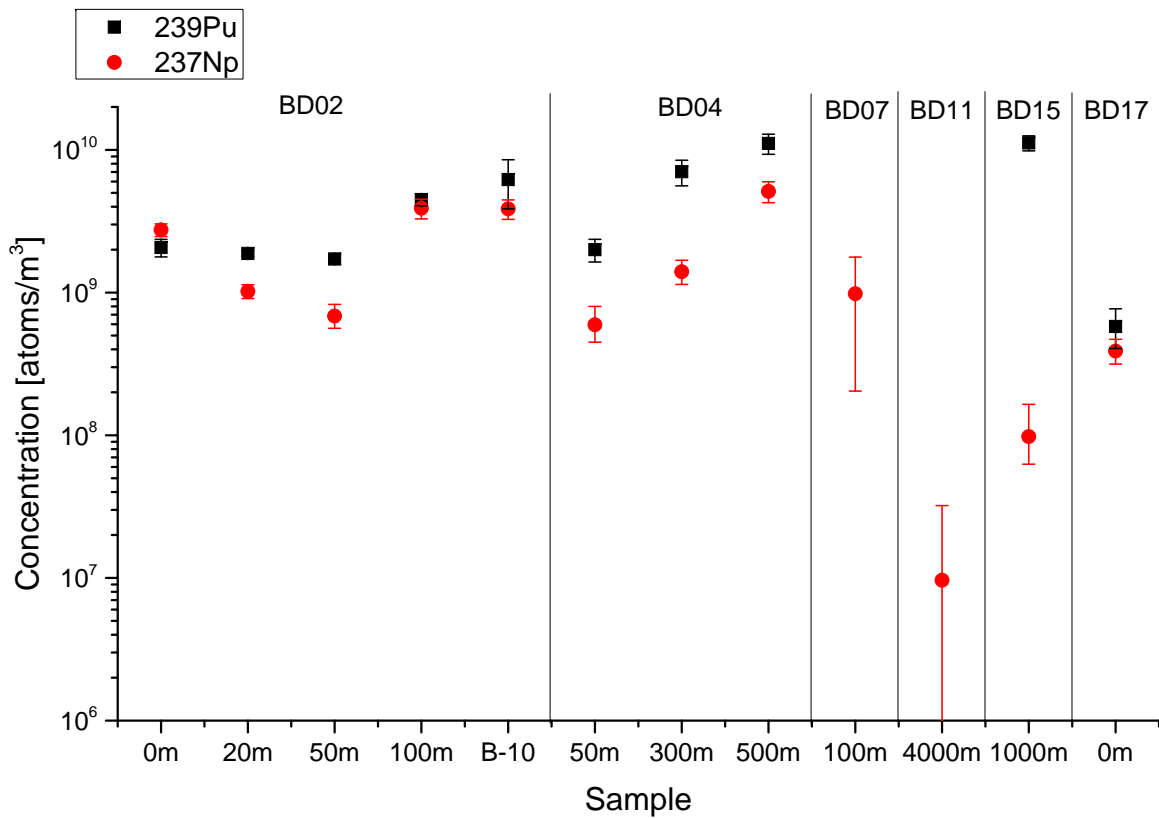


Figure 7.6.: Final ^{237}Np (red dots) concentrations in comparison with ^{239}Pu (black squares) in [atoms/m³] measured by AMS with 1σ uncertainty.

sion sources is not possible. Samples without ^{239}Pu measurement are not considered in this plot. Within 2-3 σ most values fit to global fallout (horizontal green line). Variations of the $^{237}\text{Np}/^{239}\text{Pu}$ ratio could be caused by a chemical recovery for a specific sample different from the average obtained in Ch. 5.3, so that these results should not be interpreted in detail. Nevertheless, it should be noticed that the value for BD15-1000m is remarkably low and the ratio of BD02-0m is rather high. There is no point in interpreting the low ratio of BD15-1000m as originating from the FDNPP accident (horizontal red line) considering the Pu results and the large distance to the Japanese coast. This ratio is probably rather caused by the different behaviour of Np and Pu in sea water as in the previous section and demonstrates the limits in using a ratio of different elements for source identification in natural waters. The same might hold for the relatively large isotopic ratio of BD02-0m.

7. Results and Discussion of the Ocean Water Samples

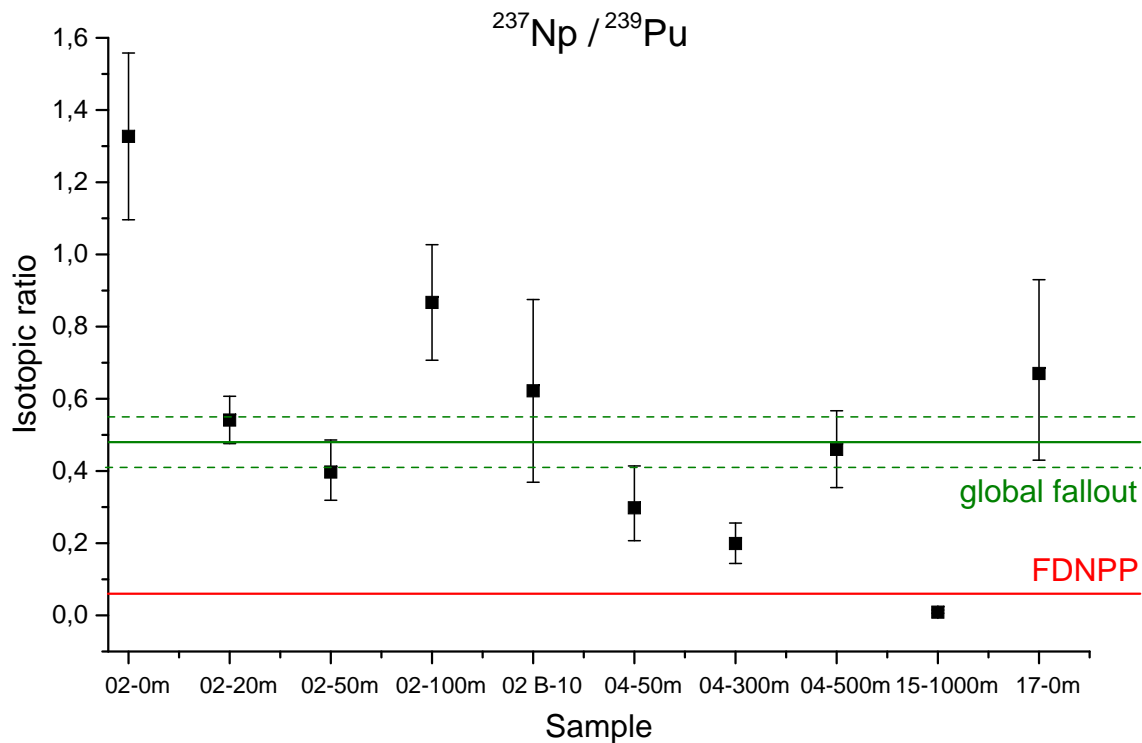


Figure 7.7.: Isotopic ratio $^{237}\text{Np}/^{239}\text{Pu}$ in the Pacific Ocean water samples, which show a large scattering, so that source identification is possible only to a limited extent.

7.4. Upper limit of dissolved ^{239}Pu activity released by the FDNPP accident

From the results for the average $^{241}\text{Pu}/^{239}\text{Pu}$ ratio of BD02 an estimate on the upper limit of Pu released by the FDNPP accident which is dissolved in the Pacific Ocean can be calculated. Using a simple mixing model, the contribution x from n sources denoted by i with characteristic ratio R_i to a measured ratio R_m is

$$R_m = \sum_i^n x_i \cdot R_i \quad (7.1)$$

with

$$\sum_i^n x_i = 1$$

The mixing ratio of global and close-in fallout at sampling station BD02 before the accident is not exactly known, but in general $^{240}\text{Pu}/^{239}\text{Pu}$ ratios ranging from 0.20 to 0.24

7.4. Upper limit of dissolved ^{239}Pu activity released by the FDNPP accident

have been measured in sea water off the east coast of Japan [3], so that the average $^{240}\text{Pu}/^{239}\text{Pu} = 0.22$ is used in the following calculation. Consequently, to calculate the proportion of Pu originating from FDNPP, x_F , the following system of equations taking into account global fallout (GF), close-in fallout (CF) and an emission from Fukushima (F), had to be solved:

$$\begin{aligned} 0.22 &= x_{GF} \cdot R(240/239)_{GF} + x_{CF} \cdot R(240/239)_{CF} \\ 0.0012 &= x_{GF} \cdot R(241/239)_{GF} + x_{CF} \cdot R(241/239)_{CF} + x_F \cdot R(241/239)_F \\ x_{GF} + x_{CF} + x_F &= 1 \end{aligned} \quad (7.2)$$

With an average $^{241}\text{Pu}/^{239}\text{Pu}$ ratio of $0.0006 + 0.0006$, the measured ratio is lower than the ratio of all three possible sources and hence, can be explained exclusively by global fallout. Therefore, it is reasonable to only consider the positive error of the measured value which adds up to 0.0012 and the minimum values of global and close-in fallout to calculate an upper limit for the contribution from the Fukushima accident. Inserting the numbers for the respective isotopic ratios from Ch. 2.5 and from Ch. 3.5 in eq. 7.2, results in a maximum Fukushima proportion of 0.20 % to the Pu inventory in the water column. The ^{239}Pu and ^{240}Pu inventory of the water column was calculated by fitting each concentration linearly in two sections, i.e. 0 m - 50 m and 50 m - 139 m (corresponds to sample B-10), in the first place, in order to describe the concentration as a function of depth $f(z) = m \cdot z + t$. Then, by section wise integration over the depth z , the inventory I depending on the maximum depth of the water column d for Pu was obtained

$$I(d) = \int_0^d f_1(z) dz \quad \text{for } z \leq 50\text{m} \quad (7.3)$$

$$I(d) = \int_0^{50} f_1(z) dz + \int_{50}^d f_2(z) dz \quad \text{for } z > 50\text{m} \quad (7.4)$$

which becomes

$$\begin{aligned} I_1(d) &= \frac{1}{2} \cdot m_1 \cdot d^2 + d \cdot t_1 \quad \text{for } d \leq 50\text{m} \\ I_2(d) &= \frac{1}{2} \cdot m_2 \cdot d^2 + d \cdot t_2 + 68.92 \frac{\text{mBq}}{\text{m}^2} \quad \text{for } d > 50\text{m} \end{aligned} \quad (7.5)$$

For BD02 with a maximum depth of 149 m the total inventory of ^{239}Pu and for ^{240}Pu is 0.48 Bq/m^2 and 0.33 Bq/m^2 , respectively.

As the sea bed rises towards the coast line, the maximum depth of the water column depends on the distance D to the coast. With a depth below 200 m, BD02 was assumed to be located in the neritic zone of the ocean, i.e. on the continental shelf [155] where the decrease of the ocean bed with increasing distance to the coast can be very well described

on the depth in eq. (7.4) into account, so that eq. (7.5) can be transformed to

$$A(^{239}\text{Pu}) = 0.20\% \left(\int_0^\pi \int_0^{13\text{km}} I_1(r, \varphi) \cdot r dr d\varphi + \int_0^\pi \int_{13\text{km}}^{39\text{km}} I_2(r, \varphi) \cdot r dr d\varphi \right) \quad (7.9)$$

where the dependency of the borders of integration on φ is not considered for this estimate. The upper limit for the ^{239}Pu activity emitted from FDNPP, which is compatible with the detected $^{241}\text{Pu}/^{239}\text{Pu}$ ratio within 1σ uncertainty, hence is 10 MBq. The corresponding ^{240}Pu and ^{241}Pu activity of 12 MBq and 18 GBq were derived from the characteristic isotopic ratios of FDNPP. Compared to the atmospheric release of ^{239}Pu of 31 TBq due to the Chernobyl accident, these numbers are negligibly small. It should be noticed that as a very particle-reactive element, Pu is likely to sediment rather quickly (compare Ch. 2.2.2). For this reason, no radial Pu concentration profile which is increasing towards FDNPP was included, as the sedimentation rate is also expected to increase in more shallow waters, leading to a faster removal of Pu from the water column. Concentrations of ^{241}Pu in sediments off the Fukushima coast after the accident were usually below the detection limit of the applied method. The atom ratio measured closest to FDNPP in sediment was $^{241}\text{Pu}/^{239}\text{Pu} = 0.00340 \pm 0.00036$ and was assigned to close-in fallout [55].

7.5. Discussion of BD17-0m

Sample BD17-0m shows a significantly lower $^{240}\text{Pu}/^{239}\text{Pu}$ ratio of 0.04 (+0.04, -0.03) and also a lower concentration of Pu in general, than all other samples investigated in this study. With a large probability, it can be excluded that these results are simply artefacts of the AMS measurement, as samples BD17-0m and BD15-1000m had been already measured in a previous beam time at VERA with comparable results which is demonstrated by Tab. 7.2. The measured values are cited with 1σ uncertainties. For asymmetric errors, only the positive value is given in Tab. 7.2. Complete results can be found in Appendix B. Even though the error of the $^{240}\text{Pu}/^{239}\text{Pu}$ ratio in sample BD17-0m obtained in the second beam time is quite large, because of low statistics, it is also smaller than the ratio for global fallout. This gives confidence that 0.04 is the actual atomic ratio of BD17-0m.

As discussed in Ch. 2.5, this very different atomic ratio might indicate the presence of a Pu source different from those which are usually detected in the Pacific Ocean. In addition to Russian submarines and fallout from low yield nuclear weapons as it can be found at the Semipalatinsk test site, for example [40], a low atomic Pu ratio is the characteristic signature of weapon grade plutonium. The first two explanations are regarded as unlikely as contamination source in the Pacific Ocean. As a possible source for the detected type of Pu, Hanford Site was identified, where several reactors for weapon grade Pu production

7. Results and Discussion of the Ocean Water Samples

| sample | Beam time | $N(^{239}\text{Pu})$ | $N(^{240}\text{Pu})$ | $^{240}\text{Pu}/^{239}\text{Pu}$ |
|------------|-----------|-----------------------------|-----------------------------|-----------------------------------|
| BD15-1000m | I | $(2.5 \pm 0.29) \cdot 10^8$ | $(5.0 \pm 0.29) \cdot 10^7$ | 0.20 ± 0.03 |
| | II | $(1.7 \pm 0.14) \cdot 10^8$ | $(4.1 \pm 0.39) \cdot 10^7$ | 0.25 ± 0.03 |
| BD17-0m | I | $(1.3 + 0.42) \cdot 10^7$ | $(5.6 + 4.8) \cdot 10^5$ | $0.04 (+0.04, -0.03)$ |
| | II | $(6.2 + 4.3) \cdot 10^6$ | $(2.4 + 9.6) \cdot 10^5$ | < 0.13 |

Table 7.2.: Comparison of results for BD15-1000m and BD17-0m from beam time I (November 2015) and II (July 2015) at VERA. For results with asymmetric error, only the positive error is cited.

were operated from 1944-1971 [156]. The location of sample BD17-0m with respect to Hanford Site is shown on the map in Fig. 7.9. It is well known that small amounts of the fuel elements were emitted to the close-by Columbia River, due to fuel element failures. The water used as coolant in the primary circuit was hold for some hours for the decay of the short-lived nuclides, but then was directly returned to the river [156]. Depending on its operation mode, Pu with a $^{240}\text{Pu}/^{239}\text{Pu}$ ratio of 0.0522 ± 0.0005 were found in Hanford Site soils and ratios below 0.04 were detected in some groundwater samples collected close to the site [157]. Thus, it is possible that small amounts of Pu from river sediments are re-mobilized and then discharged into the ocean until today. Since the Columbia River transports large amounts of water and sediment to the Pacific Ocean, also the annual discharge of 2.6 GBq of $^{239+240}\text{Pu}$ was detected at the estuary of the Columbia River in 1978-1979 [158]. However, only $(3.5 \pm 0.9)\%$ of this Pu activity were assigned to Hanford, whereas the predominant part was identified as global fallout. BD17-0m shows a slightly lower salinity of 32.861 g/kg than the other surface water samples of this study (around 34.01 g/kg), which indicates only a small proportion of fresh water, so that it is remarkable that BD17-0m shows the pure weapon grade Pu signature. Furthermore, a more recent study on Pu in the water of the Columbia River reported a $^{240}\text{Pu}/^{239}\text{Pu}$ of 0.18 which can be interpreted as global fallout [157]. These are arguments against a recent input of weapon grade Pu which had been re-mobilized from Columbia River sediments. A re-mobilization from ocean sedimentation seems more probable. But still, a mixture with global fallout would be expected due to the large distance of 772 km to the estuary of the Columbia River. Consequently, further investigation of the $^{240}\text{Pu}/^{239}\text{Pu}$ ratios in sea water collected off the coast of Oregon and Washington state are required. If the findings of the present study can be confirmed, to my knowledge, this would be the first detection of Hanford-derived Pu in the Pacific Ocean.

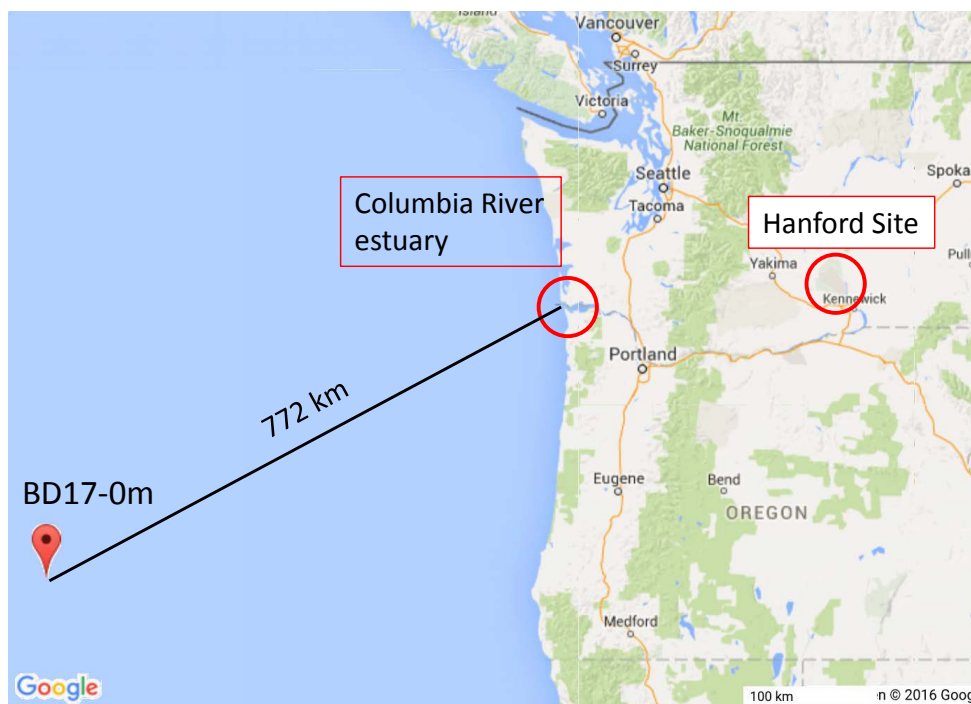


Figure 7.9.: Map showing the location of BD17-0m with respect to the Columbia River and Hanford site. [159], modified.

8. Conclusion and Outlook

The plutonium ratio $^{240}\text{Pu}/^{239}\text{Pu}$ as well as the $^{241}\text{Pu}/^{239}\text{Pu}$ ratio was measured in Pacific Ocean water samples collected in autumn 2012, in order to answer the question concerning the presence of transuranium elements in the Pacific Ocean due to the FDNPP accident. Furthermore, the determination of the ^{237}Np concentration in the same ocean water samples improves the very limited data on the ^{237}Np distribution in ocean water. In contrast to previous studies, very low atomic ^{241}Pu concentrations of around 10^6 atoms/m³ could be detected in small sample volumes of 20 L ocean water. This was possible due to the application of the ultra-sensitive detection method accelerator mass spectrometry (AMS) in combination with a highly efficient chemical suppression of the isobar ^{241}Am in the order of 10^{-4} . The separation chemistry based on extraction chromatography was adjusted to the requirements of the laboratory at the Maier-Leibnitz-Laboratory (MLL) and to three different detection techniques, i.e. radiometric detection, ICP-MS and AMS. All mentioned detection methods could be successfully applied to the processed sea water samples, but usually considerably lower recoveries for both Pu and Np were found by ICP-MS than by activity measurements, which is not fully understood. These variations introduced an additional error of 10 % on the ^{237}Np concentration, where no isotopic spike material is commercially available. For the verification of the sample preparation and the AMS detection procedure, the concentration of $^{239-241}\text{Pu}$ and ^{237}Np in the certified reference material IAEA-443 was analyzed at the Maier-Leibnitz-Laboratory (MLL) in Munich. The very good agreement of the experimental results with the literature values demonstrates the feasibility of actinide detection in natural waters at the MLL in general. 3 of the 12 Pacific Ocean water samples analyzed in this work at VERA (Vienna Environmental Research Accelerator), showed a slightly elevated $^{240}\text{Pu}/^{239}\text{Pu}$ ratio compared to global fallout of up to 0.23 (+0.042, -0.031) and one more sample contained a rather large error. A differentiation between a Fukushima and a tropospheric close-in fallout contribution is not possible in these four samples, as both emission sources have a $^{240}\text{Pu}/^{239}\text{Pu}$ signature of around 0.3. In contrast, the detected $^{241}\text{Pu}/^{239}\text{Pu}$ ratios with a mean value of $6.5(+3.0, -1.1)\cdot 10^{-4}$ is clearly compatible with nuclear weapon fallout and no contribution from Fukushima is visible in any of the investigated samples. From these results an upper limit of the dissolved fraction of Pu emitted by the FDNPP of 10 MBq ^{239}Pu was estimated, which strongly supports the general opinion of a negligible emission of actinides into the Pacific Ocean from the FDNPP accident. The remaining 30 ocean wa-

8. Conclusion and Outlook

ter samples cannot improve the findings of this study further, as the sampling stations are located too far away from FDNPP (>1000 km). As sedimentation rates of Pu are rather high, it was already pointed out by Zheng et al [4], that sediment samples collected within a 30 km radius from FDNPP are especially interesting regarding their Pu signature. Elevated $^{240}\text{Pu}/^{239}\text{Pu}$ ratios found in sediment samples at slightly larger distances to FDNPP, were interpreted as combination of global and close-in fallout [55, 160]. ^{241}Pu concentrations were usually below the detection limit, indicating also little contribution from FDNPP. From these data and the results of this work, it can be concluded that even at the high temperatures of a core meltdown, the actinides are quite well confined in the molten fuel matrix and only a minor fraction is transferred to the coolant. One of the background samples, which was collected at a distance of 772 km to the US west coast, showed a significantly decreased $^{240}\text{Pu}/^{239}\text{Pu}$ ratio of 0.04 (+0.04, -0.03), which is usually assigned to weapon grade Pu. For this reason, it is supposed that Hanford Site, a former reprocessing plant for weapon grade Pu, could be the contamination source. As this would be the first detection of Pu in ocean water discharged by Hanford Site, further data are required to confirm these findings. No additional samples off the US west coast from the KH-12-4 cruise are available. This example demonstrates very well the importance of constantly improving the data on the environmental Pu concentration and isotopic ratio distributions for a better understanding of its behaviour in the world oceans and the emission sources. The analysis of the remaining ocean water samples can serve this purpose.

Compared to Pu, there are hardly any data on environmental concentrations of ^{237}Np published, so that this work presents probably the first depth profile of ^{237}Np in the water column of the Pacific Ocean. As several averages had to be taken to obtain the ^{237}Np concentration in the sea water, a detailed interpretation of individual sample results is not recommended. In general, the data indicate a more narrow subsurface maximum of the ^{237}Np distribution located closer to the water surface compared to Pu, which would resemble to more soluble elements like Sr or Cs. However, this implies that the interpretation of $^{237}\text{Np}/^{239}\text{Pu}$ ratios for source identification especially in sea water is little informative as it would depend on the depth. Consequently, it would be more useful to use a ratio relative to an element with a similar chemical behaviour like e.g. ^{129}I . At least in surface waters (0 - 300 m) promising results on using $^{237}\text{Np}/^{129}\text{I}$ ratios have been reported [161]. Certainly more data, in particular from water columns with greater depth, are required for a definite statement. These data can be provided by the remaining ocean water samples not processed within the frame of this work. For a better precision of the results, an isotopic spike is urgently needed. In the course of this work, the possibility of producing ^{235}Np ($T_{1/2}=396.1$ d) at the Tandem Accelerator of the MLL has been intensively discussed and the production using the reaction $^{232}\text{Th}(^6\text{Li}, 3n)^{235}\text{Np}$ seems feasible, so that efforts in this direction will be increased.

A. α - and γ -decay energies

| Nuclide | Emitted particle | Energy (keV) | Intensity (%) |
|---------|------------------|--------------|---------------|
| Pu-238 | α | 5499 | 71,04 |
| | | 5456 | 28,85 |
| Pu-239 | α | 5157 | 70,79 |
| | | 5144 | 17,14 |
| | | 5106 | 11,87 |
| Pu-240 | α | 5168 | 72,74 |
| | | 5124 | 27,16 |
| Pu-242 | α | 4902 | 76,53 |
| | | 4858 | 23,44 |
| Np-237 | α | 4788 | 47,64 |
| | | 4771 | 23,0 |
| | | 4767 | 9,5 |
| | | 4640 | 6,43 |
| | | 4665 | 3,46 |
| | | 4817 | 2,430 |
| | | 4873 | 2,410 |
| | | 4804 | 2,02 |
| | | 4712 | 1,174 |
| Np-239 | γ | 106,1 | 25,9 |
| | | 277,6 | 14,4 |
| | | 228,2 | 11,32 |
| | | 209,8 | 3,42 |
| | | 334,3 | 2,72 |
| | | 315,9 | 1,59 |
| Am-243 | α | 5275 | 86,74 |
| | | 5233 | 11,46 |
| | | 5181 | 1,383 |

B. Individual sample results

| sample | nuclide | ^{242}Pu count rate [Hz] | number of atoms | isotopic ratio |
|------------|-------------------|--------------------------------------|-----------------------------------|------------------------------|
| BLK-P | ^{239}Pu | 37 | $3.2^{+0.6}_{-0.5} \cdot 10^6$ | - |
| | ^{240}Pu | 43 | $3.5^{+1.2}_{-0.8} \cdot 10^5$ | $0.11^{+0.04}_{-0.03}$ |
| | ^{241}Pu | 45 | $1.6^{+6.3}_{-1.0} \cdot 10^4$ | $0.005^{+0.020}_{-0.003}$ |
| | ^{237}Np | 36 | $2.7^{+3.4}_{-1.0} \cdot 10^5$ | $0.08^{+0.11}_{-0.03}$ |
| BLK-A | ^{239}Pu | 11 | $3.4^{+1.3}_{-0.7} \cdot 10^6$ | - |
| | ^{240}Pu | 12 | $3.4^{+3.1}_{-1.0} \cdot 10^5$ | $0.10^{+0.10}_{-0.04}$ |
| | ^{241}Pu | 13 | $0.0^{+2.1}_{-0.0} \cdot 10^5$ | $0.00^{+0.06}_{-0.00}$ |
| | ^{237}Np | 22 | $2.7^{+6.7}_{-1.2} \cdot 10^5$ | $0.08^{+0.20}_{-0.04}$ n.a. |
| BD02-0m | ^{239}Pu | 39 | $(4.5 \pm 0.6) \cdot 10^7$ | - |
| | ^{240}Pu | 47 | $(8.0 \pm 0.5) \cdot 10^6$ | 0.177 ± 0.027 |
| | ^{241}Pu | 48 | $1.6^{+9.3}_{-2.0} \cdot 10^4$ | < 0.0025 |
| | ^{237}Np | 25 | $(6.0 \pm 0.6) \cdot 10^7$ | 1.33 ± 0.23 |
| BD02-20m | ^{239}Pu | 36 | $(4.16 \pm 0.19) \cdot 10^7$ | - |
| | ^{240}Pu | 39 | $(9.1 \pm 0.7) \cdot 10^6$ | 0.220 ± 0.019 |
| | ^{241}Pu | 41 | $6.6^{+7.9}_{-2.2} \cdot 10^4$ | $0.0016^{+0.0024}_{-0.0006}$ |
| | ^{237}Np | 34 | $(2.28 \pm 0.25) \cdot 10^7$ | 0.54 ± 0.07 |
| BD02-50m I | ^{239}Pu | 25 | $(3.97 \pm 0.33) \cdot 10^7$ | - |
| | ^{240}Pu | 27 | $7.89^{+0.28}_{-0.26} \cdot 10^6$ | $0.206^{+0.021}_{-0.020}$ |
| | ^{241}Pu | 28 | $5.4^{+1.1}_{-2.4} \cdot 10^4$ | $0.001^{+0.004}_{-0.001}$ |
| | ^{237}Np | 21 | $5^{+8}_{-3} \cdot 10^5$ | $0.40^{+0.09}_{-0.08}$ |

Table B.1.: Individual sample results - part 1.

B. Individual sample results

| sample | nuclide | ^{242}Pu count rate [Hz] | number of atoms | isotopic ratio |
|--------------|-------------------|--------------------------------------|-----------------------------------|------------------------------|
| BD02-50m II | ^{239}Pu | 2.1 | $4.0_{-0.7}^{+1.0} \cdot 10^7$ | - |
| | ^{240}Pu | 2.2 | $7.78_{-0.15}^{+0.25} \cdot 10^6$ | $0.20_{-0.05}^{+0.09}$ |
| | ^{241}Pu | 2.4 | $0.0_{-0.0}^{+1.3} \cdot 10^6$ | $0.000_{-0.000}^{+0.034}$ |
| | ^{237}Np | 21 | $1.46_{-0.26}^{+0.28} \cdot 10^7$ | $0.22_{-0.05}^{+0.07}$ |
| BD02-100m | ^{239}Pu | 33 | $9.9_{-1.8}^{+0.9} \cdot 10^7$ | - |
| | ^{240}Pu | 36 | $(1.82 \pm 0.07) \cdot 10^7$ | 0.186 ± 0.019 |
| | ^{241}Pu | 36 | $3.5_{-1.6}^{+8.0} \cdot 10^4$ | $0.0002_{-0.0002}^{+0.0011}$ |
| | ^{237}Np | 21 | $(8.4 \pm 1.3) \cdot 10^7$ | 0.87 ± 0.16 |
| BD02 B-10 | ^{239}Pu | 35 | $(1.4 \pm 0.5) \cdot 10^8$ | - |
| | ^{240}Pu | 39 | $(2.58 \pm 0.14) \cdot 10^7$ | 0.19 ± 0.07 |
| | ^{241}Pu | 40 | $1.2_{-0.3}^{+0.9} \cdot 10^5$ | $0.0008_{-0.0004}^{+0.0008}$ |
| | ^{237}Np | 22 | $(8.4 \pm 1.3) \cdot 10^7$ | 0.62 ± 0.25 |
| BD04-50m | ^{239}Pu | 30 | $(4.6 \pm 0.8) \cdot 10^7$ | - |
| | ^{240}Pu | 35 | $(8.4 \pm 0.5) \cdot 10^6$ | 0.19 ± 0.04 |
| | ^{241}Pu | 38 | $4.8_{-1.8}^{+8.5} \cdot 10^4$ | $0.0007_{-0.0005}^{+0.0025}$ |
| | ^{237}Np | 5 | $1.3_{-0.3}^{+0.4} \cdot 10^7$ | $0.30_{-0.09}^{+0.12}$ |
| BD04-300m | ^{239}Pu | 37 | $(1.54 \pm 0.31) \cdot 10^8$ | - |
| | ^{240}Pu | 42 | $(2.97 \pm 0.10) \cdot 10^7$ | 0.19 ± 0.04 |
| | ^{241}Pu | 44 | $9.2_{-3.1}^{+7.0} \cdot 10^4$ | $0.0005_{-0.0002}^{+0.0006}$ |
| | ^{237}Np | 22 | $(3.0 \pm 0.6) \cdot 10^7$ | 0.20 ± 0.06 |
| BD04-500m I | ^{239}Pu | 52 | $(2.3 \pm 0.4) \cdot 10^8$ | - |
| | ^{240}Pu | 58 | $(4.30 \pm 0.28) \cdot 10^7$ | 0.192 ± 0.33 |
| | ^{241}Pu | 60 | $1.7_{-0.4}^{+0.7} \cdot 10^5$ | $0.0007_{-0.0002}^{+0.0004}$ |
| | ^{237}Np | 8 | $(1.03 \pm 0.17) \cdot 10^8$ | 0.46 ± 0.11 |
| BD04-500m II | ^{239}Pu | 0.34 | $8.3_{-2.6}^{+6.0} \cdot 10^7$ | - |
| | ^{240}Pu | 0.41 | $3.7_{-1.0}^{+1.8} \cdot 10^7$ | $0.5_{-0.2}^{+0.4}$ |
| | ^{241}Pu | - | n.a. | n.a. |
| | ^{237}Np | - | - | - |

Table B.2.: Individual sample results - part 2.

| sample | nuclide | ^{242}Pu count rate [Hz] | number of atoms | isotopic ratio relative to ^{239}Pu |
|------------|-------------------|--------------------------------------|----------------------------------|---|
| BD07-100m | ^{239}Pu | 0.036 | n.a. | n.a. |
| | ^{240}Pu | 0.048 | n.a. | n.a. |
| | ^{241}Pu | 0.084 | n.a. | n.a. |
| | ^{237}Np | 41 | $2.1^{+1.7}_{-1.6} \cdot 10^7$ | n.a. |
| BD11-4000m | ^{239}Pu | 0.011 | n.a. | n.a. |
| | ^{240}Pu | 0.028 | n.a. | n.a. |
| | ^{241}Pu | 0.039 | n.a. | n.a. |
| | ^{237}Np | 52 | $4.7^{+3.2}_{-1.9} \cdot 10^5$ | n.a. |
| BD15-1000m | ^{239}Pu | 25 | $(2.53 \pm 0.29) \cdot 10^8$ | n.a. |
| | ^{240}Pu | 29 | $(5.03 \pm 0.29) \cdot 10^7$ | $0.20^{+0.03}_{-0.03}$ |
| | ^{241}Pu | 30 | $3.4^{+3.6}_{-1.4} \cdot 10^5$ | $0.001^{+0.015}_{-0.001}$ |
| | ^{237}Np | 29 | $2.4^{+1.4}_{-0.8} \cdot 10^6$ - | $0.009^{+0.006}_{-0.003}$ |
| BD17-0m | ^{239}Pu | 36 | $(1.9 \pm 0.4) \cdot 10^7$ | - |
| | ^{240}Pu | 43 | $1.3^{+0.5}_{-0.3} \cdot 10^6$ | $0.04^{+0.04}_{-0.03}$ |
| | ^{241}Pu | 44 | $0.7^{+2.1}_{-0.4} \cdot 10^5$ | $0.003^{+0.017}_{-0.003}$ |
| | ^{237}Np | 86 | $8.9^{+1.8}_{-1.6} \cdot 10^6$ | $0.67^{+0.26}_{-0.24}$ |
| BD15-1000m | ^{239}Pu | 49 | $(1.73 \pm 0.14) \cdot 10^8$ | - |
| | ^{240}Pu | 48 | $(4.2 \pm 0.4) \cdot 10^7$ | $0.25^{+0.03}_{-0.03}$ |
| | ^{241}Pu | 46 | $0.7^{+3.7}_{-0.7} \cdot 10^5$ | < 0.0024 |
| | ^{237}Np | 20 | $4.2^{+2.3}_{-0.8} \cdot 10^6$ | $0.012^{+0.014}_{-0.005}$ |
| BD17-0m | ^{239}Pu | 27 | $1.1^{+0.4}_{-0.3} \cdot 10^7$ | - |
| | ^{240}Pu | 29 | $8.2^{+9.5}_{-3.1} \cdot 10^5$ | < 0.13 |
| | ^{241}Pu | 27 | $0.4^{+1.5}_{-0.8} \cdot 10^6$ | < 0.31 |
| | ^{237}Np | 35 | $9.4^{+1.4}_{-1.1} \cdot 10^6$ | $0.38^{+0.11}_{-0.10}$ |
| BLK-I | ^{239}Pu | 75 | $4.7^{+0.7}_{-0.6} \cdot 10^6$ | - |
| | ^{240}Pu | 71 | $5.3^{+1.8}_{-1.2} \cdot 10^5$ | - |
| | ^{241}Pu | 87 | $2^{+4}_{-1} \cdot 10^4$ | - |
| | ^{237}Np | 71 | $2.2^{+0.4}_{-0.3} \cdot 10^6$ | - |

Table B.3.: Individual sample results - part 3. The results in the lower part of the table were measured in a previous beam time.

C. Results for Pu and Np recovery

| sample matrix | volume [ml] | method | Al(NO ₃) ₃ | ²⁴² Pu yield [%] | ^{239/237} Np yield [%] |
|---------------|-------------|-----------------------------------|-----------------------------------|-----------------------------|---------------------------------|
| fresh water | 20 | DOWEX 1-x8 | - | n.a. | 48.1 ± 2.2 |
| fresh water | 20 | TEVA, 0.2M oxalic acid | yes | 92.4 ± 2.9 | 33.3 ± 3.1 |
| fresh water | 20 | TEVA, change to HCL for elution | yes | n.a. | 7.5 ± 0.7 |
| fresh water | 20 | TEVA, Fe separation before column | yes | n.a. | 88.9 ± 8.4 |
| fresh water | 20 | TEVA | yes | 88.9 ± 2.8 | 107 ± 10 |
| sea water | 550 | TEVA | yes | 91.4 ± 4.3 | 82.9 ± 7.9 |
| sea water | 550 | TEVA | no | n.a. | 93.1 ± 9.0 |
| sea water | 3000 | TEVA | no | 88.8 ± 4.3 | 66.8 ± 5.9 |
| IAEA-443 | 600 | TEVA | yes | 109 ± 11 | n.a. |
| IAEA-443 | 600 | TEVA | no | 114 ± 12 | 96.9 ± 7.8 |
| sea water | 550 | TEVA+UTEVA | yes | < D.L. | 55.4 ± 6.8 |
| sea water | 550 | TEVA+UTEVA | yes | 40.5 ± 4.5 | 49.0 ± 7.2 |
| sea water | 520 | TEVA+UTEVA | yes | 54.8 ± 3.9 | 46.0 ± 5.1 |
| Pacific Ocean | 2750 | TEVA+UTEVA | yes | 144 ± 12 | 34.6 ± 3.8 |
| Pacific Ocean | 2750 | TEVA+UTEVA | yes | 118 ± 9 | 50.9 ± 5.7 |

Table C.1.: Complete lists of experimentally obtained chemical recoveries of the Pu and Np tracers in different sample matrices with 1 sigma uncertainties detected by activity measurement (upper half) and ICP-MS (lower half), n.a.: not analyzed.

D. Further chemical separation techniques

D.1. Solvent extraction

The most prominent example for solvent extraction is the PUREX process which is used to separate Pu and U from fission products and other actinides for the reprocessing of spent nuclear fuel [162]. During solvent extraction the elements of interest, which are in the aqueous phase, e.g. in nitric acid, are transferred to a highly selective organic solvent by mixing [163]. For an unexperienced user, however, the subsequent separation of the two phases is not trivial, so that recoveries can be rather low depending on the abilities of the user. Due to the high selectivity of the different solvents, several extraction steps might be needed, to separate several radionuclides from each other completely. Furthermore, after the back-extraction of the respective elements, organic liquid wastes accumulate which require separate disposal. Because of the rather high effort, solvent extraction is not used very often for the analysis of environmental samples [12].

D.2. Ion exchange chromatography

A more convenient method for the separation of actinides is ion exchange chromatography, where radionuclides in solution are poured onto a column filled with a chemically active resin. Depending on the chemical characteristics of the different elements, they either pass through the column or sorb to the resin. The latter can be eluted then from the column by different diluted acids or complexing agents. A further separation can be achieved during elution with respect to the different sorption strength of different actinides on the resin. In general, it can be distinguished between anion and cation exchange resins, depending on the functional group of the resin which can be either e.g. a sulfonic $-\text{SO}_3\text{H}$ group in case of the cation exchanger or e.g. a quaternary ammonium ion $-\text{N}(\text{CH}_3)_3\text{OH}$ in case of an anion exchange resin [112]. After dissociation of the H^+ and the OH^- , respectively, the functional group of the cation exchange resin ends up with a negative charge where cations can adsorb, whereas the anion exchange resin can bind anions, due to the remaining positive charge of the functional group. Even though actinides form

D. Further chemical separation techniques

positive ions, anion exchangers are more efficiently used for their separation and thus are more widespread in the analysis of actinides than cation exchangers. This is because cation exchangers are only selective for ions with a valence state between +I and +III [12]. Dissolved in HNO_3 or HCl , the actinides form anionic nitrate or chlorid complexes according to their oxidation state which are retained on the column. For example, Pu and Am can be efficiently separated from each other by ion exchange chromatography, as Pu forms nitrate complexes in oxidation state +IV in 8 M HNO_3 whereas Am in its most prominent oxidation state +III does not. Consequently, Pu stays on the column whereas Am passes through. From the large variety of possible oxidation states of the actinides, it is clear that the oxidation states have to be carefully adjusted to obtain reasonable recoveries. For this purpose, different oxidizing and reducing agents as Fe(II) sulfamate, ascorbic acids are added to the sample solution which has to be present as 7-8 M HNO_3 to fix the the oxidation state of the respective radionuclides. This solution is then called column load solution.

Fig. D.1 shows a possible separation procedure according to the problem of this work, which is the effective separation of Am, Pu and Np. After the separation of Am(III) which passes through the column, Pu(IV), which is bound to the resin as a nitrite complex, has to be reduced to +III before it can be eluted from the column. For this purpose, a strong reducing agent as e.g. hydrazine hydrochloride, hydroxylamine, HI or HBr has to be used. However, it is well known, that especially the first two reagents are highly toxic and also explosive [164, 165]. HI and HBr are very strong acids and form a strong vapor of I_2 and Br_2 which are also extremely hazardous. As the sample preparation was first planned to be performed at the MLL which is equipped with exhaust hoods with only low performance, this procedure was not feasible due to safety reasons. Most conventional reducing agents other than those named before, do not fulfill the requirements of α -spectrometry, ICP-MS and AMS. Furthermore, it is recommended to use dilute HNO_3 -HF for an enhanced recovery of Np during elution, as F^- ions complex Np very efficiently. In general, elution of Np is also possible without HF by decreasing the NO_3^- concentration by rinsing the resin with dilute HNO_3 . The procedure without HF and using HI for Pu elution was tested at the Radiochemie München within the scope of this work, but did not show satisfying results (see Ch. 5.3).

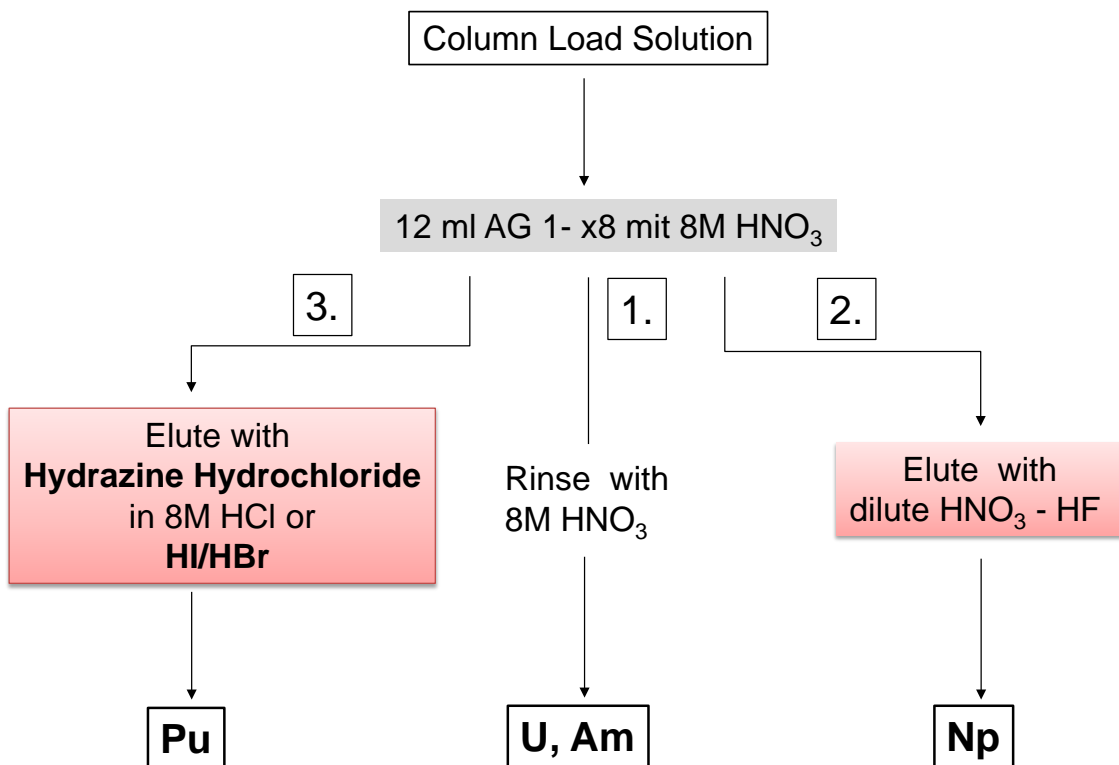


Figure D.1.: Flow chart of a possible Pu, Am and Np separation method using ion exchange chromatography. Marked in red are the elution steps which posed a problem for handling in the chemistry lab of the MLL, as hazardous substances are involved.

E. Purification and characterization of the ^{237}Np solution

The ^{237}Np concentration in the solution, received from the RCM, was determined by detecting the γ activity of its daughter nuclide ^{233}Pa ($T_H = 27.0$ d) by a high-purity Ge-detector and assuming secular equilibrium between ^{237}Np and ^{233}Pa . The corresponding γ spectrum which was recorded for 1800 s is presented in Fig. E.1 in the interesting energy range from 0 to 600 keV. More detailed information on the set-up used for γ spectrometry at the RCM can be found in Ch. 5.2.1.

From the several lines of ^{233}Pa which can be identified in Fig. E.1, the predominant 312.17 keV gamma line with the highest yield of 38.60 % was chosen to calculate the total ^{233}Pa activity of the ^{237}Np solution. The activity was determined to 9.95 ± 0.79 kBq.

Due to the production way of ^{237}Np by irradiation, it cannot be excluded that considerable amounts of ^{239}Pu and ^{240}Pu were also built up. These increased concentrations might cause contaminations in the chemistry lab of the MLL during the preparation of the $^{237}\text{Np}/^{242}\text{Pu}$ standard sample. Also in the ion source, a sample several order of magnitudes more concentrated than the expected trace level of the environmental samples, could lead to cross-talk and might lead to wrong concentrations of ^{239}Pu and ^{240}Pu . Also a contamination of the sample by ^{242}Pu would lead to a wrong $^{237}\text{Np}/^{242}\text{Pu}$ ratio in the standard sample. However, it cannot be told from the γ spectrum in Fig. E.1 whether there are elevated levels of the α -emitters ^{239}Pu , ^{240}Pu and ^{242}Pu . The energies of the γ 's emitted by the those nuclides are below 100 keV and therefore, are superimposed by the X-ray spectrum of different elements, especially U. For this reason, it was decided to clean the ^{237}Np standard solution from possible Pu impurities and determine their remaining concentration and the ^{237}Np concentration by α -spectrometry afterwards.

E.0.1. Purification of the ^{237}Np solution provided by the RCM

Approximately one half of the initial ^{237}Np standard solution were purified in order to keep activities which have to be handled as small as possible on the one hand but on the other hand to obtain sufficient statistics in the activity measurements. By weighing the solution and using the results for the ^{233}Pa activity from the γ spectrometry the initial ^{237}Np was determined to be 4.64 kBq \pm 0.37 kBq. For the cleaning of the ^{237}Np solution

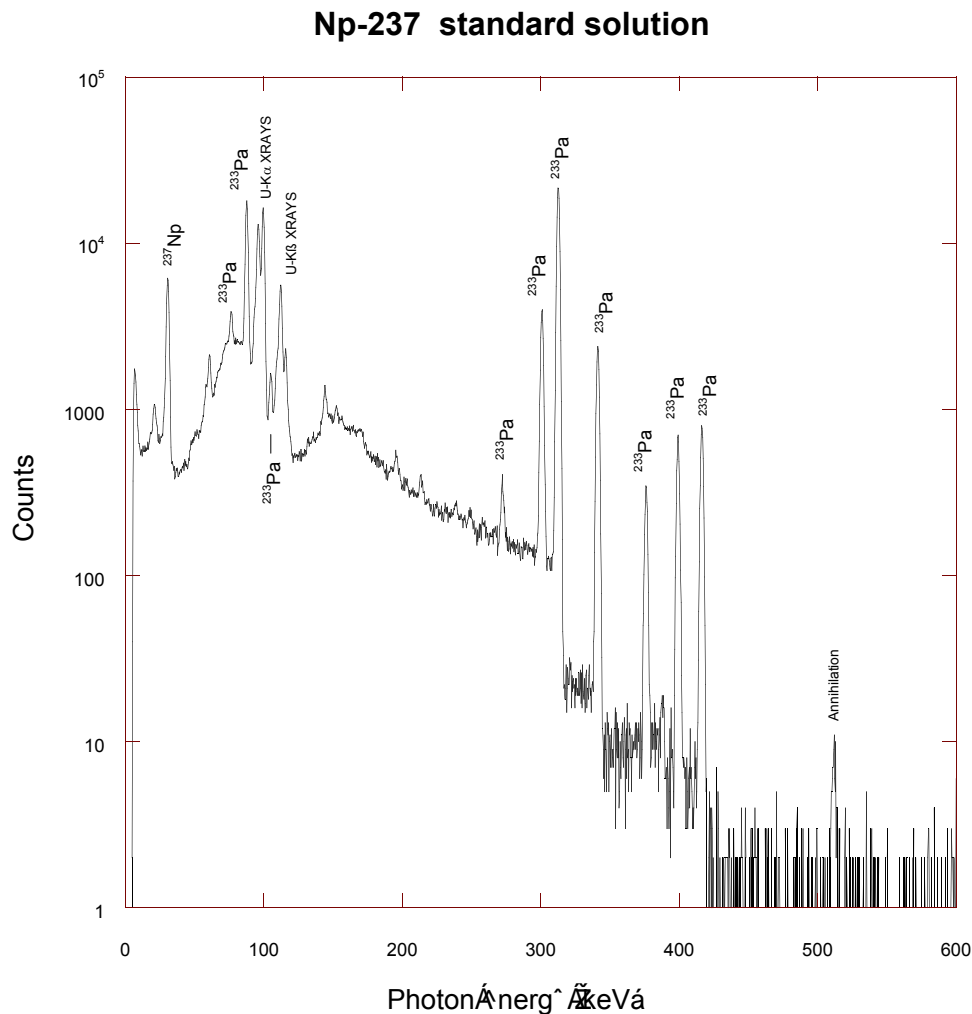


Figure E.1.: γ spectrum of the ^{237}Np solution from the RCM detected by a high-purity Ge-detector. Several emission lines of the ^{237}Np daughter nuclide ^{233}Pa can be identified, which were used to calculate the activity of ^{237}Np .

from the Pu impurities the procedure described in Ch. 4.2.4 using a single TEVA column was applied. After the separation a quick scan of all three fractions and the column itself for the ^{233}Pa activity was done with γ spectrometry. Approximately 17 Bq of ^{233}Pa were found in the Pu fraction, 220 Bq in the Np fraction, 1 kBq in the Am fraction. The main part of ^{233}Pa seemed to be on the column but could not be quantified due to the unknown geometry. Obviously, Pa did not follow in the Np fraction due to the different chemical characteristics of Pa and hence, the secular equilibrium of ^{237}Np and ^{233}Pa was broken by the separation process. This demonstrates that the procedure was optimized for the separation of Am, Pu and Np and thus, the application to different actinides is not straightforward. For the characterization of the purified Np fraction, an aliquot of 0.4988 g was taken aside for α spectrometry. The aliquot was electro-deposited as described in Ch. 5.2.1 at a voltage of 12 V and currents between 0.28 A and 0.29 A.

E.0.2. Characterization of the final ^{237}Np solution and standard sample preparation

The ^{237}Np α preparation was measured for 340000 s in an Integrated Alpha Spectrometer from Canberra [123] which is equipped with a 450 mm² PIPS detector with a detection efficiency of $8.53 \cdot 10^{-2} \pm 3.98 \cdot 10^{-5}$. The spectrum on the left side of Fig. E.2 nicely compares to the α energies emitted by the decay of ^{237}Np . Consequently, the peak structure can be clearly identified as ^{237}Np emission lines which were evaluated with the program Genie 2000 Alpha Analysis, available from Canberra using the relative α -emission yields, given in Appendix A, to obtain the specific activity of the purified ^{237}Np solution. As the resolution of the detector was not sufficient to analyze and fit every line individually, regions of interest were defined grouping together several peaks. The respective emission yields were then added up in the calculation of the overall ^{237}Np activity. A table of the α energies and the respective yields of the relevant nuclides can be found in the Appendix A.

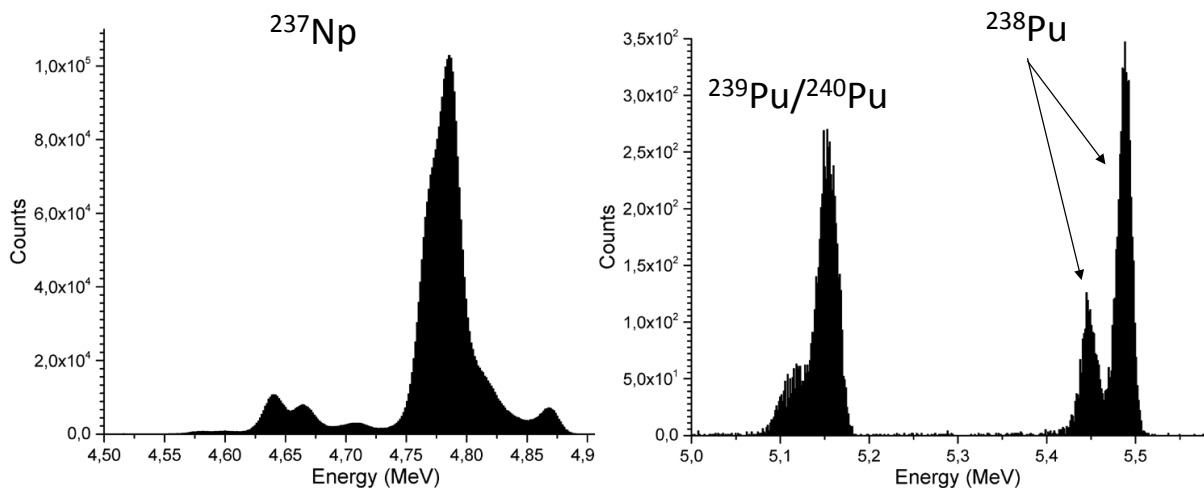


Figure E.2.: α -spectrum of the ^{237}Np solution after the purification. Left side: the distinct lines can be attributed to the alpha emission of ^{237}Np . Right side: at higher energies small concentrations of impurities are visible which correspond to $^{239}\text{Pu}/^{240}\text{Pu}$ and ^{238}Pu , respectively. Different scales on the y axis are used to improve the visibility of the Pu impurities.

The specific activity obtained from the different regions of interest for the purified ^{237}Np solution are listed in Tab. E.1 with one sigma uncertainty. However, the individual values vary strongly, which has to be taken into account when calculating the error weighted mean value for the specific activity of ^{237}Np . For this reason, the error derived from the standard deviation of the mean value was added to the propagated statistical error leading to the final result of $229 \text{ Bq/g} \pm 21 \text{ Bq/g}$. In order to obtain a suitable concentration for analysis by AMS, a dilution series with four steps was performed. The dilution used for

E. Purification and characterization of the ^{237}Np solution

| Region of interest [keV] | emission yield [%] | Specific activity [Bq/g] |
|--------------------------|--------------------|--------------------------|
| 4612.3 - 4687.6 | 10.3 | 202 ± 0.58 |
| 4690.5 - 4731.7 | 1.71 | 280 ± 1.1 |
| 4728.9 - 4852.6 | 84.6 | 221 ± 0.14 |
| 4854.0 - 4889.5 | 2.92 | 267 ± 0.82 |

Table E.1.: Results for the specific activity of the purified ^{237}Np solution for the individual regions of interest with one sigma uncertainty.

the standard samples finally had a concentration of $7.08 \pm 0.64 \cdot 10^9$ $^{237}\text{Np}/\text{g}(\text{solution})$. At higher energies of the α spectrum shown on the left side of Fig.E.2 contaminations which can be attributed to $^{239}\text{Pu}/^{240}\text{Pu}$ and ^{238}Pu are visible. However, only 6 events with an energy close to 4,902 MeV were detected, which corresponds to the most pronounced α line of ^{242}Pu with a yield of 76.53% [166]. This corresponds to a specific activity of 0.54 mBq/g and an atomic ratio of $^{242}\text{Pu}/^{237}\text{Np} = 4.1 \cdot 10^{-7}$. Using a typical number of around $3.0 \cdot 10^9$ ^{237}Np atoms, would produce a ^{242}Pu contamination of $1.2 \cdot 10^3$ atoms in the standard sample, which is negligible.

F. Prepared $^{237}\text{Np}/^{242}\text{Pu}$ standard samples

| Name | Number of ^{237}Np atoms | Number of ^{242}Pu atoms | $^{237}\text{Np}/^{242}\text{Pu}$ ratio |
|-------|-----------------------------------|-----------------------------------|---|
| STD 1 | $1.09(10)\cdot 10^9$ | $5.68(6)\cdot 10^9$ | 0.191(17) |
| STD 2 | $1.21(11)\cdot 10^9$ | $5.68(6)\cdot 10^9$ | 0.214(20) |
| STD 3 | $2.69(24)\cdot 10^9$ | $5.66(6)\cdot 10^9$ | 0.48(4) |
| STD 4 | $1.65(15)\cdot 10^9$ | $1.988(20)\cdot 10^9$ | 0.83(8) |
| STD 5 | $2.53(23)\cdot 10^9$ | $1.988(20)\cdot 10^9$ | 1.27(12) |

Table F.1.: Prepared $^{237}\text{Np}/^{242}\text{Pu}$ standard samples.

G. Certificates



IRMM

Institute for Reference Materials and Measurements

CERTIFICATE SPIKE ISOTOPIC REFERENCE MATERIAL IRMM-085

$3.909\ 8(60) \cdot 10^{-8} \text{ mol } (^{242}\text{Pu}) \cdot \text{kg}^{-1} \text{ (solution)}$

The Spike Isotopic Reference Material is supplied with an isotope amount content of ^{242}Pu certified as above.

The amount of other plutonium isotopes present are related to the ^{242}Pu content through the following certified amount ratios:

| | |
|---|-----------------|
| $n(^{238}\text{Pu})/n(^{242}\text{Pu})$: | 0.000 008 3(56) |
| $n(^{239}\text{Pu})/n(^{242}\text{Pu})$: | 0.000 826 8(40) |
| $n(^{240}\text{Pu})/n(^{242}\text{Pu})$: | 0.000 107 9(40) |
| $n(^{241}\text{Pu})/n(^{242}\text{Pu})$: | 0.000 005 4(24) |
| $n(^{244}\text{Pu})/n(^{242}\text{Pu})$: | 0.000 015 0(40) |

This corresponds to an isotopic composition with the following abundances :

| amount fraction ($\cdot 100$) | | mass fraction ($\cdot 100$) | |
|-----------------------------------|---------------|-----------------------------------|---------------|
| $n(^{238}\text{Pu})/n(\text{Pu})$ | 0.000 83(56) | $m(^{238}\text{Pu})/m(\text{Pu})$ | 0.000 82(56) |
| $n(^{239}\text{Pu})/n(\text{Pu})$ | 0.082 60(40) | $m(^{239}\text{Pu})/m(\text{Pu})$ | 0.081 58(40) |
| $n(^{240}\text{Pu})/n(\text{Pu})$ | 0.010 78(40) | $m(^{240}\text{Pu})/m(\text{Pu})$ | 0.010 69(40) |
| $n(^{241}\text{Pu})/n(\text{Pu})$ | 0.000 54(24) | $m(^{241}\text{Pu})/m(\text{Pu})$ | 0.000 54(24) |
| $n(^{242}\text{Pu})/n(\text{Pu})$ | 99.903 75(92) | $m(^{242}\text{Pu})/m(\text{Pu})$ | 99.904 87(92) |
| $n(^{244}\text{Pu})/n(\text{Pu})$ | 0.001 50(40) | $m(^{244}\text{Pu})/m(\text{Pu})$ | 0.001 51(40) |

The molar mass of the plutonium in this sample is $242.056\ 028(28) \text{ g}\cdot\text{mol}^{-1}$

From the certified values, the following amount content and mass fractions are derived:

| | |
|------------------------------|--|
| $3.913\ 5(60) \cdot 10^{-8}$ | $\text{mol (Pu)} \cdot \text{kg}^{-1} \text{ (solution)}$ |
| $9.464(14) \cdot 10^{-9}$ | $\text{kg } (^{242}\text{Pu}) \cdot \text{kg}^{-1} \text{ (solution)}$ |
| $9.473(14) \cdot 10^{-9}$ | $\text{kg (Pu)} \cdot \text{kg}^{-1} \text{ (solution)}$ |



**International Atomic Energy Agency
Department of Nuclear Sciences and Applications
IAEA Environment Laboratories**

Vienna International Centre, P.O. Box 100, 1400 Vienna, Austria

REFERENCE SHEET

CERTIFIED REFERENCE MATERIAL

IAEA-443

**NATURAL AND ARTIFICIAL RADIONUCLIDES IN SEA WATER
FROM THE IRISH SEA**

Certified values for massic activities

| Radionuclide | Certified value [Bq kg ⁻¹] | Expanded uncertainty [Bq kg ⁻¹] ^(*) |
|-----------------------------------|---|---|
| ³ H | 37.2 | 0.5 |
| ⁴⁰ K | 11.4 | 0.4 |
| ⁹⁰ Sr | 0.110 | 0.005 |
| ¹³⁷ Cs | 0.36 | 0.01 |
| ²³⁴ U | 0.044 | 0.002 |
| ²³⁵ U | 0.00185 | 0.00010 |
| ²³⁸ U | 0.039 | 0.002 |
| ²³⁸ Pu | 0.0031 | 0.0001 |
| ²³⁹⁺²⁴⁰ Pu | 0.0147 | 0.0002 |
| ²⁴¹ Am ^(**) | 0.0197 | 0.0010 |

^(*) Estimated expanded uncertainty with a coverage factor k=2, corresponding to a level of confidence of approximately 95%, as defined in the Evaluation of measurement data - Guide to the expression of uncertainty in measurement JCGM100:2008 [1].

^(**) The values should be corrected for in-growth from ²⁴¹Pu.

Reference date for decay correction: 1 January 2007

Information values for massic activities

| Radionuclide | Information value | Combined expanded uncertainty |
|-------------------|-------------------------|-------------------------------|
| | [mBq kg ⁻¹] | [mBq kg ⁻¹] |
| ²³⁰ Th | 0.5 | 0.1 |
| ²³² Th | 0.19 | 0.03 |
| ²³⁹ Pu | 8.2 | 0.8 |
| ²⁴⁰ Pu | 7.0 | 0.6 |
| ²⁴¹ Pu | 161 | 19 |

Reference date for decay correction: 1 January 2007

Origin and preparation of the material

In collaboration with IAEA-MEL, the Federal Maritime and Hydrographic Agency (BSH), Hamburg, Germany, collected about 3600 litres of surface water from the Irish Sea on-board Research Vessel *Valdivia* on September 7, 1993. Sampling was performed while cruising between two shallow (ca. 20 m water depth) stations located at 54°24,89' N - 3°33,62' W and 54°23,2'N - 3°33,45'W. Water was sampled from 5 m water depth, stored in 600 L containers and acidified to pH<1 immediately without prior filtration. A part of the sample was forwarded to IAEA-MEL and was used for the IAEA-381 interlaboratory comparison on anthropogenic and natural radionuclides. The results obtained from 28 laboratories were reported and the IAEA-381 Certified Reference Material was issued [2-3].

In 2005, 1100 L of this sample, stored at the then Risø National Laboratory, Denmark, were provided to IAEA-MEL. The sample was then transferred into a container of 1500 L and mixed for 4 hours using two pumps, aliquoted into 5 L cubitainers and coded as IAEA-443. All units were sterilized according to ISO standards at 25 kGy in an irradiation facility.

Characterization study

The IAEA-443 candidate reference material was characterized in an interlaboratory comparison (ILC) with participation of 28 laboratories, including 10 expert laboratories, from Austria, Belgium, Denmark, Finland, France, Germany, Hungary, Ireland, Morocco, Netherlands, Norway, Japan, Portugal, Slovakia, Spain, Sweden, U.K., U.S.A, and the IAEA Laboratory in Monaco.

Laboratories were requested to determine as many natural and anthropogenic radionuclides as possible by the analytical method of their choice. The following methods were used: gamma-spectrometry, low background gamma-spectrometry, alpha-spectrometry, beta counting and/or mass spectrometry.

Assignment of values - Certification procedure

The assigned property values were established on the basis of results reported by participating laboratories to the IAEA Environment Laboratories in Monaco. The medians for the sets of individual data were chosen as the best estimations of the property values [4-8] and are reported as certified values when:

- (i) at least 5 laboratory means were available, reported from at least 3 different laboratories and
- (ii) the relative uncertainty of the median did not exceed $\pm 5\%$ for activities higher than 100 Bq kg⁻¹, $\pm 10\%$ for activities from 1 to 100 Bq kg⁻¹ and $\pm 20\%$ for activities lower than 1 Bq kg⁻¹.

An activity value was considered as an information value if at least 5 laboratory means calculated from the results of at least 2 different laboratories were available.

H. List of Pacific ocean water samples

| station | depth [m] | latitude | | longitude | | salinity |
|---------|------------|------------|---|-------------|---|----------|
| BD02 | 0 | 37° 19.83 | N | 141° 27.59 | E | n.a. |
| BD02 | 20 | 37° 19.83 | N | 141° 27.59 | E | 33.740 |
| BD02 | 50 | 37° 19.83 | N | 141° 27.59 | E | 34.178 |
| BD02 | 100 | 37° 19.83 | N | 141° 27.59 | E | 34.033 |
| BD02 | B-10 (139) | 37° 19.83 | N | 141° 27.59 | E | 34.048 |
| BD04 | 0 | 37° 48.469 | N | 143° 52.476 | E | n.a. |
| BD04 | 20 | 37° 48.469 | N | 143° 52.476 | E | 34.352 |
| BD04 | 50 | 37° 48.466 | N | 143° 52.467 | E | 34.754 |
| BD04 | 100 | 37° 48.466 | N | 143° 52.467 | E | 34.691 |
| BD04 | 200 | 37° 48.466 | N | 143° 52.467 | E | 34.492 |
| BD04 | 300 | 37° 48.466 | N | 143° 52.467 | E | 34.319 |
| BD04 | 400 | 37° 48.5 | N | 143° 52.5 | E | 34.276 |
| BD04 | 500 | 37° 48.5 | N | 143° 52.5 | E | 34.111 |
| BD04 | 600 | 37° 48.5 | N | 143° 52.5 | E | 33.999 |
| BD07 | 100 | 46° 59.986 | N | 160° 4.988 | E | 33.127 |
| BD07 | 300 | 47° 0.02 | N | 160° 5.01 | E | 34.003 |
| BD07 | 600 | 47° 0.02 | N | 160° 5.01 | E | 34.250 |
| BD07 | 1000 | 47° 0.03 | N | 160° 4.913 | E | 34.419 |

Table H.1.: List of Pacific Ocean water samples with geographic coordinates - part 1. Salinity is given in terms of PSU (Practical Salinity Unit) and therefore has no dimensions. B denotes “bottom”.

H. List of Pacific ocean water samples

| station | depth [m] | latitude | | longitude | | salinity |
|---------|-----------|-----------|---|------------|---|----------|
| BD07 | 2000 | 47° 0.035 | N | 160° 4.992 | E | 34.607 |
| BD07 | 3000 | 47° 0.035 | N | 160° 4.992 | E | 34.663 |
| BD07 | 4000 | 47° 0.006 | N | 160° 4.987 | E | 34.684 |
| BD07 | 5000 | 47° 0.006 | N | 160° 4.987 | E | 34.685 |
| BD07 | B | 47° 0.006 | N | 160° 4.987 | E | 34.688 |
| BD11 | 0 | 47° 0.05 | N | 179° 59.85 | W | n.a. |
| BD11 | 200 | 46° 59.99 | N | 179° 59.98 | W | 33.666 |
| BD11 | 500 | 47° 0.06 | N | 179° 59.94 | E | 34.069 |
| BD11 | 2000 | 46° 59.98 | N | 179° 59.99 | E | 34.585 |
| BD11 | 3000 | 47° 0 | N | 179° 59.92 | E | 34.655 |
| BD11 | 4000 | 47° 0 | N | 179° 59.92 | E | 34.679 |
| BD11 | 5000 | 47° 0.05 | N | 179° 59.85 | W | 34.688 |
| BD11 | B | 47° 0.05 | N | 179° 59.85 | W | 34.682 |
| BD15 | 0 | 50° 50.06 | N | 160° 0.0 | W | n.a. |
| BD15 | 100 | 50° 50.04 | N | 159° 59.93 | W | 33.181 |
| BD15 | 300 | 50° 49.94 | N | 160° 0.09 | W | 34.003 |
| BD15 | 600 | 50° 49.87 | N | 159° 59.95 | W | 34.229 |
| BD15 | 1000 | 50° 49.87 | N | 159° 59.95 | W | 34.398 |
| BD15 | 2000 | 50° 49.85 | N | 160° 0.25 | W | 34.586 |
| BD15 | 3000 | 50° 49.85 | N | 160° 0.25 | W | 34.625 |
| BD15 | 4000 | 50° 50.06 | N | 160° 0 | W | 34.676 |
| BD15 | B | 50° 50.06 | N | 160° 0 | W | 34.682 |
| BDS2 | 0 | 50° | N | 140° | W | n.a. |
| BD17 | 0 | 43° 0.05 | N | 132° 39.91 | W | 32.861 |

Table H.2.: List of Pacific Ocean water samples with geographic coordinates - part 2. Salinity is given in terms of PSU (Practical Salinity Unit) and therefore has no dimensions. B denotes “bottom”.

List of Abbreviations

| | |
|--------------|--|
| AMS | Accelerator mass spectrometry |
| BWR | Boiling Water Reactor |
| EDX-Analysis | Energy Dispersive X-Ray Analysis |
| ESA | Electrostatic Analyzer |
| FCV | Free Column Volume |
| FDNPP | Fukushima Daiichi nuclear power plant |
| GAMS | Gas-filled Analyzing Magnet System |
| GRS | Gesellschaft für Reaktorsicherheit |
| HPCI | high pressure injection |
| HZDR | Helmholtz Zentrum Dresden-Rossendorf |
| IAEA | International Atomic Energy Agency |
| IC | isolation condensor |
| ICP-MS | Inductively Coupled Plasma Mass Spectrometry |
| INPO | The Institute of Nuclear Power Operations |
| KIT | Karlsruhe Institute of Technology |
| LLNL | Lawrence Livermore National Laboratory |
| LPCI | low pressure coolant injection |
| MCP | Micro channel plate |
| MLL | Maier-Leibnitz-Laboratory |
| MOX | Mixed Oxide Fuel |
| PCV | primary containment vessel |
| PPG | Pacific Proving Grounds |
| PSU | Practical Salinity Unit |
| RCIC | reactor core isolation system |
| RCM | Radiochemie München |

H. List of Pacific ocean water samples

RHR residual heat removal

ROI Region of Interest

RPV reactor pressure vessel

SCRAM Safety Control Rod Activator Mechanism

SHC shutdown cooling

TEPCO The Tokyo Electric Power Company

ToF Time-of-Flight

TRU transuranium elements

VERA Vienna Environmental Research Accelerator

List of Figures

| | |
|---|----|
| 2.1. Eh-pH diagram for the Pu-O-H system (a), the Np-O-H system (b) and the Am-O-H system (c) | 21 |
| 2.2. Production paths of the transuranium elements in a thermal nuclear reactor. | 25 |
| 2.3. Depth profiles of $^{239+240}\text{Pu}$ at different stations in the central NW Pacific Ocean. Credit [29]. | 29 |
| 3.1. Picture of the 6 units of FDNPP before the accident | 32 |
| 3.2. Technical Data of Unit 1-4 of FDNPP during normal operation. Adapted from [73]. | 33 |
| 3.3. Principle plant layout of FDNPP I | 34 |
| 3.4. Photograph of the four units of FDNPP I after the accident. Credit [69]. . . | 40 |
| 3.5. Map of aerial dose rates in the prefectures close to FDNPP (November 2011). | 42 |
| 3.6. Concentrations of ^{131}I , ^{134}Cs and ^{137}Cs close to the intake of Unit 3 from March 2011 to July 2013. | 45 |
| 3.7. Section of the chart of nuclides showing the actinide region. | 47 |
| 3.8. $^{240}\text{Pu}/^{239}\text{Pu}$ and $^{241}\text{Pu}/^{239}\text{Pu}$ ratios in soil and litter samples close to FDNPP compared to global fallout, atmospheric fallout in Japan and fallout from the Chernobyl accident. | 50 |
| 4.1. Track of cruise KH-12-4 from Tokyo to Vancouver and sampling positions . | 55 |
| 4.2. Location of sampling stations BD02 and BD04 with respect to FDNPP . . | 57 |
| 4.3. Picture of rotary evaporator and heat bath | 58 |
| 4.4. Photography of sample during the concentration step using $\text{Fe}(\text{OH})_3$ co-precipitation. | 61 |
| 4.5. Dependency of Pu(IV) and Pu(V) recovery on Fe^{3+} concentration during $\text{Fe}(\text{OH})_3$ cluster co-precipitation | 62 |
| 4.6. Dependence of the adsorption onto the TEVA resin on the molarity of HNO_3 and HCl for different elements. | 64 |
| 4.7. Influence of the presence of different salts on the retention (k' -factor) of Np(IV) on the TEVA resin | 65 |
| 4.8. Flow chart of the separation procedure for Am, Pu and Np using TEVA resin. | 67 |

List of Figures

| | | |
|-------|---|-----|
| 4.9. | Dependence of the adsorption onto the U/TEVA resin on the molarity of HNO_3 for different elements. | 68 |
| 4.10. | Flow chart of the separation procedure using an additional U/TEVA column in tandem with the TEVA column. | 69 |
| 5.1. | α -spectrum of Atlantic water sample with ^{242}Pu spike | 74 |
| 5.2. | Basic setup of an ICP-QMS instrument using a quadrupole mass separator. | 75 |
| 6.1. | Schematical drawing of the AMS setup at the MLL in Munich. | 81 |
| 6.2. | Technical drawing of the single-cathode Cs-sputter ion source. Courtesy of P. Hartung, modified. | 82 |
| 6.3. | Detection system at the TOF beam line at the MLL | 84 |
| 6.4. | Layout of VERA after the upgrade in 2004 for the detection of nuclides with masses larger than 150 amu. | 86 |
| 6.5. | Spectrum with different stable beams measured at the MLL, superimposed on each other. | 90 |
| 6.6. | AMS spectra of the actinides at the MLL and VERA. | 92 |
| 6.7. | E versus ToF spectrum of $^{242}\text{Pu}^{10+}$ spike and $^{239}\text{Pu}^{10+}$ measured at the MLL | 95 |
| 7.1. | AMS results for IAEA-443 reference material | 100 |
| 7.2. | Measured concentration of $^{239-241}\text{Pu}$ in Pacific Ocean water samples. | 102 |
| 7.3. | Specific activity of $^{239,240}\text{Pu}$ (a) and ^{241}Pu (b) in Pacific Ocean water samples. | 104 |
| 7.4. | Isotopic ratios $^{240}\text{Pu}/^{239}\text{Pu}$ (a) and $^{241}\text{Pu}/^{239}\text{Pu}$ (b) of the Pacific Ocean water samples. | 106 |
| 7.5. | Measured concentration of ^{237}Np in Pacific Ocean water samples. | 108 |
| 7.6. | Final concentrations of ^{237}Np in Pacific Ocean water samples. | 109 |
| 7.7. | Isotopic ratio $^{237}\text{Np}/^{239}\text{Pu}$ in Pacific Ocean water samples. | 110 |
| 7.8. | Visualization of the relevant parameters for the calculation of the Pu inventory in the ocean segment. | 112 |
| 7.9. | Map showing the location of BD17 with respect to the Columbia River and Hanford site. | 115 |
| D.1. | Flow chart of a possible Pu, Am and Np separation method using ion exchange chromatography | 129 |
| E.1. | γ spectrum of the ^{237}Np solution from the RCM | 132 |
| E.2. | α -spectrum of the ^{237}Np solution after the purification. | 133 |

List of Tables

| | |
|--|-----|
| 2.1. Nuclear characteristics of most relevant Pu and Np isotopes | 18 |
| 2.2. Typical concentration of most important inorganic constituents in sea water | 23 |
| 2.3. Summary of isotopic ratios originating from different sources. | 27 |
| 3.1. Source term of the radioactive contamination of the Pacific Ocean due to the FDNPP accident | 46 |
| 3.2. Results for average inventory of FDNPP I in Bq/tHM and the correspond- ing atomic ratios calculated in different analyses. | 48 |
| 4.1. Massic activities of ^{239}Pu , ^{240}Pu and ^{241}Pu in the reference material IAEA- 443. | 54 |
| 4.2. Pacific Ocean water samples which were prepared for the analysis with AMS. | 56 |
| 4.3. Contaminations of ^{239}Pu , ^{240}Pu , ^{241}Pu introduced by the spike solution . . | 60 |
| 5.1. Chemical recoveries of Pu and Np tracer in different sample matrices . . . | 77 |
| 7.1. AMS results for IAEA-443 reference material | 101 |
| 7.2. Comparison of results for BD15-1000m and BD17-0m from different beam times | 114 |
| B.1. Individual sample results - part 1. | 121 |
| B.2. Individual sample results - part 2. | 122 |
| B.3. Individual sample results - part 3. | 123 |
| C.1. Summary of chemical recoveries of Pu and Np tracer. | 125 |
| E.1. Results for the specific activity of the purified ^{237}Np solution | 134 |
| F.1. Prepared $^{237}\text{Np}/^{242}\text{Pu}$ standard samples. | 135 |
| H.1. List of Pacific Ocean water samples with geographic coordinates - part 1. . | 141 |
| H.2. List of Pacific Ocean water samples with geographic coordinates - part 2. . | 142 |

Bibliography

- [1] D.J. Assinder. A review of the occurrence and behaviour of neptunium in the Irish Sea. *J. Environ. Radioact.*, 44:335–347, 1999.
- [2] K.O Buessler. The isotopic signature of fallout plutonium in the North Pacific. *J. Environ. Radioact.*, 36(1):69 – 83, 1997.
- [3] J. Zheng et al. Isotopic evidence of plutonium release into the environment from the Fukushima DNPP accident. *Sci. Rep.*, 2(304), 2012.
- [4] J. Zheng, K. Tagami, and S. Uchida. Release of plutonium isotopes into the environment from the fukushima daiichi nuclear power plant accident: what is known and what needs to be known. *Environ. Sci. Technol.*, 47(17):9584–9595, 2013.
- [5] International Atomic Energy Agency. *The Fukushima Daiichi Accident, Technical Volume 1/5*. IAEA, Vienna, 2015. <http://www-pub.iaea.org/MTCD/Publications/PDF/AdditionalVolumes/P1710/Pub1710-TV1-Web.pdf> (Accessed 07.09.2015).
- [6] GEOTRACES - An International Study of the Marine Biochemical Cycles of Trace Elements and their Isotopes. www.geotraces.org/outreach/geotraces-brochure (Accessed 23.08.15).
- [7] C. Wallner. *Beschleunigermassenspektrometrie mit Supernova-erzeugten Aktiniden*. PhD thesis, Technische Universität München, 2000.
- [8] P. Ludwig, T. Faestermann, G. Korschinek, G. Rugel, I. Dillmann, L. Fimiani, S. Bishop, and P. Kumar. Search for Superheavy elements with $292 \leq A \leq 310$ in nature with accelerator mass spectrometry. *Phys. Rev. C*, 85:024315, 2012.
- [9] J. Lachner, I. Dillmann, T. Faestermann, G. Korschinek, M. Poutivtsev, G. Rugel, Ch. Lierse von Gostomski, A. Türler, and U. Gerstmann. Attempt to detect primordial ^{244}Pu on Earth. *Phys. Rev. C*, 85, 2012.
- [10] E. P. Horwitz, M. L. Dietz, R. Chiarizia, H. Diamond, III Maxwell, S. L., and M. R. Nelson. Separation and preconcentration of actinides by extraction chromatography using a supported liquid anion exchanger: application to the characterization of high-level nuclear waste solutions. *Anal. Chim. Acta*, 310:63–78, 1995.
- [11] S. L. Maxwell, B. A Culligan, V. D. Jones, S. T. Nichols, and G. W. Noyes. Rapid determination of ^{237}Np and Pu isotopes in water by inductively-coupled plasma mass spectrometry and alpha spectrometry. *J Radioanal Nucl Chem*, 287(1), 2010.
- [12] J. Lehto and X. Hou. *Chemistry and Analysis of Radionuclides*. Wiley-VCH Verlag,

Bibliography

- 2011.
- [13] F. Quinto, R. Golser, M. Lagos, M. Plaschke, T. Schäfer, P. Steier, and H. Geckeis. Accelerator Mass Spectrometry of Actinides in Ground- and Seawater: An Innovative Method Allowing for the Simultaneous Analysis of U, Np, Pu, Am, and Cm Isotopes below ppq Levels. *Anal. Chem.*, 87(11):5766–5773, 2015.
 - [14] T. Shinonaga, P. Steier, M. Lagos, and Ohkura T. Airborne Plutonium and Non-Natural Uranium from the Fukushima DNPP Found at 120 km Distance a Few Days after Reactor Hydrogen Explosions. *Environ. Sci. Technol.*, 48:3808–3814, 2014.
 - [15] G.T. Seaborg. The Plutonium Story. In *Berkeley Laboratory/Lawrence Livermore National Laboratory Conference, Actinides 1981*, Pacific Grove, CA, September 10–15, 1981.
 - [16] G. T. Seaborg and M. L. Perlman. Search for Elements 94 and 93 in Nature. presence of 94^{239} in Pitchblende. *J. Am. Chem. Soc.*, 70:1571–1573, 1948.
 - [17] C. A. Levine and G.T. Seaborg. The occurrence of plutonium in nature. *J. Am. Chem. Soc.*, 73(7):3278–3283, 1951.
 - [18] W. A. Myers and M. Lindner. Precise determination of the natural abundance of ^{237}Np and ^{239}Pu in Katanga Pitchblende. *J. nucl. inorg. Chem.*, 33(10):3233–3238, 1971.
 - [19] J. Magill, G. Pfennig, and Galy. J. Karlsruher Nuklidkarte. Forschungszentrum Karlsruhe GmbH, 2006. 7. edition.
 - [20] W. Runde. The chemical interactions of actinides in the environment. *Los Alamos Sci.*, (26):392–410, 2000.
 - [21] B. Allard, U. Olofsson, and B. Torstenfelt. Environmental Actinide Chemistry. *Inorg. Chim. Acta*, 94:205–221, 1984.
 - [22] G. R. Choppin and B. E. Stout. Actinide Behaviour in Natural Waters. *Sci. Total Environ.*, 83:203–216, 1989.
 - [23] N. Takeno. Atlas of Eh-pH diagrams, Geological Survey of Japan Open File Report 419. Technical report, National Institute of Advanced Industrial Science and Technology, Research Center for Deep Geological Environments, 2005.
 - [24] C. Walther et al. New insights in the formation processes of Pu(IV) colloids. *Radiochim. Acta*, 97(199-207), 2009.
 - [25] L. S. Natrajan, A. N. Swinburne, M. B. Andrews, S. Randall, and S. L. Heath. Redox and environmentally relevant aspects of actinide(IV) coordination chemistry. *Coordin. Chem. Rev.*, 266-267:171–193, 2014.
 - [26] R.H. Byrne, S. Mecking, R.A. Feely, and X. Liu. Direct observations of basin-wide acidification of the North Pacific Ocean. *Geophys. Res. Lett.*, 37(2), 2010.
 - [27] L.H.N. Cooper. Oxidation-Reduction Potential in Sea Water. *J. Mar. Biol. Assoc. UK*, 22(1):167–176, 1937.
 - [28] P.I. Mitchell, J. Vives i. Batlle, A.B. Downes, O.M. Condren, L.L. Vintró, and

- Sánchez-Cabeza J.A. Recent observations on the physico-chemical speciation of plutonium in the Irish sea and the western Mediterranean. *Appl. Radiat. Isotopes*, 46(11):1175 – 1190, 1995.
- [29] L. L. Vintró, P. I. Mitchell, K. J. Smith, P. J. Kershaw, and H. D. Livingston. Transuranium nuclides in the world's oceans. In H. D. Livingston, editor, *MARINE RADIOACTIVITY*, pages 79–108. Elsevier Ltd., 2004.
- [30] R.J. Pentreath, B.R. Kershaw, P.J. and Harvey, and M.B. Lovett. The behaviour of certain long-lived radionuclides in the marine environment. In *Behaviour of long-lived radionuclides associated with deep-sea disposal of radioactive wastes*, pages 101–115. International Atomic Energy Agency (IAEA), 1986.
- [31] E.R. Sholkovitz. The Geochemistry of Plutonium in Fresh and Marine Water Environments. *Earth Sci. Rev.*, 19:95–161, 1983.
- [32] H. D. Livingston, P.P. Povinec, T. Ito, and O. Togawa. The behaviour of plutonium in the Pacific Ocean. *Radioactiv. Environm.*, 1:267–292, 2001.
- [33] D.M. Taylor. The Biodistribution and Toxicity of Plutonium, Americium and Neptunium. *Sci. Total Environ.*, 83:217–225, 1989.
- [34] J.C. Nenot and J.W. Stather. *The Toxicity of Plutonium, Americium and Curium*. Pergamon Press, 1979.
- [35] W. J. Bair. Toxicology of inhaled Plutonium - Experimental animal studies. Technical report, Pacific Northwest Laboratories, Battelle Memorial Institute, 1971.
- [36] G. L. Voelz, J.N.P. Lawrence, and E. R. Johnson. Fifty Years of Plutonium Exposure to the Manhattan Project Plutonium Workers: An Update. *Health Phys.*, 73(4), 1997.
- [37] D. D. Mahlum and W. J. Clarke. Neptunium-237 Toxicity in the Rat-I. Histopathologic and Chemical Observations in Liver and Kidney. *Health Phys.*, 12(1), 1966.
- [38] S. Fetter, V. A. Frolov, M. Miller, R. Mozley, O. F. Prilutsky, S. N. Rodionov, and R. Z. Sagdeev. Detecting Nuclear Warheads. *Science & Global Security*, 1:225–302, 1990.
- [39] J. Gray, S. R. Jones, and A. D. Smith. Discharges to the environment from the Sellafield Site, 1951-1992. *J. Radiol. Prot.*, 15(2):99–131, 1995.
- [40] P. Lindahl, S.-H. Lee, P. Worsfold, and M. Keith-Roach. Plutonium isotopes as tracers for ocean processes: A review. *Mar. Environ. Res.*, 69:73–84, 2010.
- [41] G. T. Seaborg and W. D. Loveland. *THE ELEMENTS BEYOND URANIUM*. John Wiley & Sons, Inc., 1990.
- [42] J. Kuwabara, M. Yamamoto, D.J. Assinder, K. Komura, and K. Ueno. Sediment profiles of ^{237}Np in the Irish Sea: estimation of the total amount of ^{237}Np from Sellafield. *Radiochim. Acta*, 73:73–81, 1996.
- [43] T. Mizutani, J. Koarashi, and M. Takeishi. Monitoring of Low-Level Radioactive Liquid Effluent in Tokai Reprocessing Plant. *J. Nucl. Sci. Technol.*, 46(7):665–672,

Bibliography

- 2009.
- [44] International Atomic Energy Agency IAEA, Vienna, Austria. *ENVIRONMENTAL CONSEQUENCES OF THE CHERNOBYL ACCIDENT AND THEIR REMEDIATION: TWENTY YEARS OF EXPERIENCE*, 2006. http://www-pub.iaea.org/mtcd/publications/pdf/pub1239_web.pdf (Accessed 10.01.2016).
 - [45] United Nations Scientific Committee on the Effects of Atomic Radiation UNSCEAR, New York, USA. *Exposures and effects of the Chernobyl Accident (ANNEX J)*, 2000. <http://www.unscear.org/unscear/en/chernobyl.html> (Accessed 10.01.2016).
 - [46] United Nations Scientific Committee on the Effects of Atomic Radiation UNSCEAR, New York, USA. *Sources and Effects of Ionizing Radiation (VOLUME I)*, 2008. www.unscear.org/unscear/en/publications/2008_1.html (Accessed 10.01.2016).
 - [47] N.-O. Bergkvist and R. Ferm. Nuclear Explosions 1945 - 1998. Technical report, DEFENCE RESEARCH ESTABLISHMENT, Division of Systems and Underwater Technology, 2000.
 - [48] E.P. Hardy, P.W. Krey, and H.L. Volchok. Global Inventory and Distribution of Fallout Plutonium. *Nature*, 241:444–445, 1973.
 - [49] T. M. Beasley, J. M. Kelley, T.C. Maiti, and L. A. Bond. $^{237}\text{Np}/^{239}\text{Pu}$ Atom Ratios in Integrated Global Fallout: a Reassessment of the Production of ^{237}Np . *J. Environ. Radioactivity*, 38(2):133–146, 1998.
 - [50] W.F. Libby. Radioactive Fallout. In *Proc. Nat. Acad. of Sci.*, volume 44, pages 800–820, 1958.
 - [51] M. Kelley, L. A. Bond, and T. M. Beasley. Global distribution of Pu isotopes and ^{237}Np . *Sci. Total Environ.*, 237/238:483–500, 1999.
 - [52] V.T. Bowen, V.E. Noshkin, H.D. Livingston, and H.L. Volchok. Fallout Radionuclides in the Pacific Ocean: Vertical and Horizontal Distributions, Largely from GEOSECS Stations. *Earth Planet Sc. Lett.*, 49:411–434, 1980.
 - [53] S.-H. Lee, P. P. Povinec, E. Wyse, M. K. Pham, G.-H. Hong, C.-S. Chung, S.-H. Kim, and H.-J. Lee. Distribution and inventories of ^{90}Sr , ^{137}Cs , ^{241}Am and Pu isotopes in sediments of the Northwest Pacific Ocean. *Mar. Geol.*, 216:249–263, 2005.
 - [54] M. Yamamoto, T. Ishiguro, K. Tazaki, K. Komura, and U. Kaoru. ^{237}Np in Hemp-Palm Leaves of Bontenchiku for Fishing Gear Used by the Fifth Fukuryu-Marui: 40 Years after "Bravo". *Health Phys.*, 70(5), 1996.
 - [55] J. Zheng, T. Aono, S. Uchida, J. Zhang, and M. C. Honda. Distribution of Pu isotopes in marine sediments in the Pacific 30 km off Fukushima after the Fukushima Daiichi nuclear power plant accident. *Geochem. J.*, 46:361–369, 2012.
 - [56] K. Hirose. Complexation-scavenging of plutonium in the ocean. In H. Metivier, editor, *Radioprotection. Pt.1. Inventories, behaviour and processes*, volume 29, pages 225–230. 1997.

- [57] M. Yamada and J. Zheng. ^{239}Pu and ^{240}Pu inventories and $^{240}\text{Pu}/^{239}\text{Pu}$ atom ratios in the equatorial Pacific Ocean water column. *Sci. Total Environ.*, 430:20–27, 2012.
- [58] W. Bu, J. Zheng, Q. Guo, T. Aono, K. Tagami, S. Uchida, H. Tazoe, and M. Yamada. Ultra-trace plutonium determination in small volume seawater by sector field inductively coupled plasma mass spectrometry with application to Fukushima seawater samples. *J. Chromatogr. A.*, 1337:171–178, 2014.
- [59] C.S. Kim, C.K. Kim, and K.J. Lee. Simultaneous analysis of ^{237}Np and Pu isotopes in environmental samples by ICP-SF-MS coupled with automated sequential injection system. *J. Anal. At. Spectrom.*, 19:743–750, 2004.
- [60] J. W. Mietelski, J. Dorda, and B. Was. Pu-241 in samples of forest soil from Poland. *Appl. Radiat. Isot.*, 51:435 – 447, 1999.
- [61] INPO (Institute of Nuclear Power Operations). *Special Report on the Nuclear Accident at the Fukushima Daiichi Nuclear Power Station*, 2011. http://www.nei.org/filefolder/11_005_Special_Report_on_Fukushima_Daiichi_MASTER_11_08_11_1.pdf (Accessed 30.07.2013).
- [62] WHO (World Health Organisation). *Preliminary dose estimation from the nuclear accident after the 2011 Great East Japan Earthquake and Tsunami*, 2012. http://apps.who.int/iris/bitstream/10665/44877/1/9789241503662_eng.pdf (Accessed 21.03.2013).
- [63] G. Steinhauser, A. Brandl, and T.E. Johnson. Comparison of the Chernobyl and Fukushima nuclear accidents: A review of the environmental impacts. *Sci. Total Environ.*, 470-471:800–817, 2014.
- [64] G. Steinhauser, A. Brandl, and T.E. Johnson. Erratum to “Comparison of the Chernobyl and Fukushima nuclear accidents: A review of the environmental impacts” [Sci Total Environ 470-471 (2014) 800-817]. *Sci. Total Environ.*, 487:575, 2014.
- [65] International Atomic Energy Agency (IAEA), Vienna. *IAEA International Fact Finding Expert Mission of the Fukushima Daiichi NPP Accident Following the Great East Japan Earthquake and Tsunami*, 2011. www-pub.iaea.org/MTCD/meetings/PDFplus/2011/cn200/documentation/cn200_Final-Fukushima-Mission_Report.pdf (Accessed 25.08.2015).
- [66] TEPCO (Tokyo Electric Power Company). *Fukushima Nuclear Accident Analysis Report*, 2012. www.tepco.co.jp/en/press/corp-com/release/betu12_e/images/120620e0104.pdf (Accessed 31.07.2013).
- [67] GRS (Gesellschaft für Reaktorsicherheit). *Fukushima Daiichi - Unfallablauf, radiologische Folgen*, 2015. www.grs.de/sites/default/files/pdf/fukushima_2015_s-55_0.pdf (Accessed 30.08.2015).
- [68] Government of Japan - Nuclear Emergency Response Headquarters. *Report of Japanese Government to the IAEA Ministerial Conference on Nuclear*

Bibliography

- Safety - The Accident at TEPCO's Fukushima Nuclear Power Stations*, 2011. www.iaea.org/newscenter/focus/fukushima/japan-report.
- [69] The National Diet of Japan. *The official report of The Fukushima Nuclear Accident Independent Investigation Commission*, 2012. http://www.nirs.org/fukushima/naiic_report.pdf (Accessed 21.03.2013).
- [70] M. Hirano, T. Yonomoto, M. Ishigaki, N. Watanabe, Y. Maruyama, Y. Sibamoto, T. Watanabe, and K. Moriyama. Insights from review and analysis of the Fukushima Dai-ichi accident. *J. Nucl. Sci. Technol.*, 49(1):1–17, 2012.
- [71] globalenergyobservatory.org/geoid/3248 (Accessed 25.08.15).
- [72] U.S. Nuclear Regulatory Commission, Technical Training Center, Osborne Office Center, 5746 Marlin Road, Suite 200, Chattanooga, TN 37411-5677. *Boiling Water Reactor (BWR) Systems*. www.nrc.gov/reading-rm/basic-ref/teachers/03.pdf (Accessed 02.09.2015).
- [73] GRS (Gesellschaft für Reaktorsicherheit). Technische Daten Fukushima Nr.1 im Normalbetrieb. fukushima.grs.de/sites/default/files/Technische_Daten_Reaktoren_Fukushima_Nr_1_0.pdf (Accessed 25.01.2013).
- [74] OECD Nuclear Energy Agency (NEA), 12, *boulevarddesÎles* 92130 Issy-les-Moulineaux, France. *Basic Design Information for Boiling Water Reactors BWR3 & BWR4*, 2011. www.oecd-nea.org/press/2011/BWR-basics_Fukushima.pdf.
- [75] World Nuclear Association. Fukushima accident, 2012. www.world-nuclear.org/info/Safety-and-Security/Safety-of-Plants/Fukushima-Accident (Accessed 28.09.2015).
- [76] International Atomic Energy Agency IAEA, Tokyo and Fukushima Prefecture, Japan. *Final Report-The Follow-up IAEA International Mission on Remediation of Large Contaminated Areas Off-Site the Fukushima Daiichi Nuclear Power Plant*, 2014. www.iaea.org/sites/default/files/final_report230114_0.pdf (Accessed 07.09.2015).
- [77] A. Stohl, P. Seibert, G. Wotawa, D. Arnold, J. F. Burkhart, S. Eckhardt, C. Tapia, A. Vargas, and T. J. Yasunari. Xenon-133 and caesium-137 releases into the atmosphere from the Fukushima Dai-ichi nuclear power plant: determination of the source term, atmospheric dispersion, and deposition. *Atmos. Chem. Phys.*, 12:2313–2343, 2012.
- [78] United Nations Scientific Committee on the Effects of Atomic Radiation UNSCEAR, New York, USA. *Sources, Effects and Risks of Ionizing Radiation, UNSCEAR 2013 Report - Volume I*, 2014. www.unscear.org/docs/reports/2013/14-06336_Report_2013_Annex_A_Ebook_website.pdf (Accessed 07.10.2015).
- [79] J. M. Schwantes, C. R. Orton, and R. A. Clark. Analysis of a Nuclear Accident: Fission and Activation Product Releases from the Fukushima Daiichi Nuclear Fa-

- cility as Remote Indicators of Source Identification, Extent of Release, and State of Damaged Spent Nuclear Fuel. *Environ. Sci. Technol.*, 46:8621–8627, 2012.
- [80] G. Steinhauser, V Schauer, and K. Shozugawa. Concentration of Strontium-90 at Selected Hot Spots in Japan. *PLoS ONE*, 8, 2013.
- [81] B. Qiu. Kuroshio And Oyashio Currents. In J.H. Steele, editor, *Encyclopedia of Ocean Sciences*. Academic Press, 2001.
- [82] S. Yoshida, A.M. Macdonald, S.R. Jayne, I.I. Rypina, and K.O. Buesseler. Observed eastward progression of the Fukushima ^{134}Cs signal across the North Pacific. *Geophys. Res. Lett.*, 42:7139–7147, 2015.
- [83] Y. Masumoto et al. Oceanic Dispersion Simulations of ^{137}Cs Released from the Fukushima Daiichi Nuclear Power Plant. *Elements*, 8:207–212, 2012.
- [84] J. N. Smith, R. M. Brown, W. J. Williams, M. Robert, R. Nelson, and S. B. Moran. Arrival of the Fukushima radioactivity plume in North American continental waters. *PNAS*, 112(5):1310–1315, 2014.
- [85] TEPCO. *Increases in the Concentration of Radioactive Materials in Seawater and Groundwater on the Ocean Side of the Site: Current Situation and Countermeasures*, 2013. www.tepco.co.jp/en/decommission/planaction/images/handouts_130722_07-e.pdf (Accessed 20.10.2015).
- [86] P. P. Povinec, K. Hirose, and M. Aoyama. Radiostrontium in the Western North Pacific: Characteristics, Behaviour, and the Fukushima Impact. *Environ. Sci. Technol.*, 46:10356–10363, 2012.
- [87] A. Sakaguchi, A. Kadokura, P. Steier, K. Tanaka, Y. Takahashi, H. Chiga, A. Matsushima, S. Nakashima, and Y. Onda. Isotopic determination of U, Pu and Cs in environmental waters following the Fukushima Daiichi Nuclear Power Plant accident. *Geochem. J.*, 46:355–360, 2012.
- [88] P. Bailly du Bois, P. Laguionie, D. Boust, I. Korsakissok, D. Didie, and B. Fiévet. Estimation of marine source-term following Fukushima Dai-ichi accident. *J. Environ. Radioact.*, 114:2–9, 2012.
- [89] K.O. Buessler et al. Fukushima-derived radionuclides in the ocean and biota off Japan. *PNAS*, 109(16):5984–5988, 2012.
- [90] T. Kobayashi, H. Nagai, M. Chino, and H. Kawamura. Source term estimation of atmospheric release due to the Fukushima Dai-ichi Nuclear Power Plant accident by atmospheric and oceanic dispersion simulations. *J. Nucl. Sci. Technol.*, 50(3):55–264, 2013.
- [91] H. Kawamura, T. Kobayashi, A. Furuno, T. In, Y. Ishikawa, T. Nakayama, S. Shima, and T. Awaji. Preliminary Numerical Experiments on Oceanic Dispersion of ^{131}I and ^{137}Cs Discharged into the Ocean because of the Fukushima Daiichi Nuclear Power Plant Disaster. *J. Nucl. Sci. Technol.*, 48(11):1349–1356, 2011.

Bibliography

- [92] Nucleonica. Nucleonica Nuclear Science Portal, www.nucleonica.net/ (Accessed 04/02/16), 2016. Version 3.0.62.0001, Karlsruhe.
- [93] M. J. Bell. ORIGEN - The ORNL Isotope Generation and Depletion Code. *ORNL-4628*, 1973.
- [94] A. G. Croff. Origen2 - A Revised and Updated Version of the Oak Ridge Isotope Generation and Depletion Code. *ORNL-5621*, 1980.
- [95] S.M. Bowman, L.C. Leal, O.W. Hermann, and C.V. Parks. ORIGEN-ARP, A Fast and Easy-to-Use Source Term Generation Tool. *J. Nucl. Sci. Technol.*, 37:sup1:575–579, 2000.
- [96] I. R. Cameron. *Nuclear Fission Reactors*. Plenum Press, 1982. chapter 3.
- [97] K. Nishihara, H. Iwamoto, and K. Suyama. Estimation of Fuel Compositions in Fukushima-Daiichi Nuclear Power Plant, JAEA-Data/Code 2012-018. Technical report, Japan Atomic Energy Agency (JAEA), 2012.
- [98] G. Kirchner, P. Bossew, and M. De Cort. Radioactivity from Fukushima Dai-ichi in air over Europe; part 2: what can it tell us about the accident? *J. Environ. Radioact.*, 114:35–40, 2012.
- [99] C. DiSanzo, J. Vujic, M. Bandstra, D. H. Chivers, K. Vetter, and T. Aucott. The Fukushima Accidents: Simulation of the NPP Inventory and Comparison with Experimental Measurements of the Fallout by the UC Berkeley Team. In *Proceedings of GLOBAL 2011*, number 449457, Makuhari, Japan, Dec. 2011.
- [100] J. Leppänen. *Serpent - a Continuous-energy Monte Carlo Reactor Physics Burnup Calculation Code*, 2015. <http://montecarlo.vtt.fi/> (Accessed 20/12/15).
- [101] V. Hannstein. private communications.
- [102] W. Bu, J. Zheng, T. Aono, J.W. Wu, K. Tagami, S. Uchida, Q.J. Guo, and M. Yamada. Pu Distribution in Seawater in the Near Coastal Area off Fukushima after the Fukushima Daiichi Nuclear Power Plant Accident. *J. Nucl. Radiochem. Sci.*, 15(1):1–6, 2015.
- [103] M. K. Pham et al. A certified reference material for radionuclides in the water sample from Irish Sea (IAEA-443). *J. Radioanal. Nucl. Chem.*, 288:603–611, 2011.
- [104] M. B. Lovett, S. J. Boggis, and P. Blowers. The determination of alpha-emitting nuclides of plutonium, americium and curium in environmental materials: Part I. Sea water. Technical report, Ministry of Agriculture, Fisheries and Food, Directorate of Fisheries Research, Lowestoft, 1990.
- [105] *Reference Sheet, Certified Reference Material IAEA-443*. International Atomic Energy Agency, Vienna International Centre, P.O. Box 100, 1400 Vienna, Austria, 2013.
- [106] K.O. Buessler, M. Aoyama, and M. Fukasawa. Impacts of the Fukushima Nuclear Power Plants on Marine Radioactivity. *Environ. Sci. Technol.*, 45:9931–9935, 2011.
- [107] www.gps-coordinates.net (Accessed 09.09.15).

- [108] R. Eigl, M. Srnicik, P. Steier, and G. Wallner. $^{236}\text{U}/^{238}\text{U}$ and $^{240}\text{Pu}/^{239}\text{Pu}$ isotopic ratios in small (2 L) sea and river water samples. *J. Environ. Radioact.*, 116:54–58, 2013.
- [109] K. M. Wong. Radiochemical determination of plutonium in sea water, sediments and marine organisms. *Anal. Chim. Acta*, 56:355–364, 1971.
- [110] G. A. Burney and R. M. Harbour. *Radiochemistry of Neptunium*. Technical Information Center, Office of Information Services, UNITED STATES ENERGY COMMISSION, 1974.
- [111] <http://www.eichrom.com/eichrom/products/extraction.aspx> (Accessed 10.07.2015).
- [112] W.D. Loveland, D.J. Morrissey, and G.T. Seaborg. *Modern nuclear chemistry*. John Wiley & Sons, Inc., 2006.
- [113] <http://www.eichrom.com/eichrom/radiochem/> (Accessed 10.07.2015).
- [114] E. P. Horwitz, R. Chiarizia, and M. L. Dietz. A Novel Strontium-Selective Extraction Chromatographic Resin*. *Solvent Extr. Ion. Exc.*, 10(2):313–336, 1992.
- [115] Eichrom ideas. Eichrom industries, INC., 1996.
- [116] L. Perna, M. Betti, J. M. Barrero Moreno, and R. Fuoco. Investigation on the use of UTEVA as a stationary phase for chromatographic separation of actinides on-line to inductively coupled plasma mass spectrometry. *J. Anal. At. Spectrom.*, 16:26–31, 2001.
- [117] E. P. Horwitz, M. L. Dietz, R. Chiarizia, and Diamond H. Separation and pre-concentration of uranium from acidic media by extraction chromatography. *Anal. Chim. Acta*, 266:25–37, 1992.
- [118] N. Famulok, T. Faestermann, L. Fimiani, J. Gómez-Guzmán, K. Hain, G. Korschinek, P. Ludwig, and S. Schönert. Ultrasensitive detection method for primordial nuclides in copper with Accelerator Mass Spectrometry. *Nucl. Instr. Methods Phys. Res., Sect. B*, 361:193–196, 2015.
- [119] Referat für Gesundheit und Umwelt. *Jährlicher Bericht - 2008, Entnahme von Tertiärgrundwasser durch Münchner Firmen*, 2008. www.rismuenchen.de/RII/RII/DOK/SITZUNGSVORLAGE/1529270.pdf (Accessed 02.02.2016).
- [120] T. Mayer-Kuckuck. *Kernphysik*. Teubner-Studienbücher: Physik, 1984.
- [121] G.F Knoll. *Radiation Detection and Measurement*. John Wiley & Sons, Inc., 2010.
- [122] A. Alke. Präparation von Pu-236 durch protonen-bestrahlung von U-238. Master's thesis, Fachhochschule Isny, 2008.
- [123] Canberra Industries, Inc. *Alpha AnalystTM Integrated Alpha Spectrometer*, 2009. www.canberra.com/products/radiochemistry_lab/pdf/Alpha-Analyst-SS-C36474.pdf (Accessed 04.02.16).
- [124] J.F. Wacker, G.C. Eiden, and S.A. Lehn. Mass Spectrometric Radionuclide Analy-

Bibliography

- ses. In B. Kahn, editor, *Radioanalytical Chemistry*. Springer, 2007.
- [125] S. Wilbur. Rapid Analysis of High-Matrix Environmental Samples Using the Agilent 7500cx ICP-MS. Technical report, Agilent Technologies, Inc., 2007.
- [126] K.L. Linge and K.E. Jarvis. Quadrupole ICP-MS: Introduction to Instrumentation, Measurement Techniques and Analytical Capabilities. *Geostand. Geoanal. Res*, 33(4):445–467, 2009.
- [127] W. Kutschera et al. VERA: A new AMS facility in Vienna. *Nucl. Instr. Methods Phys. Res., Sect. B*, 123(1-4):47–50, 1997.
- [128] A. Priller, R. Golser, P. Hille, W. Kutschera, W. Rom, P. Steier, A. Wallner, and E. Wild. First performance tests of VERA. *Nucl. Instr. Methods Phys. Res., Sect. B*, 123:193–198, 1997.
- [129] P. Steier, R. Golser, W. Kutschera, A. Priller, C. Vockenhuber, and S. Winkler. VERA, an AMS facility for "all" isotopes. *Nucl. Instr. Methods Phys. Res., Sect. B*, 223-224:67–71, 2004.
- [130] C. Tuniz, J. R. Bird, D. Fink, and G. F. Herzog. *Accelerator Mass Spectrometry - Ultrasensitive Analysis for Global Science*. CRC Press LLC, 1998.
- [131] K. Knie, T. Faestermann, and G. Korschinek. AMS at the Munich gas-filled analyzing magnet system GAMS. *Nucl. Instrum. Methods Phys. Res., Sect. B*, 123(1-4):128–131, 1997.
- [132] P. Ludwig. *Search for ^{60}Fe of Supernova Origin in Earth's Microfossil Record*. PhD thesis, Technische Universität München, 2015.
- [133] J. C. Rucklidge, G. C. Wilson, and L. R. Kilius. In situ trace element determination by AMS. *Nucl. Instr. Methods*, 52(3 - 4):507–511, 1990.
- [134] H.-A. Synal, M. Stocker, and M. Suter. MICADAS: A new compact radiocarbon AMS system. *Nucl. Instr. Methods Phys. Res., Sect. B*, 259(1):7–13, 2007.
- [135] L. Fimiani. *Instellar radionuclides in Lunar samples*. PhD thesis, Technische Universität München, 2014.
- [136] B. Deneva. Development of accelerator mass spectrometry for ^{93}Zr . Master's thesis, Technische Universität Wien, 2015.
- [137] R. Middleton. A versatile high intensity negative ion source. *Nucl. Instr. Methods Phys. Res.*, 214(2-3):139–150, 1983.
- [138] K. Hain. *Accelerator Mass Spectrometry relevant for Nuclear Waste Transmutation*. PhD thesis, Technische Universität München, 2011.
- [139] N. Bohr. The Penetration of Atomic Particles Through Matter. *Mat. Fys. Medd. Dan. Vid. Selsk.*, 18(8), 1948.
- [140] T. Faestermann, G. Dollinger, and W. Carli. Calibration of the New Analyzing Magnet. In *Jahresbericht*. Beschleunigerlabor von LMU und TUM, 1996.
- [141] Canberra Industries, Inc. *Passivated Implanted Planar Silicon (PIPSTM) Detectors*, 2012.

- [142] P. Ludwig. Search for Superheavy Elements in Nature with Accelerator Mass Spectrometry. Master's thesis, Technische Universität München, 2010.
- [143] S. R. Winkler, P. Steier, J. Buchriegler, J. Lachner, J. Pitters, A. Priller, and R. Golser. He stripping for AMS of ^{236}U and other actinides using a 3 MV tandem accelerator. *Nucl. Instr. Methods Phys. Res., Sect. B*, 361:458–464, 2015.
- [144] T.-L. Ku, K. G. Knauss, and G. G. Mathieu. Uranium in open ocean: concentration and isotopic composition. *Deep Sea Res.*, 24:1005–1017, 1977.
- [145] J. Lachner, M. Christl, C. Vockenhuber, and H.-A. Synal. Detection of UH^{3+} and ThH^{3+} molecules and ^{236}U background studies with low-energy AMS. *Nucl. Instr. Methods Phys. Res., Sect. B*, 294:364–368, 2013.
- [146] B. R. Harvey and G.A. Sutton. The Properties of ^{235}Np as a Tracer and Yield Monitor in Studies of the Environmental Behaviour of Neptunium. *Nucl. Instr. Methods Phys. Res. A*, 254:172–181, 1987.
- [147] L. K. Fifield, R. G. Cresswell, M.L. di Tada, T.R. Ophel, J. P. Day, A. P. Clacher, S. J. King, and N. D. Priest. Accelerator mass spectrometry of plutonium isotopes. *Nucl. Instr. Methods Phys. Res. B*, 117(3):295–303, 1996.
- [148] R. Middleton. 'A Negative-Ion Cookbook', University of Pennsylvania, 1990.
- [149] F. Dellinger, W. Kutschera, O. Forstner, R. Golser, A. Priller, P. Steier, A. Wallner, and G. Winkler. Upper limits for the existence of long-lived isotopes of roentgenium in natural gold. *Phys. Rev. C*, 83(1):015801(1)–(9), 2011.
- [150] L. K. Fifield, A. P. Clacher, K. Morris, S. J. King, R. G. Cresswell, J. P. Day, and F. R. Livens. Accelerator mass spectrometry of the planetary elements. *Nucl. Instr. Methods Phys. Res. B*, 123:400–404, 1997.
- [151] G. Feldman and R. Cousins. A Unified Approach to the Classical Statistical Analysis of Small Signals. *Phys. Rev. D*, 57(7):3873–3889, 1998.
- [152] K.A. Olive and others (PDG). *Chin. Phys. C*, 38(090001), 2014.
- [153] Seawater. www.britannica.com/science/seawater/Density-of-seawater-and-pressure (accessed 20.01.16), 2016.
- [154] K. Hirose. Plutonium in the Ocean Environment: Its Distributions and Behavior. *J. Nucl. Radiochem. Sci.*, 10(1):R7–R16, 2009.
- [155] Neritic zone. www.britannica.com/science/neritic-zone (accessed 25.01.16), 2016.
- [156] D.E. Robertson, Silker W.B., J.C. Langford, Petersen M.R., and R.W. Perkins. Transport and depletion of radionuclides in the Columbia River. In *Radioactive contamination of the marine environment*, pages 141–155, 1973.
- [157] M. Dai, K.O. Buesseler, and S.E. Pike. Plutonium in groundwater at the 100K-Areas of the US DOE Hanford Site. *J. Contam. Hydrol.*, 76(3-4):167–189, 2004.
- [158] T.M. Beasley, L.A. Ball, and B.A. Blakesley. Plutonium and Americium Export to the North-east Pacific Ocean by Columbia River Runoff. *Estuar. Coast Shelf S.*, 13:659–669, 1981.

Bibliography

- [159] www.mapcoordinates.net/en (accessed 26.01.16).
- [160] W. Bu, J. Zheng, T. Aono, K. Tagami, S. Uchida, J. Zhang, Honda M.C., Q.J. Guo, and M. Yamada. Vertical distributions of plutonium isotopes in marine sediment cores off the Fukushima coast after the Fukushima Dai-ichi Nuclear Power Plant accident. *Biogeosciences*, 10:2497â2511, 2013.
- [161] T.M. Beasley, L.W. Cooper, J.M. Grebmeier, K. Aagaard, J.M. Kelley, and L.R. Kilius. $^{237}\text{Np}/^{129}\text{I}$ Atom Ratios in the Arctic Ocean: Has ^{237}Np from Western European and Russian Fuel Reprocessing Facilities Entered the Arctic Ocean? *J. Environ. Radioactivity*, 39(3):255–277, 1998.
- [162] H.A.C. McKay. *The PUREX process*. United States: CRC Press, Inc., 1990.
- [163] M. Cox and J. Rydberg. Introduction to Solvent Extraction. In *Solvent Extraction - Principles and Practice*. (Rydberg, J. and others, Eds.), Marcel Dekker, 2005.
- [164] *Material Safety Data Sheet, Hydroxylamine solution*. Sigma-Aldrich Chemie GmbH, Riedstrasse 2, D-89555 STEINHEIM, 2013.
- [165] *Material Safety Data Sheet, Hydrazine solution*. Sigma-Aldrich Chemie GmbH, Riedstrasse 2, D-89555 STEINHEIM, 2015.
- [166] <http://laraweb.free.fr/> (Accessed 30.01.2015).

Acknowledgement

There is a considerable number of people who made this work possible and supported in different ways in sometimes quite difficult times. Therefore, I would like to thank:

- Studienstiftung des deutschen Volkes, for the financial support of this work and the possibility to meet and discuss with many other PhD students.
- Walter Henning, for encouraging me to apply for the scholarship of the Studienstiftung and for supervising this work even at this large distance.
- Gunther Korschinek and Thomas Faestermann, for introducing me to AMS in the first place, for sharing their incredible experience in experimental physics with me and for countless discussions on many exciting aspects of physics and sometimes also organizational issues.
- Christoph Lierse von Gostomski and Florian Kortmann (RCM), for helping out with a chemistry lab twice. I would like to express my sincere gratitude for this support, because otherwise I really wouldn't have known how to finish my thesis. Thank you, Flo, for always being available and willing to help with smaller and bigger problems in the lab.
- Peter Steier (VERA), for your readiness to help in very difficult times by offering the possibility of AMS measurements at VERA. I really would like to thank you very much for your straightforward assistance. The same holds for the whole VERA group who keep the set-up running.
- the AMS group (Peter Ludwig, Leticia Fimiani, José Guzmán, Boyana Deneva), for help during the experiments and a very pleasant working atmosphere. Special thanks to Leticia for keeping spirits high with cake and Asado and to Peter for the careful proof-reading of parts of this work.
- Jacqueline Walser (RCM), for tips and tricks in a radiochemistry lab and for always being in a good mood.
- Gisela Grünewald (RCM), for the evaluation of the γ -spectrometry data.
- Masatoshi Yamada (Hirosaki University), for providing the Pacific Ocean water samples.
- Taeko Shinonaga, for the introduction to actinide chemistry in environmental samples.
- Alexander Diener (former KIT), Bastian Breustedt (KIT), Aline Ritter (HZDR), Sabrina Gurlit (HZDR), for the ICP-MS measurements. Thank you, Alex, for check-

Bibliography

ing the results over and over again.

- Volker Hannstein (GRS), for the reactor core calculations using the Serpent code.
- The whole staff of the accelerator lab of the MLL, i.e. the operators (“old” and “new”), the workshop, L. Beck and C. Singer, for their continuous assistance over the last 4.5 years. I really enjoyed being part of this institute (and also will in the future).
- My family, for their wholehearted support in all situations and the ups and downs we have been through together, especially in the last 9 years.